Analytic Solutions to the Laplace, Poisson, and Biharmonic Equations with Internal Boundaries: Theory and Application to Microfluidic Dynamics

by

Chengzhao "Richard" Zhang

Submitted to the Department of Mathematics
in partial fulfillment of the requirements for the degree of

Doctor of Philosophy in Applied Mathematics

at the

MASSACHUSETTS INSTITUTE OF TECHNOLOGY

May 2021

Author . . . .
Department of Mathematics
May 7th, 2021

Certified by . . . .
Rodolfo Ruben Rosales
Professor
Thesis Supervisor

Accepted by . . . .
Jonathan Kelner
Chairman, Department Committee on Graduate Studies

Analytic Solutions to the Laplace, Poisson, and Biharmonic Equations with Internal Boundaries: Theory and Application to Microfluidic Dynamics

by

Chengzhao "Richard" Zhang

Submitted to the Department of Mathematics
on May 7th, 2021, in partial fulfillment of the
requirements for the degree of
Doctor of Philosophy in Applied Mathematics

Abstract

This dissertation focuses on developing analytical methods for elliptic partial differential equations with conditions imposed on internal boundaries. Internal boundaries are formed where materials with different properties meet to form interfaces. These interfaces arise in a variety of physical and engineering contexts such as in the evaporation of water droplets, dielectric double-spheres, and soft-material Janus drops. The solutions to problems with interfaces are often singular where the interfaces meet the boundaries, or two interfaces meet. This causes difficulties when attempting to solve these problems solely with numerical approaches. In contrast, analytical approaches (while limited to relatively simple geometries) lend significant insight into the nature of the singularities, with full resolutions in some cases. Potentially this knowledge can then be used to improve the quality of numerical solutions for more generic situations.

We will focus here on four important elliptic PDE problems: Laplace, Poisson, biharmonic, and Stokes flow. Chapter 1 introduces our main analytic result known as the Parity Split Method (PSM), developed in the context of the Laplace and the Poisson equation. Chapter 2 takes the results from Chapter 1 and applies them to the problem of a thermally driven evaporative liquid bridge in a long V-shaped channel. The problem involves solving a coupled temperature-concentration system of Laplace equations. Complex analysis based analytic solutions to the concentration equation are also developed along the way. Chapter 3 extends the PSM to the biharmonic equation and addresses several numerical issues related to solving for the fluid flow near a soft-material Janus drop.

Thesis Supervisor: Rodolfo Ruben Rosales
Title: Professor

Acknowledgments

"It was the best of times, it was the worst of times, it was the age of wisdom, it was the age of foolishness, it was the epoch of belief, it was the epoch of incredulity, it was the season of light, it was the season of darkness, it was the spring of hope, it was the winter of despair." The words of Charles Dickens have never been truer. After all, I would've never imagined to be finishing my PhD during the COVID-19 Pandemic. The emptiness of 2-490 resonates with the white noise coming from my computer as I am typing up these words. Outside the Simons Building, the season of spring is gently kissing the grass of the Killian Court even though the stubborn wintry chill of Boston is still making its last attempt to blast through the city. The sporadic, socially distant, mask-wearing pedestrians and joggers bustle along the Memorial Drive on a slow Friday morning, against the background of the Great Dome of MIT. The Neoclassical architecture guards this great Institute so *solemnly, peacefully, and majestically* as if the cacophony of the mundane world is but a little dust particle in its eons of presence along the Charles River. Ever since the start of the quarantine, we have been isolated and far from one another. But in some other way, the pandemic brought us closer. When I defended my dissertation on April 28th, 2021 at 9:00am EDT via Zoom, more than 200 attendees showed up from all over the world. This could've not happened during normal times.

A lot of the 200 people who showed up are friends from the MIT Visiting Student Association (VISTA), whom I am dedicating this dissertation to first and foremost. When I first met the founders of VISTA in February 2018, I would've not thought that this would be my family for the remaining times at MIT. Thank you for your collective energy, passion, and kindness, and for showing me the power of a real community and the true meaning of a home away from home. People like *Francesco Benedetti, Giannandrea Inchingolo, Tanja Mueller, Dominik Gau (+Steffi + Melanie), Holden Lai, Luca Alfeo, Monika Feldmann, Simone Bruno, Stefano Deluca, Nuno Marques, Raksmy Nop, Ana Morello, Bassel Tarabay, Diego Sandoval, Gregoire Chomette, Kumar Kishen, Luana Morrocco, Daniel Bergen (+Nefeli + Ines), Fabio Caltanissetta, Geraldine Chanteux, Hakan Yilmaz, Diana Bonilla, Don van Elst, Andrea Pertoldi, Steven Schenk, Jorge Marques Silva, Jurgis Ruza, Luca Montanelli (+Jenny Jang), Max Elsen, Valentin Klusener, Valentina Negri (+Pang), Caio Benatti Moretti, Lorenzo Santollini, Evelyne Ringoot, Lisa Kraus, Luca Ballotta, Katharina*

Kempf, Sofia Gorbatchev, Michael Uggowitzer, Dennis Gankin, Martijn van Galen, Cristina Marquez, Niki Gatzionis, Richard Karl, Taka Morikawa, Marcella Franco, etc. are **some of the most beautiful, kindest, and humblest people on this planet**. And the list really goes on. To all the parties we had and all the shots we took, thank you so much, VISTA, for giving me an incredible time at MIT.

Another very important community that I have been doubling down at MIT is FAIL!. When we started this little project back in 2018, it was just an experiment. But then it transformed into a whole new tight community of academics, entrepreneurs, and young professionals who are struggling with high self-expectations, self-doubts, and impostor syndrome. For the 10+ live conferences and numerous online events we organized, 50+ speakers engaged, 100+ volunteers, and hundreds of thousands of audiences, I toast to you all, and especially to the FAIL! Board: *Francesco Benedetti, Giannandrea Inchingolo, Tanja Mueller, Luca Alfeo, Jurgis Ruza, Luca Ballotta, Valentina Negri, Eleonora Ricci, Nico Parow, Fabio Cruz, and Simone Bruno.* Thank you for making my life at MIT less anxious and more tolerable! (FYI: I like the name "John Richard":))

Of course, not all of my friends come from any identifiable communities that I fostered. Thanks *Tobi Egle* for all these years of unique, heartwarming and irreplaceable companionship (go Bee-Chaz), *Ranjan Anantharaman* for cooking for me and for being there when I needed it the most (eg. 2020 New Year's Eve), *Francesco Benedetti* for all your sage advice and omnipresence in my life, *German Parada* for those unforgettable nights of cocktail mixing in Ashdown, *Rene Ahlsdorf* for the endless regular Sunday conversations and wisdom into AI, healthcare, and dating, *Sungwoo Jeong* for the always-too-short coffee times, *Sabrina Smai* for our favorite song and dance, *Aziza Sulton Ahson* for the unwavering support both at Pillar and elsewhere, *Wenyan Deng* for the never-ending socio-economic-political discussions, *Jose Luis Lara* for the math memes and long-lasting friendship all the way from Finland, *Felix Feist* for his genuine kindness and purple love, *Matthias Ginterseder* for his witting humor and a constant ear to listen, *Matteo Gardini* for the fulfilling coffees and dinners during his short and sweet stay at MIT, and *Ferah Akiriru* for the decades of friendship and common pure love for Marvel (Wakanda Forever!).

In addition, how can I forget all the mentors who helped me along the way? These mentors are not just smart and brilliant, but also are just good people. Personally, I think society over-indexes on people who are smart and brilliant. But the truth is that everyone is brilliant

in a place like MIT; brilliance is a cheap commodity that is no longer the sole judging criterion for a mentor. Quoting Prof. Allan Adams from MIT Physics, "find the mentors that are good to you, not just brilliant. Because brilliance is cheap, and good is special." My one and only advisor, *Prof. Ruben Rosales*, is one of the kindest and most caring advisors that one could ever hope for. He not only cares about my research but also my mental health and well-being. So thank you, Ruben! *Prof. Gilbert Strang*, my other committee member, has dedicated his entire life to the education of mathematics and has been and will always be my role model going forward. Thank you Gil! And of course, *Prof. Pedro Saenz*, my third committee member, never let go of me and my project despite its immense difficulty. Thank you Pedro! There are so many other mentors who believed in me when I might not even believe in myself, and here goes the very incomplete list: *Francesco Benedetti, Oleg Pianykh, John Werner, Reinaldo Normand, Jamie Goldstein, Russ Wilcox, Sarah Hodges, Parker McKee, Friedrich Ulfers, Gorick Ng, Jake Livengood, Emily Taylor, Danielle Reddy, Maisie O'Brien, Jose Diaz-Alban, Luisa Apostol, Sue Lambe-Sarinana, Mar Hershenson, Peter Polga-Hecimovich, Jinane Abounadi, etc.*

Last but not the least, I want to say how much I love my mom and dad, Chunxiao Zhang and Bing Zhang. They have created an impossibly ideal ambiance for me to grow up and sacrificed so much to come to Canada and the United States to make my dream possible. No word can express how much I am feeling about my own family.

As I am closing my MIT chapter and heading down a new journey in Palo Alto, I am grateful to all the good and bad experiences in the past five years. Quoting the famous Chinese military strategist Zhuge Liang during the Three Kingdom, " 今當遠離，臨表涕零, 不知所云。" (I depart now on a long expedition. Blind by my own tears, I know not what to write.).

Chengzhao "Richard" Zhang 張承昭, May 7th, 2021. 10:20am. 2-490. Massachusetts Institute of Technology

Contents

List of Figures

List of Tables

Chapter 1

Introduction

1.1 The Parity Split Method for Poisson's Equation

Many physical problems require solving elliptic partial differential equations with interfaces, such as the electric potential for electromagnetic double spheres [28, 41, 42], temperature and concentration of vapor above a slowly evaporating sessile drop [59, 10, 3, 47], and the concentration of soft materials under Laplacian growth [20, 2]. In all such problems, the interfaces are modeled as infinitely thin surfaces. Then the quantities of interest, such as temperature, material concentration, or potential, often must satisfy jump conditions across the interfaces. Several numerical approaches have been developed to solve problems of this type, such as, the Immersed Boundary Method (IBM) [39], the Immersed Interface Method (IIM) [29, 30, 31], the Ghost Fluid Method [16, 15, 21, 17], and the Correction Function Method (CFM) [34].

Additional difficulties arise when the internal interface meets the external boundary at the "triple-line" points (See Figure B-1), and can trigger "triple-line singularities (TLS)". Elliptic problems are notorious for developing singular behavior at places where the boundary or the boundary conditions lack smoothness. For corner singularities, the behavior of the solutions is well understood [13, 12, 19, 18, 38]. We are not aware of similar studies for the type of singularities that arise at triple line points. In this paper, we propose a new analytical method, which we call the Parity Split Method (PSM), which allows us to solve elliptic problems with TLS for certain restricted geometries. For those geometries, the PSM eliminates the interface and replaces the original elliptic problem by sub-problems without the interface. If the geometry is such that separation of variables provides a spectral basis

to express the solutions of the sub-problems with the interface removed, then our approach provides a fast converging spectral basis for the original problem with the interface.

Suitable PDE which PSM can be applied for include Poisson's equation, biharmonic equation, and Stokes' equation. In this chapter, we present the method in the context of Laplace's equation and later generalize to Poisson's equation. Section 2.1 sets up the problem of interest in the generic form. Section 2.2 introduces the Parity Split Method in the context of Laplace's equation. Section 2.3 works out explicit examples for Laplace's in various 2D and 3D domains. Section 2.4 extends the method to Poisson's and relaxes several conditions set in Section 2.1. Section 2.5 elucidates an important technicality in the PSM.

1.2   Evaporation of a Liquid Bridge in a V-Shaped Channel

We will demonstrate the power of the Parity Split Method via the problem of thermally driven microfluidic evaporation. The evaporation of liquid on a substrate is of paramount significance in a wide range of engineering applications, such as inkjet printing, micro-fabrications, and DNA sequencing. A tremendous amount of theoretical and experimental investigations have been done to advance the understanding of quasi-static evaporation. Seminal works include those in [5, 7, 22, 24, 43, 23, 3, 10, 11, 37, 51, 47]. Throughout these studies, topics of interests involve pattern formation during drying [6], material flux across the liquid-vapor interface [11, 48], and lifetimes of evaporating liquid [51, 52, 47, 48]. We are particularly interested in the study of material flux and lifetime of a thermally-driven evaporating liquid in a V-shaped channel. The geometry of V-shaped channels appears in numerous modern heat transfer microelectronic devices, such as micro heat pipes [54]. Such devices often rely on the evaporation of liquid in the channels to achieve the desirable heat transfer. As a result, material flux and evaporation lifetime can be appropriate metrics to characterize the efficiency of the transfer mechanisms. Extensive theoretical, numerical, and experimental studies have been conducted to understand the evaporation of a liquid in a V-shaped channel, including [55, 40, 33, 32, 59].

Most of the aforementioned works use either experimental or purely numerical approaches. However, in a V-shaped channel, the length often vastly exceeds its width, which should render the problem effectively two-dimensional – thus potentially amenable to analytic treatment using conformal mapping and other complex analysis tools. Unfortunately,

a straight reduction of 3D elliptical problems in unbounded domains to 2D is often problematic. For example, while developing an analytical solution for Stokes flow inside an evaporating drop, Masoud [35] noted that "...a solution does not exist for diffusive flux in 2D" because the 2D solution varies "logarithmically" at infinity [35]. Schofield, Wray, Pritchward, and Wilson encounter the same issue when studying the lifetimes of two-dimensional sessile droplets [48]. o get around this issue, in this work we do not do a straight reduction to 2D. Instead we write a suitably modified 2D problem, which can be solved (analytically) using the Parity Split Method and tools from complex analysis.

In this thesis we present an analytical solution to a 2D model problem involving the thermally-driven evaporation of a liquid in an infinitely long V-shaped channel. We obtain exact (analytical) expressions for the temperature distribution and vapor concentration, from which we compute the vapor flux and the evaporating lifetime for the liquid. To formulate the model we follow the spirit in [48], and transform the far-field conditions (which would either invalidate or trivialize the 2D problem) into boundary conditions along a "mathematical" boundary. In Section 3.1, we present the governing equations, with boundary conditions that render meaningful solutions. In Section 3.2, we present the solutions to temperature and concentration. In particular, we use the Parity Split Method introduced in Chapter 2 to analytically implement the jump conditions in temperature at the liquid-vapor interface, and introduce a (novel as far as we know) complex analysis technique to solve for the concentration. Finally, we use the obtained analytical expressions to compute the evaporative lifetime in Section 3.3 and discuss their significance in Section 3.4.

1.3 Preliminary Results on Biharmonic Equation

Named after the ancient Roman double-faced god, Janus drops are liquid droplets formed by two immiscible liquids. Famously referred by the Nobel Prize winner P. G. de Gennes in 1991 [4], Janus drops have found their way into numerous applications, from material self-assembly and smart sensing to drug deliveries and imaging [14, 26]. Upon immersed in a solute, Janus drops are easily re-orientable by externally controlled variables such as temperature, relative concentrations of the solute, and any surfactant applied on the surfaces of the drops. Note that Janus drops occur within the context of micro-fluidics, and thus its behavior is governed by the Stokes equations.

Our work in Janus drops was initially motivated by experiments conducted at the Physical Mathematics Laboratory at the UNC Chapel-Hill Department of Mathematics [45], showing how a Janus drop in a liquid may re-orient, and displace, in response to an applied external thermal gradient — due to flows triggered by the Marangoni effect. Our objective was to develop a simple (analytical) formula for the drop dynamics, which could then be used (for example) as the building block to model the behavior of a large collection of drops.

Our intention was to use, as the starting point for our analysis, the work by Shklyaev, et. al [49, 8, 50, 9]. In particular, *Dynamics of a Janus Drop in an External Flow* [49], these authors present a semi-analytical technique (based on mode expansions) to calculate the steady motion of a Janus drop under a uniform external flow. They approximate the Janus drop as a perfect sphere with different material compositions in the upper and lower hemispheres, with a flat interface across the equator. Next the authors write the governing equations in each of the three regions (upper and lower hemisphere, and external region — see Figure B-14), and write the appropriate jump conditions across the interfaces. Finally they propose "mode" expansions for the solutions in each region, with constants to be determined by a linear system that results upon imposing the jump conditions. The most interesting feature of this method is that the proposed expansions satisfy the jump conditions across the equatorial interface automatically, "term-by-term".

Unfortunately, upon performing a detailed examination of the work in [49], we encountered significant "puzzles", that worried us, while trying to understand the proposed solution. Our attempts to fix these issues lead to the current work. The issues are: (i) The "modes" satisfying the equatorial jump conditions are simply written. There is no attempt at motivating, or explaining, why they should have the proposed form. Thus the obvious question: is there a general principle behind them, or are these just smart guesses? (ii) Since the proposed solutions involve an infinite series, one may again wonder: Is the set of modes involved complete, and linearly independent? (iii) Assuming that the answer to (ii) is yes, another problem arises: On the one hand, as explained earlier, the presence of a triple-point (along the equator — see Figure B-14) causes a singularity in the solution there, which implies that the proposed series must converge slowly. On the other hand, the linear system that must be solved to find the coefficients is numerically poorly conditioned. Thus it is very hard to accurately compute more than a few coefficients. This results in a "visually" satisfactory solution, which (however) fails to satisfy the stress jump conditions

20

across the Janus drop surface, exhibiting a rather massive case of the Gibbs phenomena. The questions here are then: What is the source of the poor conditioning, and can it be fixed? Alternatively: is there a way to extract the singular part of the series, so that the rest converges reasonably fast?

The work in this thesis gives a positive answer to the questions in (i) and (ii) above in various related settings, although the work for the specific case of the Stokes equations is not yet complete. As for (iii) we do not have a complete answer, but we know that it is not a phenomena restricted to Janus drops in 3D, as we have found the exact same problem for a similar problem in 2-D, the "Janus cylinder". This research is presented in Chapter 4, as follows: Section 4.1 introduces the 3D Janus problem in [49], and describes in some detail the issues reported in the prior paragraph. In section 4.2 we examine the Stokes equations in 2D, which can be reduced to the biharmonic equation, and present some results that are needed to formulate the Parity Split Method (PSM) in this case. In Section 4.3 we introduce the 2D "Janus cylinder" problem, and show how to solve it using the PSM. Section 4.4 proposes a way to fix the large condition number issue (for the linear system arising in section 4.3) via the use of novel basis functions and numerical pre-conditioning. Finally, Section 4.5 concludes the chapter and identifies potential future directions for this line of work.

Chapter 2

Parity Split Method for the Poisson Equation; Triple-Line Singularities

2.1 Problem Formulation

In this chapter we consider Poisson's problem over a domain Ω (in 2D or 3D, say), with boundary $\partial\Omega$, split in two sub-domains, Ω_1 and Ω_2, by an interface Γ — see Figure B-1. The equations are as follows

$$
\begin{cases}
\Delta u = h, & \text{in } \Omega, \\[4pt]
u = f, & \text{on } \partial\Omega, \\[4pt]
[u]|_\Gamma = b, \\[4pt]
[\nu\,\hat{n}\cdot\nabla u]|_\Gamma = w,
\end{cases}
\tag{2.1}
$$

where the brackets indicate the jumps in the enclosed variables across the interface

$$
[u]_\Gamma = u_1(x) - u_2(x), \qquad\qquad x \in \Gamma, \tag{2.2}
$$

$$
[\nu\,\hat{n}\cdot\nabla u]_\Gamma = \left(\nu_1\,\hat{n}\cdot\nabla u_1\right)(x) - \left(\nu_2\,\hat{n}\cdot\nabla u_2\right)(x), \qquad\qquad x \in \Gamma, \tag{2.3}
$$

Here: h, f, b, and w, are given functions (defined in the appropriate domains), we use the subscripts 1 and 2 to indicate quantities defined in each of the sub-domains (e.g.: u_i is the solution in Ω_i), $\hat{n}$ is the unit normal to Γ (pointing towards Ω_1), and the ν_i are positive (generally not equal) constants.

Note 2.1. *(**Boundary conditions**). Here we consider the case with Dirichlet boundary*

conditions. However, the approach we will introduce can be easily extended to other types of boundary conditions, such as Neumann. ♣

Note 2.2. (The function ν). *ν is defined by $\nu = \nu_1$ for Ω_1 and $\nu = \nu_2$ for Ω_2.* ♣

Note 2.3. (Physical motivation). *This type of problem arises when, for example, seeking the steady state temperature distribution in a domain with two different (constant) heat diffusivities, ν_1 and ν_2. In this case f is the temperature on the boundary, h arises because of heat sources in the domain, $b = 0$, and w corresponds to heat sources at the interface (such as those caused by the latent heat in an evaporation process) — note that $\nu_i\,\hat{n} \cdot \nabla u_i$ are the heat fluxes on each side of the interface. A non-vanishing b occurs when u represents the pressure, then b arises because of surface tension at the interface.* ♣

Note 2.4. (Notation). *Throughout this thesis $x = (x_1, ..., x_d) \in \mathbb{R}^d$ denotes a Cartesian vector, and Δ is the Laplace operator $\Delta = \sum\limits_{j=1}^{d} \partial^2_{x_j x_j}$.* ♣

In Sections 2.2–2.3, we consider the problem with no sources — i.e.: h, b, and w vanish. That is

$$
\begin{cases}
\Delta u = 0, & \text{in } \Omega \\[2mm]
u = f, & \text{on } \partial\Omega \\[2mm]
[u]|_\Gamma = 0 \\[2mm]
[\nu\,\hat{n} \cdot \nabla u]|_\Gamma = 0
\end{cases}
\tag{2.4}
$$

The source terms are added in Section 2.4.

2.2 Parity Split Method for the Laplace Equation

The PSM transforms the problem in (2.4) into an equivalent set of two problems without any interface. To do so it relies on the existence of a symmetry, relative to the interface, of the domain Ω. That is: **we assume** (2.5) that there exists a function g with the following properties:

(1) g maps Ω to Ω, and g^2 is the identity.

(2) $g(\Omega_1) = \Omega_2$. Note that then (1) implies $g(\Omega_2) = \Omega_1$.

(3) g is the identity on Γ.

(4) g is at least C^2.

(5) g preserves the Laplacian: $\Delta u(g(x)) = 0$ if $\Delta u(x) = 0$.

Note that these are rather restrictive conditions, which severely limit the possible geometries — for a more technical discussion of this issue, see Section 2.5.

Given (2.5), we use g to write the solution in terms of an "odd" and an "even" component (the "parity split").[1] We do the same for the boundary data f. Then we show that each of the components satisfies a Laplace problem with the interface Γ removed. We will also show that any solution can be written in this way.

To proceed with the program described above, we first introduce the *parity split decompositions*. Any function defined on Ω, or on $\partial\Omega$ (in particular, the solution to (2.4), and the boundary data) can be written in the form

$$u = u_e + \frac{1}{\nu}u_o \quad \text{and} \quad f = f_e + \frac{1}{\nu}f_o, \tag{2.6}$$

where the subscript "e" (resp. "o") indicates that the corresponding function is even (resp. odd) with respect to g. This decomposition is unique: with $\kappa = 1/\nu_1 + 1/\nu_2$, it is easy to see that (note **2.5**)

$$f_e(x) = \frac{1}{\kappa}\left(\frac{1}{\nu(g(x))}f(x) + \frac{1}{\nu(x)}f(g(x))\right), \tag{2.7}$$

$$f_o(x) = \frac{1}{\kappa}\left(f(x) - f(g(x))\right), \tag{2.8}$$

with similar expressions for u. Clearly f_e, f_o, etc., have the required even/odd properties.

Theorem 2.1. *If u satisfies (2.4), then u_e and u_o satisfy*

$$\begin{cases} \Delta u_e = 0, & \text{in } \Omega, \\ u = f_e, & \text{on } \partial\Omega, \end{cases} \quad \text{and} \quad \begin{cases} \Delta u_o = 0, & \text{in } \Omega, \\ u = f_o, & \text{on } \partial\Omega, \end{cases} \tag{2.9}$$

where neither of these PDE involves an internal boundary. Furthermore: if (2.9) is satisfied (with f_e even and f_o odd), then u (as defined by (2.6)) satisfies (2.4).

Proof. We begin with the proof of the second claim. This requires that we show that: (a) u is harmonic in each of Ω_1 and Ω_2, (b) $u = f$ on $\partial\Omega$, and (c) u, and the flux $\nu\,\hat{n}\cdot\nabla u$, are both continuous across the interface Γ. To prove (a) note that $u_i = u_e + \frac{1}{\nu_i}u_o$ in Ω_i for $i = 1, 2$.

---

[1] A function c is even (odd) with respect to g if $c(x) = c(g(x))$ (resp. $c(x) = -c(g(x))$).

Since u_e and u_o are harmonic throughout Ω, and ν_i is a constant, the result follows. Next: (b) follows by construction. Finally, to prove (c) we first notice that $u_e(g(x))$ and $-u_o(g(x))$ also solve (2.9). Thus, by uniqueness, u_e and u_o inherit the parity properties, that is:

$$u_e(g(x)) = u_e(x) \quad \text{and} \quad u_o(g(x)) = -u_o(x). \tag{2.10}$$

In particular
$$[u]|_\Gamma = [u_e]|_\Gamma + [(1/\nu)u_o]|_\Gamma = 0, \tag{2.11}$$

since $u_o = 0$ on Γ.

Similarly,
$$[\nu\,\hat{n}\cdot\nabla u]|_\Gamma = [\nu\,\hat{n}\cdot\nabla u_e]|_\Gamma + [\hat{n}\cdot\nabla u_o]|_\Gamma = 0. \tag{2.12}$$

Here, just as for $[u_e]|_\Gamma$

in (2.11), $[\hat{n}\cdot\nabla u_o]|_\Gamma$ vanishes because u_o is smooth throughout Ω. On the hand, the first term vanishes because $\hat{n}\cdot\nabla u_e = 0$ on Γ (which follows because u_e is even, see note **2.6**).

Note 2.5. ***Proof that (2.7–2.8) yield (2.6).*** *We have:*

$$
\begin{aligned}
f_e(x) + \frac{1}{\nu(x)}f_o(x) &= \frac{1}{\kappa}\left(\frac{1}{\nu(g(x))}f(x) + \frac{1}{\nu(x)}f(g(x))\right) + \frac{1}{\nu(x)}\frac{1}{\kappa}\left(f(x) - f(g(x))\right) \\
&= \frac{1}{\kappa}\left(\frac{1}{\nu(g(x))} + \frac{1}{\nu(x)}\right)f(x) \;=\; f(x),
\end{aligned}
\tag{2.13}
$$

where we use that $\frac{1}{\nu(g(x))} + \frac{1}{\nu(x)} = \kappa$. The proof for u is the same. ♣

Note 2.6. **The normal derivative of u_e is "odd".** *Let $A = A(x)$ be the Jacobian of g — that is $A_{nm} = \partial_{x_m}g_n$. Then* $\qquad \nabla u_e(x) = A(x)^T \nabla u_e(g(x)).$ [a]
However, as we will show in (2.67), A is proportional to an orthogonal matrix. Hence, since g is the identity on Γ, it should be either of: $A\hat{n} = \pm\hat{n}$. But g "flips" sides across Γ, so that $A\hat{n} = -\hat{n}$. Thus, from [a]*, on Γ,* $\qquad \hat{n}(x)\cdot\nabla u_e(x) = -\hat{n}(x)\cdot\nabla u_e(x).$ [b]
It follows that $\hat{n}\cdot\nabla u_e = 0$ on Γ. ♣

2.3   Examples

2.3.1   Disk (2D example)

Here we consider the example where Ω is a disk. This geometry has been the subject of extensive investigation in fluid dynamics and heat transfer theory, such as the study of drag forces on a cylinder [36, 27, 57, 25, 1]. Thus let Ω be the unit disk centered at the origin, with Ω_1 the upper half-disk, Ω_2 the lower half-disk, and interface the interval $\Gamma = \{|x| < 1, y = 0\}$ — see Figure B-2a. As usual, ν_1 and ν_2 denote the diffusivities in each of the half-disks.

Then a suitable symmetry function g is
$$g(x, y) = (x, -y), \qquad (2.14)$$
and the equation to be solved is

$$
\begin{cases}
\Delta u = 0, & x^2 + y^2 < 1, \\[2mm]
u = f, & x^2 + y^2 = 1, \\[2mm]
u|_{y=0^+} = u|_{y=0^-}, \\[2mm]
\nu_1 \frac{\partial u}{\partial y}\big|_{y=0^+} = \nu_2 \frac{\partial u}{\partial y}\big|_{y=0^-},
\end{cases}
\qquad (2.15)
$$

To write the problem as in (2.9), we split $f = f_e + \frac{1}{\nu} f_o$ following (2.7–2.8).Thus

$$f_e(x, y) = \frac{1}{\kappa} \left(\frac{1}{\nu(x, -y)} f(x, y) + \frac{1}{\nu(x, y)} f(x, -y) \right), \qquad (2.16)$$

$$f_o(x, y) = \frac{1}{\kappa} \left(f(x, y) - f(x, -y) \right), \qquad (2.17)$$

where g is as in (2.14), $\nu = \frac{1}{\nu_1}$ for $y > 0$, $\nu = \frac{1}{\nu_2}$ for $y < 0$, and $\kappa = \frac{1}{\nu_1} + \frac{1}{\nu_2}$. Note: in polar coordinates, $f(\theta) = f_e(\theta) + \frac{1}{\nu} f_o(\theta)$ is not the "standard" split into even and odd parts.

We can now solve the problems in (2.9) using the standard modes for the Laplace equation in a disk, $r^n \cos(n\,\theta)$ for u_e and $r^n \sin(n\,\theta)$ for u_o. Using then (2.6) we obtain:

$$u = u_e + \frac{1}{\nu} u_o = \sum_{n=0}^{\infty} a_n r^n \cos(n\theta) + \sum_{n=1}^{\infty} b_n \frac{1}{\nu} r^n \sin(n\theta) \qquad (2.18)$$

where

$$a_0 = \frac{1}{2\pi} \int_{-\pi}^{\pi} f_e(\theta) d\theta, \quad a_n = \frac{1}{\pi} \int_{-\pi}^{\pi} f_e(\theta) \cos(n\theta) d\theta, \quad \text{and} \quad b_n = \frac{1}{\pi} \int_{-\pi}^{\pi} f_e(\theta) \sin(n\theta) d\theta,$$

for $n = 1, 2, \ldots$. Note that this expresses the solution to (2.15) in the (somewhat) unusual basis with modes $\{r^n \cos(n\theta)\}_{n=0}^{\infty}$ and $\{\frac{1}{\nu} r^n \sin(n\theta)\}_{n=1}^{\infty}$. See Figure B-4.

2.3.2 Sphere (3D example)

Many physical problems require solving a Laplace or Poisson problem in a sphere; for example: find the electric potential of a dielectric double sphere [41, 42, 28], or the temperature field for a Janus particle. In all these problems the equations are to be solved with an interface placed at the equator (see Figure B-2a).

Using spherical coordinates $\quad \Omega = \{(r, \theta, \phi) \,|\, 0 \le r \le 1,\, 0 \le \theta \le \pi,\, 0 \le \phi \le 2\pi\}.$ $\quad$ (2.19)

Furthermore, as in the 2D problem, Ω_1 (resp. Ω_2) is the upper (resp. lower) hemisphere, Γ

is the unit disk on the plane $z = 0$ $(\theta = \pi/2)$, and $\quad g(x, y, z) = (x, y, -z)$ $\quad$ (2.20)

(reflection across the $z = 0$ plane). The equation to solve is then

$$
\begin{cases}
\Delta u = 0, & x^2 + y^2 + z^2 < 1, \\
u = f, & x^2 + y^2 + z^2 = 1, \\
u|_{z=0^+} = u|_{z=0^-}, & \text{and} \quad \nu_1 \frac{\partial u}{\partial z}|_{z=0^+} = \nu_2 \frac{\partial u}{\partial z}|_{z=0^-}
\end{cases}
\tag{2.21}
$$

Following (2.7–2.8) the parity split is

$$
f_e(x, y, z) = \frac{1}{\kappa} \left(\frac{1}{\nu(x, y, -z)} f(x, y, z) + \frac{1}{\nu(x, y, z)} f(x, y, -z) \right),
\tag{2.22}
$$

$$
f_o(x, y, z) = \frac{1}{\kappa} \left(f(x, y, z) - f(x, y, -z) \right).
\tag{2.23}
$$

Next we solve (2.9), using the basis of solutions $\{r^n Y_n^m(\theta, \phi)\}_{n=0}^{\infty}$, where Y_n^m are the spherical harmonics [58]. These have the appropriate (relative to z, i.e.: θ) parity properties: Y_n^m is even when $(n + m)$ is even and Y_n^m is odd when $(n + m)$ is odd. Putting it all together, this yields

$$
u = u_e + \frac{1}{\nu} u_o = \sum_{n=0}^{\infty} \sum_{\substack{m=-n, \\ (m+n)=even}}^{n} a_n^m r^n Y_n^m(\theta, \phi) + \sum_{n=0}^{\infty} \sum_{\substack{m=-n, \\ (m+n)=odd}}^{n} b_n^m \frac{1}{\nu} r^n Y_n^m(\theta, \phi),
\tag{2.24}
$$

where, with $\zeta = \cos(\theta)$,

$$
a_n^m = \frac{4\pi (n + m)!}{(2n + 1)(n - m)!} \int_0^{2\pi} d\phi \int_{-1}^{1} d\zeta \, f_e(\theta, \phi) \, Y_n^m(\theta, \phi),
\tag{2.25}
$$

$$
b_n^m = \frac{4\pi (n + m)!}{(2n + 1)(n - m)!} \int_0^{2\pi} d\phi \int_{-1}^{1} d\zeta \, f_o(\theta, \phi) \, Y_n^m(\theta, \phi).
\tag{2.26}
$$

The expression above is analog for this 3D case of (2.18) for the 2D case. Finally note that, for an azimuthally symmetric f, the spherical harmonics collapse to Legendre polynomials, in which case

$$
u = \sum_{n=0, 2, 4, \ldots}^{\infty} a_n r^n P_n(\cos \theta) + \sum_{n=1, 3, 5, \ldots}^{\infty} b_n \frac{1}{\nu} r^n P_n(\cos \theta),
\tag{2.27}
$$

where P_n is the Legendre polynomials of order n. Again, note the unusual basis with the modes $\{r^n P_n\}_{n \text{ even}}^{\infty}$ and $\{\frac{1}{\nu} r^n P_n\}_{n \text{ odd}}^{\infty}$ — see Figure B-5 for plots of some of these eigenmodes. We point out that a similar basis appears in equation (10) of [28], while solving for the electric potential of dielectric hemispheres. However, the authors do not explained

why such a basis is complete, nor how it was obtained (possibly through a clever and judicious guess). This approach, unfortunately, is hard to generalize, and could easily lead to intractable algebra in more complex geometries, such as in the following example.

2.3.3   2D Wedge (Continuous Basis)

The wedge geometry is often used in the design of microfluidic devices, such as microfluidic pumps, actuators, and heat pipes [55, 40, 33, 32, 59, 54]. Most wedge-shaped microfluidic devices have liquid sitting at the bottom of a wedge, forming a meniscus interface with vapor above. One is often interested in the temperature of liquid and vapor, which satisfies a Laplace equation with jump conditions imposed at the phase boundary. These conditions typically involve temperature continuity, and a nonzero added heat flux arising from the latent heat of vaporization [44]. With this motivation, we consider the Laplace equation on an infinite 2D wedge, where the interface is placed at $r = 1$ — see Figure B-2b. To be precise, we take: $\Omega = \{(r, \theta) \mid 0 \leq \theta \leq \Phi, \, 0 < r < \infty\}$, where Φ is the wedge angle, Γ is the intersection of Ω with $r = 1$, $\Omega_1 = \{x \in \Omega \mid r < 1\}$, $\Omega_2 = \{x \in \Omega \mid r > 1\}$, and we use polar coordinates. The symmetry function is then

$$g(r, \theta) = \left(\frac{1}{r}, \theta\right). \tag{2.28}$$

The equation to be solved is [2]

$$\begin{cases} \Delta u = 0, & \text{in} \quad \Omega, \\ u = f_1(r) \ \text{at} \ \theta = 0, & \text{and} \quad u = f_2(r) \ \text{at} \ \theta = \Phi, \\ u|_{r=1^-} = u|_{r=1^+}, & \text{and} \quad \nu_1 \frac{\partial u}{\partial r}|_{r=1^-} = \nu_2 \frac{\partial u}{\partial r}|_{r=1^+}. \end{cases} \tag{2.29}$$

Note that, if $u^{(i)}$ satisfies this equation with $f_i = 0$, then $u = u^{(1)} + u^{(2)}$. Furthermore, the problems satisfied by the $u^{(i)}$ are equivalent via the transformation $\theta \to \Phi - \theta$. Thus, *without loss of generality, we assume $f_1 = 0$.* Dropping the subscript and superscript notations, we then have:

$$\begin{cases} \Delta u = 0, & \text{in} \quad \Omega, \\ u = 0 \ \text{at} \ \theta = 0, & \text{and} \quad u = f(r) \ \text{at} \ \theta = \Phi, \\ u|_{r=1^-} = u|_{r=1^+}, & \text{and} \quad \nu_1 \frac{\partial u}{\partial r}|_{r=1^-} = \nu_2 \frac{\partial u}{\partial r}|_{r=1^+}. \end{cases} \tag{2.30}$$

---

[2]Here there are no heat sources at the interface. In Section 2.4, we consider a case with a heat source produced by the latent heat of vaporization.

Next follow the procedure in (2.6–2.9), § 2.2. First a parity split on f, using (2.28),

$$f_e(r) = \frac{1}{\kappa}\left(\frac{1}{\nu(1/r)}f(r) + \frac{1}{\nu(r)}f(1/r)\right) \quad \text{and} \quad f_o(r) = \frac{1}{\kappa}\left(f(r) - f(1/r)\right). \qquad (2.31)$$

Then $u = u_e + \frac{1}{\nu}u_o$, where

$$\begin{cases} \Delta u_e = 0, & \text{in } \Omega, \\ u_e = 0, & \theta = 0, \\ u_e = f_e, & \theta = \Phi, \end{cases} \qquad \begin{cases} \Delta u_o = 0, & \text{in } \Omega, \\ u_o = 0, & \theta = 0, \\ u_o = f_o, & \theta = \Phi. \end{cases} \qquad (2.32)$$

Separation of variables yields the elementary solutions $r^{\pm\tilde{\alpha}}\sin(\tilde{\alpha}\theta)$ and $r^{\pm\tilde{\alpha}}\cos(\tilde{\alpha}\theta)$, where $\tilde{\alpha}$ is an arbitrary complex constant. Since we will need to expand the boundary data along the edge $\theta = \Phi$, with homogeneous boundary condition on the other edge, we select $\tilde{\alpha} = i\,\alpha$ purely imaginary — see note **2.7**. This leads to:[3]

$$\text{(a) } \cos(\alpha\,\log(r))\,\sinh(\alpha\,\theta) \quad \text{and} \quad \text{(b) } \sin(\alpha\,\log(r))\,\sinh(\alpha\,\theta). \qquad (2.33)$$

$$\text{(c) } \cos(\alpha\,\log(r))\,\cosh(\alpha\,\theta) \quad \text{and} \quad \text{(d) } \sin(\alpha\,\log(r))\,\cosh(\alpha\,\theta). \qquad (2.34)$$

The homogeneous boundary condition along $\theta = 0$ then excludes (c) and (d). Furthermore: the modes in (a) are even with respect to g, and the modes in (b) are odd. Hence we can use the cosine Fourier Transform to solve for u_e, and the sine Fourier Transform for u_e. This leads to the solution:

$$u_e = \int_{-\infty}^{\infty} \cos(\alpha\log(r))\sinh(\alpha\theta)\hat{f}_e(\alpha)d\alpha, \qquad (2.35)$$

$$u_o = \int_{-\infty}^{\infty} \sin(\alpha\log(r))\sinh(\alpha\theta)\hat{f}_o(\alpha)d\alpha, \qquad (2.36)$$

where

$$\hat{f}_e(\alpha) = \frac{1}{2\pi\sinh(\alpha\Phi)}\int_{-\infty}^{\infty}\cos(\alpha\log(r))f_e(r)d(\log(r)), \qquad (2.37)$$

$$\hat{f}_o(\alpha) = \frac{1}{2\pi\sinh(\alpha\Phi)}\int_{-\infty}^{\infty}\sin(\alpha\log(r))f_o(r)d(\log(r)). \qquad (2.38)$$

Of course, this only works if f_e and f_o are sufficiently "nice". For example, integrable:

$$\int_{-\infty}^{\infty}|f_e(r)|d\log(r) < \infty \quad \text{and} \quad \int_{-\infty}^{\infty}|f_o(r)|d\log(r) < \infty. \qquad (2.39)$$

---

[3]Here α is real and we use that $r^{\pm i\alpha} = \cos(\alpha\log(r)) \pm i\sin(\alpha\log(r))$.

Unfortunately, if f does not vanish for $r \to 0$ and $r \to \infty$ (something not unrealistic), this fails.[4] Below, in § 2.3.3.1, we show how to deal with a case where (2.39) fails.

Note 2.7. (Why $\tilde{\alpha}$ real is a bad idea). *One should resist the temptation to use $\tilde{\alpha}$ real. While this could lead to a discrete basis in θ (some type of Fourier Series), eigenfunction expansions of $f(r)$ in real powers of r lead to extremely ill-conditioned problems [56].* ♣

2.3.3.1 Renormalization, the case $f = r$

Situations of interest where (2.39) fails abound. We will not attempt to deal with all of them. Instead we will do an example that illustrates some of the available techniques. Specifically we consider the example $f = r$. The parity split in this case yields

$$f_e = \frac{1}{\kappa}\left(\frac{1}{\nu(1/r)}r + \frac{1}{\nu(r)}\frac{1}{r}\right) \quad \text{and} \quad f_o = \frac{1}{\kappa}\left(r - \frac{1}{r}\right) \tag{2.40}$$

The aim is now to solve (2.32) with the boundary conditions in (2.40). The problem for u_o can be solved by inspection

$$u_o = \frac{1}{\kappa}\left(r - \frac{1}{r}\right)\frac{\sin\theta}{\sin\Phi} \tag{2.41}$$

Notice that this solution is unbounded near $r = 0$. This singular behavior should be cancelled by a corresponding singular behavior in u_e, to render a final solution that is bounded near the origin. This suggests that we "renormalize" u_e by removing the (now known) unbounded term near the origin. Thus define:

$$\tilde{u}_e = u_e - \frac{1}{\nu_1\kappa}\frac{\sin\theta}{r\sin\Phi} - \frac{1}{\nu_1\kappa}\frac{r\sin\theta}{\sin\Phi}, \tag{2.42}$$

where the second subtracted term is to keep $\tilde{u}_e$ even with respect to g in (2.28). Then $\tilde{u}_e$ satisfies the same problem as u_e, but with f_e replaced by $\tilde{f}_e$, given by:

$$\tilde{f}_e = \frac{1}{\kappa}\left(\frac{1}{\nu_2} - \frac{1}{\nu_1}\right)r \text{ for } r < 1, \quad \text{and} \quad \tilde{f}_e = \frac{1}{\kappa}\left(\frac{1}{\nu_2} - \frac{1}{\nu_1}\right)\frac{1}{r} \text{ for } r > 1. \tag{2.43}$$

Note that $\tilde{f}_e$ satisfies (2.39). Thus we can write now $\tilde{u}_e$ using (2.35) (2.37). Then u follows from $u = u_e + (1/\nu)u_o$; i.e.: (2.6). Since $\tilde{f}$ is fairly simple, explicit calculations are possible,

---

[4]Note that the case $f \to c$ as $r \to 0$ or $r \to \infty$ (same constant c) is not a problem, as then we can subtract $u = (c/\Phi)\theta$ from the solution, and reduce the problem to the $f \to 0$ situation.

which yield the final answer:

$$u(r,\theta) = \begin{cases} \frac{r\sin\theta}{\sin\Phi} + \frac{2(\nu_1-\nu_2)}{\nu_1+\nu_2}\sum_{n=1}^{\infty}(-1)^n\frac{\sin(n\pi\theta/\Phi)}{n^2\pi^2/\Phi^2-1}r^{n\pi/\Phi}, & r < 1. \\[3mm] \frac{r\sin\theta}{\sin\Phi} + \frac{2(\nu_1-\nu_2)}{\nu_1+\nu_2}\sum_{n=1}^{\infty}(-1)^n\frac{\sin(n\pi\theta/\Phi)}{n^2\pi^2/\Phi^2-1}r^{-n\pi/\Phi}, & r > 1. \end{cases} \tag{2.44}$$

Figure B-6 shows the heat map from (2.44) for a particular choices of parameters. The solution vanishes as $r \to 0$. For large r, the contribution from the infinite sum goes to zero, so that u grows linearly in r. Further: at the interface $r = 1$, the infinite series satisfies the continuity condition term-by-term. On the other hand, the fluxes at $r = 1 - dr$ and $r = 1 + dr$, formally given by

$$\nu\partial_r u(r,\theta)|_{r=1} = \begin{cases} \frac{\nu_1\sin\theta}{\sin\Phi} + \frac{2\nu_1(\nu_1-\nu_2)}{\nu_1+\nu_2}\sum_{n=1}^{\infty}(-1)^n\frac{\sin(n\pi\theta/\Phi)}{n^2\pi^2/\Phi^2-1}(n\pi/\Phi), & r = 1 - dr, \\[3mm] \frac{\nu_2\sin\theta}{\sin\Phi} + \frac{2\nu_2(\nu_1-\nu_2)}{\nu_1+\nu_2}\sum_{n=1}^{\infty}(-1)^n\frac{\sin(n\pi\theta/\Phi)}{n^2\pi^2/\Phi^2-1}(-n\pi/\Phi), & r = 1 + dr, \end{cases} \tag{2.45}$$

are not equal term-by-term. This is related to the fact that convergence is absolute for (2.44), and conditional for (2.45). In fact (2.45) makes sense only in the L^2 sense, as the $r \to 1$ limit of the corresponding expressions for $r \neq 1$ (which converge absolutely). In § 2.3.3.2 we will show how to take these limits properly.

In the rest of this subsection we sketch the steps leading to (2.44).

The first step is to calculate the Fourier Transform of $\tilde{f}_e$, using (2.37).

$$\hat{\tilde{f}}_e(\alpha) = \frac{1}{2\pi\sinh(\alpha\Phi)}\int_{-\infty}^{\infty}\cos(\alpha\xi)\,\tilde{f}_e(r)d\xi = \frac{1}{2\pi\sinh(\alpha\Phi)}\int_{-\infty}^{\infty}\exp(i\alpha\xi)\tilde{f}_e(r)d\xi,$$

where $\xi = \log(r)$, and we use that $\int_{-\infty}^{\infty}\sin(\alpha\xi)\tilde{f}_e(r)d\xi = 0$ because $\tilde{f}_e$ is even with respect to ξ. Hence

$$\begin{aligned} \hat{\tilde{f}}_e(\alpha) &= \frac{(1/\nu_2 - 1/\nu_1)}{2\kappa\pi\sinh(\alpha\Phi)}\int_{-\infty}^{0}\exp(i\alpha\xi+\xi)d\xi + \frac{(1/\nu_2 - 1/\nu_1)}{2\kappa\pi\sinh(\alpha\Phi)}\int_{0}^{\infty}\exp(i\alpha\xi-\xi)d\xi \\ &= \frac{(1/\nu_2 - 1/\nu_1)}{2\kappa\pi\sinh(\alpha\Phi)}\left(\frac{1}{1+i\alpha} + \frac{1}{1-i\alpha}\right) = \frac{(1/\nu_2 - 1/\nu_1)}{\kappa\pi\sinh(\alpha\Phi)}\left(\frac{1}{1+\alpha^2}\right) \end{aligned}$$

Then, using (2.35),

$$\tilde{u}_e = \frac{(1/\nu_2 - 1/\nu_1)}{\kappa\pi}\int_{-\infty}^{\infty}\frac{\sinh(\alpha\theta)}{\sinh(\alpha\Phi)}\frac{\cos(\alpha\xi)}{1+\alpha^2}d\alpha = \frac{(1/\nu_2 - 1/\nu_1)}{\kappa\pi}\int_{-\infty}^{\infty}\frac{\sinh(\alpha\theta)}{\sinh(\alpha\Phi)}\frac{\exp(i\alpha\xi)}{1+\alpha^2}d\alpha,$$

where we once again the second equality exploits of the imaginary part of the integrand in the last integrand. This last expression can be transformed into a series using standard

residue calculations, which yield

$$
\tilde{u}_e = \begin{cases} \frac{(1/\nu_2 - 1/\nu_1)}{\kappa}\left(\frac{\sin\theta}{r\sin\Phi} + \frac{2}{\Phi}\sum_{n=1}^{\infty} \frac{\sin\left(\frac{n\pi\theta}{\Phi}\right)r^{-n\pi/\Phi}}{\frac{n^2\pi^2}{\Phi^2}-1}(-1)^n \right), & \text{for } r < 1. \\[3mm] \frac{(1/\nu_2 - 1/\nu_1)}{\kappa}\left(\frac{r\sin\theta}{\sin\Phi} + \frac{2}{\Phi}\sum_{n=1}^{\infty} \frac{\sin\left(\frac{n\pi\theta}{\Phi}\right)r^{n\pi/\Phi}}{\frac{n^2\pi^2}{\Phi^2}-1}(-1)^n \right), & \text{for } r > 1. \end{cases}
\tag{2.46}
$$

Finally, using this expression, (2.42), (2.41), and (2.6), we obtain (2.44).

2.3.3.2 Series Acceleration and Singularity Extraction

For $r = 1$ the infinite series in (2.44) converge (absolutely) like $O(1/n^2)$, which is *not too bad, but not great either.*[5] However, the series for the fluxes in (2.45) converges conditionally, with terms decaying like $1/n$. Attempting a direct summation of these series leads to a Gibbs' phenomena, with spurious oscillations and lack of convergence in the L^∞ norm — this is illustrated in Figure B-3, which also shows that the L^2 convergence is sublinear. The reason behind this bad behavior is the triple-line singularity in the solution at $(r, \theta) = (1, \Phi)$. Since *quantities like the fluxes across the interface are often the ones of primary physical interest*, this situation is not very satisfactory, and we need to accelerate the convergence of these series. As an added benefit this will also *serve to elucidate the nature of the triple-line singularity in the solution.*

To accelerate the convergence we substitute

$$
\frac{1}{n^2\pi^2/\Phi^2 - 1} = \frac{1}{n^2\pi^2/\Phi^2} + \frac{1}{(n^2\pi^2/\Phi^2)(n^2\pi^2/\Phi^2 - 1)}
$$

into (2.44). After some cumbersome, but straightforward, manipulations this results in

$$
u(r, \theta) =
$$
$$
\begin{cases} \frac{r\sin\theta}{\sin\Phi} + \frac{2\Phi^2(\nu_1-\nu_2)}{\pi^2(\nu_1+\nu_2)}Li_2\left(-re^{i\pi\theta/\Phi}\right) + \frac{2(\nu_1-\nu_2)}{\nu_1+\nu_2}\left(\sum_{n=1}^{\infty} \frac{(-1)^n \sin(n\pi\theta/\Phi)}{(n^2\pi^2/\Phi^2)(n^2\pi^2/\Phi^2-1)}r^{n\pi/\Phi} \right) \\[2mm] \text{for } r < 1, \\[4mm] \frac{r\sin\theta}{\sin\Phi} + \frac{2\Phi^2(\nu_1-\nu_2)}{\pi^2(\nu_1+\nu_2)}Li_2\left(-\frac{1}{r}e^{i\pi\theta/\Phi}\right) + \frac{2(\nu_1-\nu_2)}{\nu_1+\nu_2}\left(\sum_{n=1}^{\infty} \frac{(-1)^n \sin(n\pi\theta/\Phi)}{(n^2\pi^2/\Phi^2)(n^2\pi^2/\Phi^2-1)}r^{-n\pi/\Phi} \right) \\[2mm] \text{for } r > 1, \end{cases}
\tag{2.47}
$$

---

[5]For $r \neq 1$ the convergence is geometrical, and much better.

33

and

$$\nu \partial_r u(r,\theta)|_{r=1} =$$

$$\begin{cases} \frac{\nu_1 \sin\theta}{\sin\Phi} + \frac{2\nu_1 \Phi(\nu_1-\nu_2)}{\pi(\nu_1+\nu_2)} Li_1\left(-e^{i\pi\theta/\Phi}\right) + \frac{2\nu_1(\nu_1-\nu_2)}{\nu_1+\nu_2}\left(\sum_{n=1}^{\infty} \frac{(-1)^n \sin(n\pi\theta/\Phi)n}{(n\pi/\Phi)(n^2\pi^2/\Phi^2-1)}\right) \\[2mm] \text{for } r < 1, \\[2mm] \frac{\nu_2 \sin\theta}{\sin\Phi} + \frac{2\nu_2 \Phi(\nu_1-\nu_2)}{\pi(\nu_1+\nu_2)} Li_1\left(-e^{i\pi\theta/\Phi}\right) + \frac{2\nu_2(\nu_1-\nu_2)}{\nu_1+\nu_2}\left(\sum_{n=1}^{\infty} \frac{(-1)^n \sin(n\pi\theta/\Phi)}{(n\pi/\Phi)(n^2\pi^2/\Phi^2-1)}\right) \\[2mm] \text{for } r > 1. \end{cases} \quad (2.48)$$

Here we have introduced the polylogarithm functions of order $s = 1$ and $s = 2$, defined by:

$$Li_s(\zeta) := \sum_{n=1}^{\infty} \frac{\zeta^s}{n^s}. \quad (2.49)$$

The computation of polylogarithm functions is optimally implemented in standard software packages, such as: MATLAB, Mathematica, and Python.

The series in (2.47–2.48) converge absolutely, even for $r = 1$ — with n-th terms $O(n^{-4})$ and $O(n^{-3})$. Figure B-3 (c-d) illustrates the point, showing no spurious oscillation. Even with just 1 term, the overall accuracy increases to 3 digits, as shown in panel (c). Furthermore, now the L^2 error is $O(N^{-3})$, while the L^∞ error is $O(N^{-2})$.

2.4   The Poisson Equation with Nonzero Jumps at Interfaces

Here we show how to use the parity method, used to solve (2.4), to the Poisson equation with a non-zero source. We also show how to solve problems with a nonzero jump in the solution at the interface; and a nonzero added flux across the interface. As before, we assume the existence of a symmetry function g for the domain Ω with the interface Γ.

2.4.1 Solving the Poisson Equation

Adding a source function, $h(x)$, to (2.4), we would like to solve the following equation

$$\begin{cases} \Delta u = h, & \text{in } \Omega \\ u = f, & \text{on } \partial\Omega \\ [u]|_\Gamma = 0 \\ [\nu\nabla u \cdot \hat{n}]|_\Gamma = 0 \end{cases} \tag{2.50}$$

We follow the procedure laid out in Section 2.2 by first performing the parity splits of boundary data as in Equation (2.7) and (2.8). In addition, we also perform a parity split on the source function, h, as

$$h_e(x) = \frac{1}{\kappa}\left(\frac{1}{\nu(g(x))}h(x) + \frac{1}{\nu(x)}h(g(x))\right) \tag{2.51}$$

$$h_o(x) = \frac{1}{\kappa}\left(h(x) - h(g(x))\right) \tag{2.52}$$

Following the arguments in (2.13), we can deduce that $h_e + \frac{1}{\nu}h_o = h$. Then we end up with two slightly modified sub-problems compared with (2.9):

$$\begin{cases} \Delta u_e = h_e, & \text{in } \Omega \\ u = f_e, & \text{on } \partial\Omega \\ \Delta u_o = h_o, & \text{in } \Omega \\ u = f_o, & \text{on } \partial\Omega \end{cases} \tag{2.53}$$

As before, the solution to Equation (2.50) can be assembled as

$$u = u_e + \frac{1}{\nu}u_o \tag{2.54}$$

A line of arguments similar to those in Section 2.2 can be pursued to show that (2.54) solves (2.50). First, we show that $\Delta u = h$ on Ω_1 and Ω_2: over Ω_1, we have that $\Delta u = \Delta u_e + \frac{1}{\nu_1}\Delta u_o = h_e + \frac{1}{\nu_1}h_o = h$; over Ω_1, we have that $\Delta u = \Delta u_e + \frac{1}{\nu_2}\Delta u_o = h_e + \frac{1}{\nu_2}h_o = h$. Secondly, we see that $u = f$ on $\partial\Omega$ as per the arguments in (2.13). Thirdly, the same arguments in Equation (2.10) - (2.12) would apply to render that $[u]|_\Gamma = 0$ and $[\nu\nabla u \cdot \hat{n}]|_\Gamma = 0$.

2.4.2 A Nonzero Jump in Solution at Interface

We are now interested in solving Equation (2.4) with a nonzero flux b across the internal interface Γ

$$\begin{cases} \Delta u = 0, & \text{in } \Omega \\ u = f, & \text{on } \partial\Omega \\ [u]|_\Gamma = b \\ [\nu \nabla u \cdot \hat{n}]|_\Gamma = 0 \end{cases} \qquad (2.55)$$

To solve (2.55), we recall that the solution to a non-homogeneous problem can be decomposed into the sum of the homogeneous solution and a particular solution. Hence, we let $u = u^h + u^p$, where u^h satisfies Equation (2.4) and u^p satisfies the equation below

$$\begin{cases} \Delta u^p = 0, & \text{in } \Omega \\ u^p = 0, & \text{on } \partial\Omega \\ [u^p]|_\Gamma = b \\ [\nu \nabla u^p \cdot \hat{n}]|_\Gamma = 0 \end{cases} \qquad (2.56)$$

To solve Equation (2.56), we will once again transform the equation into two sub-problems. From that, we will show that the solution to one sub-problem can be used to construct the solution to the other sub-problem. We let u_1^p and u_2^p be the solution to Equation (2.56) in Ω_1 and Ω_2, respectively. We let $\partial\Omega_1$ and $\partial\Omega_2$ be the exterior boundaries of the sub-domains

Ω_1 and Ω_2. Then u_1^p and u_2^p satisfy the following system of equations

$$
\begin{cases}
\Delta u_1^p = 0, & \text{in } \Omega_1 \\[2mm]
u_1^p = 0, & \text{on } \partial\Omega_1 \\[2mm]
u_1^p = \frac{\nu_2}{\nu_1+\nu_2}b, & \text{on } \Gamma
\end{cases}
\tag{2.57}
$$

$$
\begin{cases}
\Delta u_2^p = 0, & \text{in } \Omega_2 \\[2mm]
u_2^p = 0, & \text{on } \partial\Omega_2 \\[2mm]
u_2^p = -\frac{\nu_1}{\nu_1+\nu_2}b, & \text{on } \Gamma
\end{cases}
\tag{2.58}
$$

$$
[\nu\nabla u^p \cdot \hat{n}] = 0, \text{ on } \Gamma
\tag{2.59}
$$

Note that $[u^p] = u_1^p - u_2^p = b$ on Γ, in agreement with the interface solution jump in Equation (2.56). On the first glance, the conditions imposed by Equations (2.57)-(2.59) are quite strict, as (2.59) over-determines the sub-problems in (2.57) and (2.58). However, we show that the solutions can be constructed using the symmetry function.

First we proceed to solve Equation (2.57), which is a stand-alone Laplace equation with Dirichlet boundary conditions, whose solution can be obtained using a standard method (e.g.: an analytical method such as separation of variables). Having obtained u_1^p, we claim that

$$
u_2^p(x) = -\frac{\nu_1}{\nu_2}u_1^p(g(x))
\tag{2.60}
$$

We shall demonstrate that Equation (2.60) satisfies (2.58) and (2.59). First since u_1^p is harmonic and g preserves the Laplace equation, u_2^p is also harmonic. Second, to show that $u_2^p = 0$ on $\partial\Omega_2$, we recall a key property of g: $g(\Omega_2) = \Omega_1$. Thus $g(\partial\Omega_2) = \partial\Omega_1$. Hence, if $x \in \partial\Omega_2$, then $g(x) \in \partial\Omega_1$, and therefore $u_2^p(x)|_{x\in\partial\Omega_2} = -\frac{\nu_1}{\nu_2}u_1^p(g(x))|_{g(x)\in\partial\Omega_1} = 0$. Third, to see that $u_2^p = -\frac{\nu_1}{\nu_1+\nu_2}b$, we use another property of the symmetry function: $g(x) = x$ for $x \in \Gamma$. Hence if $x \in \Gamma$, $u_1^p = \frac{\nu_2}{\nu_1+\nu_2}b$, and hence $u_2^p(x) = -\frac{\nu_1}{\nu_2}\frac{\nu_2}{\nu_1+\nu_2}b = -\frac{\nu_1}{\nu_1+\nu_2}b$, as expected. Finally, to show that (2.59) holds, we compute that $[\nu\nabla u^p \cdot \hat{n}]|_\Gamma = \nu_1\nabla u_1^p(x) \cdot \hat{n}_\Gamma + \nu_2\frac{\nu_1}{\nu_2}\nabla u_1^p(g(x)) \cdot \hat{n}_\Gamma = 0$, where we use the fact that

$$
\nabla u_1^p(g(x)) \cdot \hat{n}|_\Gamma = -\nabla u_1^p(x) \cdot \hat{n}|_\Gamma
\tag{2.61}
$$

Here is the proof of Equation (2.61)

Proof. let A be the Jacobian of g and realize that it is sufficient to prove $A\hat{n}|_\Gamma = -\hat{n}$. This is because by the chain rule, $\nabla u_1^p(g(x)) = \nabla_g u_1(g)A$ (here gradient can be interpreted as a row vector). To show that $A\hat{n}|_\Gamma = -\hat{n}$, we pursue the following argument: first, because g is conformal, the Jacobian A would preserve angles, which means that if $\hat{t}$ represents a tangent unit vector at Γ, then $A\hat{n}$ is orthogonal to $A\hat{t}$. Next we shall use two facts that we will show later: (a) $A\hat{t} = \hat{t}$ and (b) over Γ, $A^2 =$ identity matrix. Because of (a), $A\hat{n}$ is also orthogonal to $\hat{t}$, which implies that $A\hat{n}$ is proportional to $\hat{n}$. Secondly, because of (b), $A\hat{n}|_\Gamma = \pm\hat{n}$. The fact that g has to map the sub-domain from one side of Γ to the other rules out the possibility that $A\hat{n}|_\Gamma = +\hat{n}$, forcing $A\hat{n}|_\Gamma = -\hat{n}$.

Lastly, to prove (a), let $z(s)$ be any arbitrary curve on Γ. Then $g(z(s)) = z(s)$. Hence $\frac{dg}{ds} = z'(s)$, which renders any tangent unit vector invariant under the Jacobian matrix multiplication. To prove (b), we know for a fact that $A(g(z))A(z) =$ identity matrix, for all $z \in \Omega$. Now choose $z \in \Gamma$ and we know that $g(z) = z$. This complete the proof. $\square$

2.4.3 A Nonzero Flux at Interface

A nonzero flux at the interface can arise in a number of physical scenarios, such as latent heat for evaporation. Mathematically, a nonzero term, w, will be added to the flux condition in Equation (2.4) to render:

$$
\begin{cases}
\Delta u = 0, & \text{in } \Omega \\
u = f, & \text{on } \partial\Omega \\
[u]|_\Gamma = 0 \\
[\nu \nabla u \cdot \hat{n}]|_\Gamma = w
\end{cases}
\tag{2.62}
$$

As before, we let $u = u^h + u^p$, where u^h is the solution to (2.4) and the particular solution u^p satisfies the following problem

$$\begin{cases} \Delta u^p = 0, & \text{in } \Omega \\ u^p = 0, & \text{on } \partial\Omega \\ [u^p]|_\Gamma = 0 \\ [\nu\nabla u^p \cdot \hat{n}]|_\Gamma = w \end{cases} \tag{2.63}$$

Similar to the previous section, we let u_1^p and u_2^p be the solution to Equation (2.63) in Ω_1 and Ω_2, respectively, with $\partial\Omega_1$ and $\partial\Omega_2$ as the exterior boundaries of the sub-domains. Then u_1^p and u_2^p can be decomposed into the following two coupled sub-problems:

$$\begin{cases} \Delta u_1^p = 0, & \text{in } \Omega_1 \\ u_1^p = 0, & \text{on } \partial\Omega_1 \\ \nabla u_1^p \cdot \hat{n} = \frac{w}{\nu_1+\nu_2}, & \text{on } \Gamma \end{cases} \tag{2.64}$$

$$\begin{cases} \Delta u_2^p = 0, & \text{in } \Omega_2 \\ u_2^p = 0, & \text{on } \partial\Omega_2 \\ \nabla u_2^p \cdot \hat{n} = -\frac{w}{\nu_1+\nu_2}, & \text{on } \Gamma \end{cases} \tag{2.65}$$

$$u_1^p = u_2^p, \text{ on } \Gamma \tag{2.66}$$

To solve this over-determined coupled system of equations, we first solve Equation (2.64), which on its own is a Laplace equation with a Robin boundary condition. Having obtained u_1^p, we claim that $u_2^p(x) = u_1^p(g(x))$. To see that this construction of $u_2^p(x)$ satisfies (2.65) and (2.66), we pursue a similar line of arguments as before. First since u_1^p is harmonic and g is Laplace preserving, u_2^p is also harmonic. Second, to show that $u_2^p = 0$ on $\partial\Omega_2$, we note that $g(\partial\Omega_2) = \partial\Omega_1$, thus if $x \in \partial\Omega_2$, then $g(x) \in \partial\Omega_1$, whence $u_2^p(x)|_{x\in\partial\Omega_2} = u_1^p(g(x))|_{g(x)\in\partial\Omega_1} = 0$. Third, to see that the normal derivative of u_2^p is $-\frac{w}{\nu_1+\nu_2}$ at the interface, we just have to invoke Equation (2.61). Finally, to show Equation (2.66), we simply note that $g(x) = x$ for $x \in \Gamma$.

2.5 On the Symmetry Function g

Recall from Section 2.2 that a symmetry function enables the use of the PSM in interfacial problems by mapping the two sub-domains onto each other, while preserving a Laplace equation. In this section, we shall give a mathematically more detailed framework for symmetry functions. The key questions we would like to address in this section are: (1) under what condition does a mapping preserve the Laplace equation? and (2) what are the possible geometries for which a symmetry function exists, and thereby where the PSM can be applied?

2.5.1 Laplace-Preserving Transformation

Question (1) can be first addressed in the generic setting. Mathematically (1) can be phrased as the following: if we let $\vec{x} \to \vec{\xi} = g(x) : X \to \Xi$ for $X, \Xi \subset \mathbb{R}^d$ be given. If $u(\xi)$ is harmonic in Ξ, what are the restrictions on g such that $v = v(x) = u(g(x))$ is also harmonic?

$$\text{We claim that the following conditions are necessary and sufficient} \qquad (2.67)$$

1. Each of the Cartesian coordinate of $g = \{g_d\}$ is harmonic

2. Let $A = A(x)$ be the Jacobian of g. Then there exists a scalar function $r = r(x) > 0$ such that $A = rO$ where O is an orthogonal matrix.

The proof of Claim (2.67) is the following

Proof. First Item 1 is necessary. For any constants $\{u_n\}$, $u = \sum u_n \xi_n$ is harmonic. Hence, $v = \sum u_n g_n$ is harmonic.

Secondly Item 2 is necessary. Let $H = H_{nm}$ be a constant and arbitrary symmetric matrix with zero trace. Then $u = \vec{\xi}^T H \vec{\xi}$ is harmonic. Then $v = \vec{g}^T H \vec{g} = \sum g_n H_{nm} g_m$ is harmonic. Thus, using Item I, we get that $0 = \Delta v = Tr\left(2A^T H A\right)$. But since H is arbitrary, we can take $H_{nm} = \delta_{np}\delta_{mq} + \delta_{nq}\delta_{mp}$, where $p \neq q$ and δ_{ij} is the Kronecker delta. This yields $0 = \sum_l A_{pl} A_{ql}$, that is the rows of A are orthogonal. Next we take $H_{nm} = \delta_{np}\delta_{mp} - \delta_{nq}\delta_{mp}$, where $p \neq q$. This then yields $0 = \sum_l A_{pl} A_{pl} - A_{ql} A_{ql}$, that is the rows of A all have the same length. Let this length be $r = r(\vec{x})$.

Thirdly, Item 1 and 2 are sufficient, which can be shown via direct computation:

- $v_{1;m} = u_{1;n}g_{n;m}$, where the index before the semicolon indicates a vector Cartesian component and the indices after the semicolon indicate partial derivatives. Here we also use the Einstein's summation notation

- $\Delta v = v_{1;nm} = u_{1;np}g_{n;m}g_{p;m} + u_{1;n}g_{n;mm} = u_{1;np}A_{nm}A_{pm} = ru_{1;nn} = r\Delta u$

Here for the third equality we use Item 1 and the definition of A. For the fourth equality we use Item 2 $\qquad\square$

2.5.2 Symmetry Functions in 2D

We claim that (2.67) has several significant implications for the symmetry functions in $2D$. In $\mathbb{R}^2$, we can use the language of complex analysis and write $z = x + iy$ and $g = u + iv$. We denote the complex conjugate of z as $\bar{z} = x - iy$. Then Item 1 of the Claim (2.67) implies that u and v are harmonic, while Item 2 of the Claim implies that either $\nabla v = i\nabla u$ (Cauchy-Riemann condition) or $\nabla v = -i\nabla u$. It follows that in $2D$, the functions that preserve the Laplace equation take the form $g(z) = f(z)$ or $g(z) = f(\bar{z})$, where f is analytic. Note that the two forms of $f(z)$ and $f(\bar{z})$ cannot coexist in a connected set. Otherwise, it would require the determinant of A in Item 2 of Claim (2.67) to vanish across the boundary between the regions of validity of each form. But an analytic function with a dense set of vanishing derivatives is identically zero. Finally, recall that as mentioned in Section 2.2, a symmetry function g maps one side of the interface Γ to the other side and must satisfy $g(z) = z$, for any $z \in \Gamma$. Therefore, a symmetry function cannot take the analytic form $g(z) = f(z)$, or else $g \equiv z$ and it would not be able to map the sub-domains from one side of Γ to the other. Hence, only the "anti-analytic" form of $g = f(\bar{z})$ is allowed.

2.5.2.1 Admissible 2D Interfaces

Having found the general form of the Laplace preserving symmetry function, we would like to leverage these functions to characterize the geometries of sub-domains and the shapes of interfaces Γ. The first attempt is enabled by the Riemann mapping theorem, which dictates that any open, connected subset of the complex plane and the unit disk can be mapped onto each other. Therefore, the strategy is to trace the mapping of the real axis from the unit disk to the open subset. Let Ω be an open and connected subset in $\mathbb{C}$. Then by the Riemann mapping theorem, there exists a bijective mapping h that maps the unit

disk in $\mathbb{C}$ to Ω. Let h^{-1} denote the inverse transformation. Then an appropriate symmetry function would be

$$g(z) = h\left(\overline{h^{-1}(z)}\right) \tag{2.68}$$

This symmetry function would trace an interface Γ given by $h(s)$ in Ω, where $-1 < s < 1$. In doing so, we would be able to collapse any interfacial problem over Ω with the interface Γ to the problem of a $2D$ sphere in Section 2.3.1.

A powerful theoretical statement nonetheless, the Riemann mapping theorem does not give a recipe for finding the mapping function h for a general domain Ω. To demonstrate the family of internal boundaries Γ traced by Equation (2.68) , we shall work with the domain of $\Omega =$ the unit disk in $\mathbb{C}$ where the mapping function h between the unit disk and itself is known to take the form of ([53])

$$h(z) = e^{i\theta} \frac{z - \alpha}{1 - \bar{\alpha}z} \tag{2.69}$$

where θ is a real number and $|\alpha| < 1$. The the family of Γ can be described as

the intersection with the unit disk of the family of circles with radius
$$R = \sqrt{y_0^2 - 1} \text{ centered at } -iy_0, where 1 < y_0 \leq \infty \tag{2.70}$$

The proof of Claim (2.70) goes as follows

Proof. The prefactor $e^{i\theta}$ in Equation (2.69) represents a rotation and can be reset to $\theta = 0$. In this way, we can write $w = x + iy$ and $\alpha = a + ib$. Here we assume that $b \neq 0$ since otherwise, $h(s) = (s - a)/(1 - as)$, which makes Γ the diagonal $[-1, 1]$.

Following the properties of bilinear mappings, we know that Γ is the intersection of circles. To locate the exact traces of circles for the mapping, we first note that since Γ is given by $w = x + iy = \frac{s - \alpha}{1 - \bar{\alpha}s}$, we can write $s = h^{-1}(w) = \frac{w + \alpha}{1 + \bar{\alpha}w}$, which enables us to write $s = h^{-1}(x + iy)$ and so

$$s = \frac{x + iy + \alpha}{1 + \bar{\alpha}(x + iy)} \tag{2.71}$$

$$= \frac{\beta + i(b + 2abx + (1 + b^2 - a^2)y + b(x^2 + y^2)))}{\rho} \tag{2.72}$$

where $\rho = |1 + \bar{\alpha}(x + iy)|^2$ and $\beta = (x + a)(1 + ax + by) + (y + b)(ay - bx)$. Since s is real, the equation of the circles must be

$$b + 2abx + (1 + b^2 - a^2)y + b(x^2 + y^2) = 0 \tag{2.73}$$

$$(x + a)^2 + \left(y + \frac{1 + b^2 - a^2}{2b}\right)^2 = \frac{(1 - a^2 - b^2)^2}{4b^2} \tag{2.74}$$

This is a circle of radius $R = \frac{1 - a^2 - b^2}{2|b|}$ centered at $\tilde{x}_0 = -a$ and $\tilde{y}_0 = -(1 + b^2 - a)/(2b)$. It is now easy to check that $R^2 + 1 = \tilde{x}_0^2 + \tilde{y}_0^2$. hence, if we define $y_0 = \sqrt{x_0^2 + y_0^2} = \sqrt{R^2 - 1}$, the circle can be rotated into the form in Equation (2.70) by an appropriate choice of θ in Equation (2.69). The range of $1 < y_0 \leq \infty$ follows because $0 < R < \infty$, with infinity corresponding to $b = 0$ □

Figure B-7 visualizes the family of the $\Gamma-$curves as controlled by the parameter y_0.

2.5.2.2 Symmetry Functions in 3D

The conditions for functions that preserve the Laplace equations are known to be extremely restrictive for $d > 2$. There are not a lot of examples of maps that satisfy them, such as the example in Section 2.3.2. Thus in its present form the parity transformation method is of limited use in dimensions higher than 2.

2.6 Conclusion

In this chapter we introduced the Parity Split Method (PSM), an analytical method for tackling elliptic PDE over domains with an internal interface, endowed with a symmetry function g. In these situations the PSM replaces original problem by (simpler and less singular) sub-problems with no interface, which can be solved using standard techniques. In particular, for some geometries, separation of variables can be used.

Note that: (i) In general, when an internal interface meets the boundary of a domain, the solutions have singularities "triple-point singularities". The PSM gives a road for (analytically) untangle the nature of these singularities. (ii) The solutions to the PMS sub-problems are symmetric (odd and even) relative to the symmetry function. This is an automatic consequence of the PSM. However, when separation of variables is possible, whether or not the PMS gives rise to "eigenmodes" for the original problem depends on the eigenmodes for the problems without an interface splitting into odd and even. This may not happen, but the PMS still works.

The method was first illustrated using the Laplace equation, with homogeneous jump conditions at the interface, over several domains: disk (2D), sphere (3D), and wedge (2D). Analytical solutions and novel eigenmode expansions resulted in each case. Next the PSM was used to solve the Poisson equation, including sources at the interface's jump conditions. Finally the conditions under which a symmetry function exists were explored, including which types of sets admit them.

As a final point: the PSM can be applied to elliptic PDE other than Laplace or Poisson. For example the biharmonic equation and the Stokes flow equations — see Chapter 4.

Chapter 3

Evaporation in a V-shaped Channel with Arbitrary Thermal Driving

3.1   Problem Statement and Mathematical Model

We consider a V-shaped channel of length $\tilde{L}_l$, side depth $\tilde{L}_w$, and opening angle Φ — see Figure B-8a. Heat is applied to the channel through the sides, with the temperature on the two sides prescribed and uniform along the channel length $\tilde{L}_l$. The bottom V-tip of the channel is at temperature T_0, while the far-field temperature is a constant, T_∞. A liquid of density ρ_1 and heat diffusivity ν_1 fills the channel up to a height $\tilde{a}$. The liquid undergoes quasi-static evaporation to the vapor region above with density ρ_2, heat diffusivity ν_2, and vapor diffusivity D. At the liquid-vapor interface, we assume that the vapor concentration is at saturation, and approximate the saturation concentration as a linear function of the temperature,[1] $C_{sat} = C_{sat}(\tilde{T})$. In the far field, we assume that the vapor concentration reaches the value HC_∞, where $0 \le H \le 1$ is the relative ambient humidity and $C_\infty = C_{sat}(T_\infty)$. Furthermore, we assume that the contact angle for the liquid-vapor interface with the wedge sides is 90° (half way between the hydrophobic and hydrophilic states). Then, in the small scale limit, this last assumption and surface tension allows us to approximate the interface as a cylindrical and centered at the tip of the wedge. Finally, we assume $\tilde{L}_l \gg \tilde{L}_w$, which (together with the prescribed uniform temperature along the channel length) allows us to reduce the problem to a two-dimensional wedge — see Figure B-8b.

---

[1]Assume temperature variations throughout the device small enough to justify this approximation.

The objective is to compute the temperature, $\tilde{T}$, throughout the device, as well as the vapor concentration, $\tilde{C}$. With these functions we can then obtain other quantities of interest, such as the vapor flux through the interface and the evaporative lifetime for the liquid.

3.1.1 Imposing Conditions at "Infinity" in $2D$

Far field conditions for the Laplace equation are reasonable for many $3D$ problems. However, in $2D$ one needs to exercise care when imposing conditions at "infinity", so as to avoid "Stokes paradox" like situations. To this end, we extend the sides of the triangular domain beyond the length $\tilde{L}_w$, so as to obtain an infinite wedge. Then we convert the far-field conditions for the temperature and concentration into boundary conditions along the extended edges of the wedge.

3.1.2 Mathematical Model

We now formalize the problem mathematically. Let $(\tilde{x}, \tilde{y})$ denote Cartesian coordinates, with origin at the wedge tip, and the x-positive axis along the right edge of the wedge. Let $(\tilde{r}, \tilde{\theta})$ be the corresponding polar coordinates. Then the wedge is represented by the domain $\Omega = \{(\tilde{r}, \tilde{\theta}) \mid 0 \leq \theta \leq \Phi\}$ — see Figure B-9a). The set Ω, in turn, is split by an interface at $\tilde{r} = \tilde{a}$, where $\tilde{r} < \tilde{a}$ (resp. $\tilde{r} > \tilde{a}$) is the region occupied by the liquid (resp. vapor).

The temperature is given, $\tilde{T} = \tilde{T}_b(r)$, along the boundaries, $\theta = 0$, Φ. Throughout this chapter we consider two types of temperature profiles along the sides: constant and linearly decreasing. While the constant temperature takes the form of $\tilde{T}_b(r) = T_\infty$, the linearly decreasing profile, $\tilde{T}_b = \tilde{T}_d$, is given by

$$\tilde{T}_d(\tilde{r}) = -\frac{T_0 - T_\infty}{\tilde{L}_w}\tilde{r} + T_0 \text{ for } \tilde{r} \leq \tilde{L}_w \quad \text{and} \quad \tilde{T}_d(\tilde{r}) = T_\infty \text{ for } \tilde{r} \geq \tilde{L}_w. \qquad (3.1)$$

This, effectively, translates the far-field conditions for the temperature, to conditions along the boundary. Similarly, for the concentration $\tilde{C}$ we impose mixed boundary condition along $\theta = 0$, Φ. Specifically: for $\tilde{r} < \tilde{L}_w$, $\tilde{C}$ we impose a no-flux boundary condition, $\frac{\partial \tilde{C}}{\partial \theta} = 0$ (no penetration along the solid boundaries of the wedge). On the other hand, for $\tilde{r} > \tilde{L}_w$, we impose the Dirichlet condition $\tilde{C} = HC_\infty$ — the concentration reaches the humidity-adjusted saturation level above the solid edge of the wedge.

At the interface $\tilde{r} = \tilde{a}$, we impose continuity in both the temperature and heat flux.[2]

---

[2]Heat flux continuity means: neglect the latent heat of evaporation; consistent with slow evaporation.

Furthermore, we assume that the concentration at the interface has the saturation level corresponding to the temperature there. That is:

$$\tilde{C}|_{\tilde{r}=\tilde{a}}(\tilde{T}) = C_{sat}(\tilde{T}) = \frac{dC_{sat}}{d\tilde{T}}|_{T_\infty}(\tilde{T} - T_\infty) + C_\infty, \tag{3.2}$$

where (as explained earlier) we linearize C_{sat}.

Finally, we consider only (slow) quasi-static evaporation, so that both temperature and concentration can be approximated as as satisfying the Laplace equation. Let $\tilde{\Delta}$ denote the (dimensional) Laplace operator in $2D$. Then the mathematical problem to be solved is:

$$
\begin{cases}
\tilde{\Delta}\tilde{T} = 0 & \text{in } \Omega, \\
\tilde{T} = \tilde{T}_b(\tilde{r}) & \text{on } \theta = 0, \Phi, \\
\tilde{T}|_{\tilde{r}=\tilde{a}^+} = \tilde{T}|_{\tilde{r}=\tilde{a}^-}, \\
\nu_1 \partial_{\tilde{r}}\tilde{T}|_{\tilde{r}=\tilde{a}^+} = \nu_2 \partial_{\tilde{r}}\tilde{T}|_{\tilde{r}=\tilde{a}^-},
\end{cases}
\quad
\begin{cases}
\tilde{\Delta}\tilde{C} = 0 & \text{for } \tilde{r} > \tilde{a}, \\
\frac{\partial \tilde{C}}{\partial \theta} = 0 & \text{on } \theta = 0, \Phi; \tilde{r} < \tilde{L}_w, \\
\tilde{C} = H C_{sat}(T_\infty), & \text{on } \theta = 0, \Phi; \tilde{r} > \tilde{L}_w, \\
\tilde{C} = \frac{dC_{sat}}{d\tilde{T}}|_{T_\infty}(T - T_\infty) + C_\infty & \text{on } \tilde{r} = \tilde{a}.
\end{cases}
\tag{3.3}
$$

3.1.3   Non-Dimensionalization

We non-dimensionalize as follows: lengths using a_0, the initial radius of the liquid interface; temperature using $\eta_T \tilde{L}_w$, where $\eta_T = (T_0 - T_\infty)/\tilde{L}_w$ is the thermal gradient parameter;[3] concentration using the characteristic concentration $C_c = C_{sat}(T_0) - HC_\infty$; and time using a characteristic lifetime for the droplet $t_c = a_0^2 \rho_1/(C_\infty D)$.[4] Thus we define the adimensional quantities: droplet size a, wedge side length L_w, temperature T, concentration C, lifetime t, cartesian coordinates (x, y), and polar coordinates (r, θ), via the formulas:

$$\tilde{a} = a\, a_0, \ \ \tilde{L}_w = L_w\, a_0, \ \ (\tilde{x}, \tilde{y}) = (\tilde{x}, \tilde{y})\, a_0, \ \ \tilde{r} = r\, a_0, \tag{3.4}$$

$$\tilde{T} = \eta_T\, \tilde{L}_w\, T + T_\infty, \tag{3.5}$$

$$\tilde{C} = C_c\, C + H\, C_\infty, \tag{3.6}$$

$$\tilde{t} = t_c\, t. \tag{3.7}$$

---

[3]Note that the thermal gradient is "easy" to control in an experiment: change T_∞.
[4]Note that our 2D "droplet" is actually an elongated bead of liquid.

Then the governing equations (3.3) take the dimensionless form:

$$
\begin{cases}
\Delta T = 0 & \text{in } \Omega, \\[4pt]
T = T_b(r) & \text{on } \theta = 0,\, \Phi, \\[4pt]
T|_{r=a^+} = T|_{r=a^-}, \\[4pt]
\partial_r T|_{r=a^+} = \frac{\nu_2}{\nu_1}\,\partial_r T|_{r=a^-},
\end{cases}
\qquad
\begin{cases}
\Delta C = 0 & \text{for } r > a, \\[4pt]
\frac{\partial C}{\partial \theta} = 0 & \text{on } \theta = 0,\, \Phi;\ r < L_w, \\[4pt]
C = 0 & \text{on } \theta = 0,\, \Phi;\ r > L_w, \\[4pt]
C = \beta T + \gamma & \text{on } r = a,
\end{cases}
\tag{3.8}
$$

where $\beta = \frac{dC_{sat}}{d\tilde{T}}\big|_{T_\infty}\frac{\eta_T \tilde{L}_w}{C_c}$ and $\gamma = \frac{C_\infty - H\,C_\infty}{C_c}$. For the constant temperature b.c. case, $T_b(r) = 0$, while the linearly decreasing profile $T_b = T_d(r)$ becomes

$$
T_d(r) =
\begin{cases}
-\frac{1}{L_w} r + 1 & \text{for } r < L_w. \\[8pt]
0 & \text{for } r > L_w.
\end{cases}
\tag{3.9}
$$

3.1.4 Justification of the Quasi-static Approximation

Equation (3.3), and its adimensional counterpart (3.8), result from a quasi-static approximation for the temperature and concentration problems. This approximation makes sense only if the lifetime of the droplet is much larger than the typical relaxation time to equilibrium for the temperature and concentration. Furthermore (to compute an accurate lifetime), it must be that during the time it takes the mass diffusion to reach steady state, the mass loss is small compared with the total mass of the liquid. Calculations showing when these two conditions are satisfied can be found in Appendix D. Note that some of these calculations borrow from the methods introduced in the later sections of this chapter.

3.2 Solution via the PSM and Complex Analysis

Our aim is to provide a completely analytical approach to solving (3.8). To do so we first solve for the temperature, which does not depend on the concentration. We consider two cases: constant and linearly decreasing temperature along the boundaries — see (3.9). While the constant temperature case has the trivial solution $T \equiv 0$,[5] the linearly decreasing b.c. requires using the Parity Split Method (PSM), introduced in Chapter 2. Once this is done we can use the thus computed value of the temperature at the interface to solve for the concentration — which requires the use of several complex variable arguments (one of

---

[5] Note that the concentration is not trivial in this case.

which, as far as we know, is novel).

3.2.1 Temperature PROBLEM with Linearly Decreasing B.C.

The aim here is to solve the temperature problem in (3.8), with the b.c. in (3.9). Specifically:

$$
\begin{cases} \Delta T & = 0 \quad & \text{in } \Omega, \\ T & = T_d(r) \quad & \text{on } \theta = 0, \, \Phi, \end{cases}
\qquad
\begin{cases} T|_{r=a+} & = T|_{r=a-}, \\ \partial_r T|_{r=a+} & = \frac{\nu_2}{\nu_1} \partial_r T|_{r=a-}. \end{cases}
\tag{3.10}
$$

To solve this problem, we first solve the following auxiliary problem

$$
\begin{cases} \Delta v & = 0 \quad & \text{in } \Omega, \\ v & = 0 \quad & \text{on } \theta = 0, \\ v & = T_d(r) \quad & \text{on } \theta = \Phi, \end{cases}
\qquad
\begin{cases} v|_{r=a+} & = v|_{r=a-}, \\ \partial_r v|_{r=a+} & = \frac{\nu_2}{\nu_1} \partial_r v|_{r=a-}. \end{cases}
\tag{3.11}
$$

Then

$$
T(r, \, \theta) = v(r, \, \theta) + v(r, \, \Phi - \theta)
\tag{3.12}
$$

Next we rescale lengths in (3.11), using a. This yields the modified problem

$$
\begin{cases} \Delta v_a & = 0 \quad & \text{in } \Omega, \\ v_a & = 0 \quad & \text{on } \theta = 0, \\ v_a & = T_d(r) \quad & \text{on } \theta = \Phi, \end{cases}
\qquad
\begin{cases} v_a|_{r=1+} & = v_a|_{r=1-}, \\ \partial_r v_a|_{r=1+} & = \frac{\nu_2}{\nu_1} \partial_r v_a|_{r=1-}, \end{cases}
\tag{3.13}
$$

where

$$
v(r, \, \theta) = v_a(r/a, \, \theta).
\tag{3.14}
$$

Below we solve (3.13) using the Parity Split Method developed in Chapter 2.

3.2.1.1 The Parity Split Method (PSM)

The PSM splits a problem like (3.13), with an internal boundary, into sub-problems without it. Once the internal boundary is eliminated, standard analytical methods[6] (such as separation of variables) can be applied to obtain the solutions to the sub-problems. In this section, we shall follow the PSM provided in Chapter 2 to solve (3.13).

First, using the symmetry function $r \to \frac{1}{r}$, we perform the parity split of the boundary

---

[6]Here we concentrate on analytical solutions, but the sub-problems could also be solved numerically.

data, $T_d(r)$, into even and odd functions

$$T_{d,e} = \frac{1}{\kappa}(\mu(1/r)T_d(r) + \mu(r)T_d(1/r)) \tag{3.15}$$

$$T_{d,o} = \frac{1}{\kappa}(T_d(r) - T_d(1/r)) \tag{3.16}$$

where κ and $\mu(r)$ are defined as

$$\kappa = 1 + \frac{\nu_1}{\nu_2} \tag{3.17}$$

$$\mu(r) = \begin{cases} 1, & r < 1 \\ \frac{\nu_1}{\nu_2}, & r > 1 \end{cases} \tag{3.18}$$

Note that $T_{d,e}$ and $T_{d,o}$ are even and odd, respectively, relative to the symmetry function. Next we define the following sub-problems in $v_{a,e}$ and $v_{a,o}$

$$\begin{cases} \Delta v_{a,e} = 0, & \text{in } \Omega \\ v_{a,e} = 0, & \text{on } \theta = 0 \\ v_{a,e} = T_{d,e}(r), & \text{on } \theta = \Phi \end{cases}, \quad \begin{cases} \Delta v_{a,o} = 0, & \text{in } \Omega \\ v_{a,o} = 0, & \text{on } \theta = 0 \\ v_{a,o} = T_{d,o}(r), & \text{on } \theta = \Phi \end{cases} \tag{3.19}$$

Note that the sub-problems have no internal boundary conditions. From here, we can write v_a as

$$v_a = v_{a,e} + \mu(r)v_{a,o} \tag{3.20}$$

The PSM claims that v_a defined in Equation (3.20) satisfies exactly Equation (3.13), including both the internal conditions at $r = a$ and external boundary conditions at $\theta = 0, \Phi$.

To solve the sub-problems in Equation (3.19), we again refer to Section 2.3.3 of Chapter 2 and use the recommended spectral eigenfunctions: $\sinh(\alpha\theta), \sin(\alpha \log r)$, and $\cos(\alpha \log r)$, where $-\infty < \alpha < \infty$. We observe only $\sinh(\alpha\theta)$ is needed because of the zero boundary condition at $\theta = 0$. Also, note that $\sin(\alpha \log r)$ and $\cos(\alpha \log r)$ are odd and even, respectively, relative to the symmetry function $r \to \frac{1}{r}$. We shall use the two functions according to the parity of the boundary conditions. We are now ready to write the solutions to Equation

(3.19)

$$v_{a,e} = \int_{-\infty}^{\infty} \cos(\alpha \log r) \sinh(\alpha\theta) \hat{v}_{a,e}(\alpha) d\alpha \tag{3.21}$$

$$v_{a,o} = \int_{-\infty}^{\infty} \sin(\alpha \log r) \sinh(\alpha\theta) \hat{v}_{a,o}(\alpha) d\alpha \tag{3.22}$$

where $\hat{v}_{a,e}$ and $\hat{v}_{a,o}$ can be *formally* computed by the corresponding boundary data $T_{d,e}$ and $T_{d,o}$ using Fourier transform with respect to the variable $\log r$

$$\hat{v}_{a,e} = \frac{1}{2\pi \sinh(\alpha\Phi)} \int_{-\infty}^{\infty} \cos(\alpha \log r) T_{d,e}(r) d(\log r) \tag{3.23}$$

$$\hat{v}_{a,o} = \frac{1}{2\pi \sinh(\alpha\Phi)} \int_{-\infty}^{\infty} \sin(\alpha \log r) T_{d,o}(r) d(\log r) \tag{3.24}$$

Notice that we say *formally* because Equation (3.23) and (3.24) would make sense if and only if $T_{d,e}$ and $T_{d,o}$ are integrable with respect to $\log r$. As a matter of fact, $T_{d,e}$ and $T_{d,o}$ defined in Equation (3.15) are not $\log r$−integrable. Therefore, to make sense of Equation (3.23) and (3.24), we would need to go back to the sub-problems (3.19) and massage the boundary conditions in order to "renormalize" the integrals in (3.23) and (3.24). We shall borrow the renormalization techniques in Section 2.3.3.1 for this problem.

First we solve for the odd sub-problem and begin by explicitly writing out $T_{d,o}(r)$ using the expression for T_d in Equation (3.9)

$$T_{d,o} = \frac{1}{\kappa}(T_d(r) - T_d(1/r)) \tag{3.25}$$

$$= \frac{1}{\kappa}
\begin{cases}
-\frac{1}{L_w}r + 1, & \text{if } 0 < r < L_w^{-1} \\
-\frac{1}{L_w}r + \frac{1}{L_w}\frac{1}{r} & \text{if } L_w^{-1} < r < L_w \\
\frac{1}{L_w}\frac{1}{r} - 1 & \text{if } r > L_w
\end{cases} \tag{3.26}$$

$$= \frac{1}{\kappa}
\begin{cases}
-\frac{1}{L_w}e^s + 1, & \text{if } -\infty < s < -\log(L_w) \\
-\frac{1}{L_w}e^s + \frac{1}{L_w}e^{-s} & \text{if } -\log L < s < \log(L_w) \\
\frac{1}{L_w}e^{-s} - 1 & \text{if } s > \log(L_w)
\end{cases} \tag{3.27}$$

where $s = \log(r)$. We notice that as $|s| \to \infty$, $|T_{d,0}| \to 1$. Hence, to remove this infinity, we

define a new function $w(r, \theta)$ that satisfies

$$\Delta w = 0 \tag{3.28}$$

$$\theta = 0 : w = 0 \tag{3.29}$$

$$\theta = \Phi : w = \frac{1}{\kappa} \begin{cases} -1, & \text{if } 0 < r < L_w^{-1} \\ 0, & \text{if } L_w^{-1} < r < L_w \\ 1, & \text{if } r > L_w \end{cases} \tag{3.30}$$

Then $v_{a,o}$ can be re-written as[7]

$$v_{a,o} = \tilde{v}_{a,o} - w \tag{3.31}$$

where $\tilde{v}_o$ satisfies

$$\Delta \tilde{v}_{a,o} = 0 \tag{3.32}$$

$$\theta = 0 : \tilde{v}_{a,o} = 0 \tag{3.33}$$

$$\theta = \Phi : \tilde{v}_{a,o} = \tilde{T}_{d,o} = \frac{1}{\kappa} \begin{cases} -\frac{1}{L_w}r, & \text{if } 0 < r < L_w^{-1} \\ -\frac{1}{L_w}r + \frac{1}{L_w}\frac{1}{r} & \text{if } L_w^{-1} < r < L_w \\ \frac{1}{L_w}\frac{1}{r} & \text{if } r > L_w \end{cases} \tag{3.34}$$

$$= \frac{1}{\kappa} \begin{cases} -\frac{1}{L_w}e^s, & \text{if } -\infty < s < -\log(L_w) \\ -\frac{1}{L_w}e^s + \frac{1}{L_w}e^{-s} & \text{if } -\log L_w < s < \log(L_w) \\ \frac{1}{L_w}e^{-s} & \text{if } s > \log(L_w) \end{cases} \tag{3.35}$$

which is integrable with respect to $\log(r)$. Hence we proceed to first compute the Fourier coefficient $\hat{\tilde{v}}_{a,o}$ of $\tilde{v}_{a,o}$ using Equation (3.24). Since $\sin(\alpha \log(r))\tilde{T}_{a,o}$ is an even function in

---

[7] Please note that here the tilde sign is simply a notation and does not mean that the quantity carries any units as per an earlier notation. I've run out of symbols and letters a long time ago

the variable $s = \log(r)$, we can write

$$\hat{\tilde{v}}_{a,o} = \frac{1}{\pi\kappa\sinh(\alpha\Phi)}\int_0^\infty \sin(\alpha\log(r))T_o(r)d(\log(r)) \tag{3.36}$$

$$= \frac{1}{\pi\kappa\sinh(\alpha\Phi)}\left(\int_0^{\log L_w}\sin(\alpha s)\left(-\frac{1}{L_w}e^s + \frac{1}{L_w}e^{-s}\right)ds + \int_{\log L_w}^\infty \frac{1}{L_w}e^{-s}\sin(\alpha s)\right)ds \tag{3.37}$$

$$= \frac{1}{\pi\kappa\sinh(\alpha\Phi)}\left(\int_0^{\log L_w}\sin(\alpha s)\left(-\frac{1}{L_w}e^s\right)ds + \int_0^\infty \frac{1}{L_w}e^{-s}\sin(\alpha s)\right)ds \tag{3.38}$$

$$= \frac{1}{\pi\kappa L_w\sinh(\alpha\Phi)}\left(-\int_0^{\log L_w}\sin(\alpha s)e^s ds + \int_0^\infty e^{-s}\sin(\alpha s)\right)ds \tag{3.39}$$

The integrals are easy to compute as

$$\int_0^\infty e^{-s}\sin(\alpha s)ds = Im\left(\int_0^\infty \exp((i\alpha - 1)s)ds\right) \tag{3.40}$$

$$= Im\left(\frac{1}{1 - i\alpha}\right) \tag{3.41}$$

$$= Im\left(\frac{1 + i\alpha}{1 + \alpha^2}\right) \tag{3.42}$$

$$= \frac{\alpha}{1 + \alpha^2} \tag{3.43}$$

while

$$\int_0^{\log L_w}\sin(\alpha s)e^s ds = Im\left(\int_0^{\log L_w}\exp((i\alpha + 1)s)ds\right) \tag{3.44}$$

$$= Im\left(\frac{\exp((i\alpha + 1)\log L_w)}{i\alpha + 1} - \frac{1}{i\alpha + 1}\right) \tag{3.45}$$

$$= Im\left(\frac{L_w\exp((i\alpha\log L_w)}{i\alpha + 1} + \frac{i\alpha - 1}{\alpha^2 + 1}\right) \tag{3.46}$$

$$= \frac{-\alpha L_w\cos(\alpha\log L_w) + L_w\sin(\alpha\log L_w)}{1 + \alpha^2} + \frac{\alpha}{\alpha^2 + 1} \tag{3.47}$$

Hence incorporating integrals (3.43) and (3.47), we can write $\hat{\tilde{v}}_{a,o}$ as

$$\hat{\tilde{v}}_{a,o} = \frac{1}{\pi\kappa L_w\sinh(\alpha\Phi)}\left(-\int_0^{\log L}\sin(\alpha s)e^s ds + \int_0^\infty e^{-s}\sin(\alpha s)\right)ds \tag{3.48}$$

$$= \frac{1}{\pi\kappa L_w\sinh(\alpha\Phi)}\left(\frac{\alpha L_w\cos(\alpha\log L) - L_w\sin(\alpha\log L_w)}{1 + \alpha^2}\right) \tag{3.49}$$

Having obtained the inverse Fourier transform $\hat{\tilde{v}}_{a,o}$, we subsequently use (3.22) to compute

53

$\tilde{v}_{a,o}$

$$\tilde{v}_{a,o} = \int_{-\infty}^{\infty} \sin(\alpha \log(r)) \sinh(\alpha\theta)\hat{\tilde{v}}_{a,o}(\alpha)d\alpha \tag{3.50}$$

$$= \frac{1}{\pi\kappa L_w} \int_{-\infty}^{\infty} \frac{\sinh(\alpha\theta)}{\sinh(\alpha\Phi)} \sin(\alpha \log(r)) \left(\frac{\alpha L_w \cos(\alpha \log L_w) - L_w \sin(\alpha \log L_w)}{1+\alpha^2} \right) d\alpha \tag{3.51}$$

$$= \tilde{v}_{a,o}^1 + \tilde{v}_{a,o}^2 \tag{3.52}$$

where

$$\tilde{v}_{a,o}^1 = \frac{1}{\pi\kappa L_w} \int_{-\infty}^{\infty} \frac{\sinh(\alpha\theta)}{\sinh(\alpha\Phi)} \sin(\alpha \log(r)) \frac{\alpha L_w \cos(\alpha \log L_w)}{1+\alpha^2} d\alpha \tag{3.53}$$

$$\tilde{v}_{a,o}^2 = -\frac{1}{\pi\kappa L_w} \int_{-\infty}^{\infty} \frac{\sinh(\alpha\theta)}{\sinh(\alpha\Phi)} \sin(\alpha \log(r)) \frac{L_w \sin(\alpha \log L_w)}{1+\alpha^2} d\alpha \tag{3.54}$$

To compute $\tilde{v}_{a,o}^1$, we use the trigonometric identity $\sin a \cos b = \frac{1}{2}\left(\sin(a+b) + \sin(a-b)\right)$ to write

$$\tilde{v}_{a,o}^1 = \frac{1}{2\pi\kappa} \left(\int_{-\infty}^{\infty} \frac{\sinh(\alpha\theta)}{\sinh(\alpha\Phi)} \frac{\alpha \sin(\alpha \log(rL_w))}{1+\alpha^2} d\alpha + \int_{-\infty}^{\infty} \frac{\sinh(\alpha\theta)}{\sinh(\alpha\Phi)} \frac{\alpha \sin(\alpha \log(\frac{r}{L_w}))}{1+\alpha^2} d\alpha \right) \tag{3.55}$$

$$= \tilde{v}_{a,o}^{1,1} + \tilde{v}_{a,o}^{1,2} \tag{3.56}$$

where

$$\tilde{v}_{a,o}^{1,1} = \frac{1}{2\pi i\kappa} \left(\int_{-\infty}^{\infty} \frac{\sinh(\alpha\theta)}{\sinh(\alpha\Phi)} \frac{\alpha \exp(i\alpha \log(rL_w))}{1+\alpha^2} d\alpha \right) = \frac{2\pi i}{2\pi i\kappa}$$

$$\begin{cases} Res\left(\frac{\sinh(\alpha\theta)}{\sinh(\alpha\Phi)} \frac{\alpha \exp(i\alpha \log(rL_w))}{1+\alpha^2}, i\right) + \sum_{n=1}^{\infty} Res\left(\frac{\sinh(\alpha\theta)}{\sinh(\alpha\Phi)} \frac{\alpha \exp(i\alpha \log(rL_w))}{1+\alpha^2}, \frac{in\pi}{\Phi}\right) \\ \text{for } rL_w > 1 \\[1em] -Res\left(\frac{\sinh(\alpha\theta)}{\sinh(\alpha\Phi)} \frac{\alpha \exp(i\alpha \log(rL_w))}{1+\alpha^2}, -i\right) - \sum_{n=1}^{\infty} Res\left(\frac{\sinh(\alpha\theta)}{\sinh(\alpha\Phi)} \frac{\alpha \exp(i\alpha \log(rL_w))}{1+\alpha^2}, \frac{-in\pi}{\Phi}\right) \\ \text{for } rL_w < 1, \end{cases}$$

$$= \frac{1}{\kappa} \begin{cases} \frac{1}{2}\frac{\sin(\theta)}{\sin(\Phi)}(rL_w)^{-1} + \sum_{n=1}^{\infty} \frac{(-L_w)^n \sin\left(\frac{n\pi\theta}{\Phi}\right)}{\Phi^2} \frac{n\pi}{\frac{n^2\pi^2}{\Phi^2}-1}(rL_w)^{-\frac{n\pi}{\Phi}}, r > \frac{1}{L_w} \\[1em] -\frac{1}{2}\frac{\sin(\theta)}{\sin(\Phi)}rL_w - \sum_{n=1}^{\infty} \frac{(-1)^n \sin\left(\frac{n\pi\theta}{\theta}\right)}{\Phi^2} \frac{n\pi}{\frac{n^2\Phi^2}{\Phi^2}-1}(rL_w)^{\frac{n\pi}{\Phi}}, r < \frac{1}{L_w} \end{cases} \tag{3.57}$$

Here we loop over the upper half plane complex domain for $rL_w > 1$ and lower for $rL_w < 1$, taking into the account that clockwise contour gives a negative sign to the evaluation of residues. Similarly, we can compute $\tilde{v}_{a,o}^{1,2}$ as

$$
\tilde{v}_{a,o}^{1,2} = \frac{1}{\kappa}
\begin{cases}
\dfrac{1}{2}\dfrac{\sin(\theta)}{\sin(\Phi)}\left(\dfrac{r}{L_w}\right)^{-1} + \displaystyle\sum_{n=1}^{\infty}\dfrac{(-1)^n \sin\left(\frac{n\pi\theta}{\Phi}\right)}{\Phi^2}\dfrac{n\pi}{\frac{n^2\pi^2}{\Phi^2}-1}\left(\dfrac{r}{L_w}\right)^{-\frac{n\pi}{\Phi}}, & r > L_w \\[4ex]
-\dfrac{1}{2}\dfrac{\sin(\theta)}{\sin(\Phi)}\left(\dfrac{r}{L_w}\right) - \displaystyle\sum_{n=1}^{\infty}\dfrac{(-1)^n \sin\left(\frac{n\pi\theta}{\theta}\right)}{\Phi^2}\dfrac{n\pi}{\frac{n^2\Phi^2}{\Phi^2}-1}\left(\dfrac{r}{L_w}\right)^{\frac{n\pi}{\Phi}}, & r < L_w
\end{cases}
\tag{3.58}
$$

Having computed $\tilde{v}_0^1$ in Equation (3.53), we move on to compute $\tilde{v}_{a,o}^2$ in Equation (3.54) following a quite similar series of steps. In the end, we get that

$$
\tilde{v}_{a,o}^2 = \tilde{v}_{a,o}^{2,1} + \tilde{v}_{a,o}^{2,2}
\tag{3.59}
$$

where

$$
\tilde{v}_{a,o}^{2,1} = -\frac{1}{\kappa}
\begin{cases}
\dfrac{\sin(\theta)}{\sin(\Phi)}\dfrac{\left(\frac{r}{L_w}\right)^{-1}}{2} + \displaystyle\sum_{n=1}^{\infty}\dfrac{(-1)^n \sin\left(\frac{n\pi\theta}{\Phi}\right)\left(\frac{r}{L_w}\right)^{-\frac{n\pi}{\Phi}}}{\Phi}\dfrac{1}{\frac{n^2\pi^2}{\Phi^2}-1}, & r > L_w \\[4ex]
\dfrac{\sin(\theta)}{\sin(\Phi)}\dfrac{\frac{r}{L_w}}{2} + \displaystyle\sum_{n=1}^{\infty}\dfrac{(-1)^n \sin\left(\frac{n\pi\theta}{\Phi}\right)\left(\frac{r}{L_w}\right)^{\frac{n\pi}{\Phi}}}{\Phi}\dfrac{1}{\frac{n^2\pi^2}{\Phi^2}-1} & r < L_w
\end{cases}
\tag{3.60}
$$

$$
\tilde{v}_{a,o}^{2,2} = \frac{1}{\kappa}
\begin{cases}
\dfrac{\sin(\theta)}{\sin(\Phi)}\dfrac{\frac{1}{rL_w}}{2} + \displaystyle\sum_{n=1}^{\infty}\dfrac{(-1)^n \sin\left(\frac{n\pi\theta}{\Phi}\right)(rL_w)^{-\frac{n\pi}{\Phi}}}{\Phi}\dfrac{1}{\frac{n^2\pi^2}{\Phi^2}-1}, & r > \frac{1}{L_w} \\[4ex]
\dfrac{\sin(\theta)}{\sin(\Phi)}\dfrac{rL_w}{2} + \displaystyle\sum_{n=1}^{\infty}\dfrac{(-1)^n \sin\left(\frac{n\pi\theta}{\Phi}\right)(rL_w)^{\frac{n\pi}{\Phi}}}{\Phi}\dfrac{1}{\frac{n^2\pi^2}{\Phi^2}-1} & r < \frac{1}{L_w}
\end{cases}
\tag{3.61}
$$

The last ingredients to compute $v_{a,o}$ in the odd sub-problem is to solve for w in Equation (3.28). To do so, we first perform a change of variable from θ to $\Phi - \theta$, so tat the equation would look like

$$
\Delta w = 0
\tag{3.62}
$$

$$
\theta = \Phi : w = 0
\tag{3.63}
$$

$$
\theta = 0 : w = \frac{1}{\kappa}
\begin{cases}
-1, & \text{if } 0 < r < L_w^{-1} \\
0, & \text{if } L_w^{-1} < r < L_w \\
1, & \text{if } r > L_w
\end{cases}
\tag{3.64}
$$

55

Next we apply the conformal transformation

$$\zeta = \zeta_1 + i\zeta_2 \tag{3.65}$$

$$= \exp\left(\frac{\pi}{\Phi}\log\left(re^{\frac{i\pi\theta}{\Phi}}\right)\right) \tag{3.66}$$

so that the equation would satisfy

$$\Delta w = 0 \tag{3.67}$$

$$w = \frac{1}{\kappa}\begin{cases} 0, & \text{if } \zeta_1 < 0, \zeta_2 = 0 \\ -1, & \text{if } 0 < \zeta_1 < L_w^{-\pi/\Phi}, \zeta_2 = 0 \\ 0, & \text{if } L_w^{-\pi/\Phi} < \zeta_1 < L_w^{\pi/\Phi}, \zeta_2 = 0 \\ 1, & \text{if } \zeta_1 > L_w^{\pi/\Phi}, \zeta_2 = 0 \end{cases} \tag{3.68}$$

The solution is well known to be

$$w(\zeta_1, \zeta_2) = \frac{1}{\kappa} - \frac{1}{\kappa}\frac{\arg(\zeta_1 + i\zeta_2 - L^{\pi/\Phi})}{\pi}$$
$$- \frac{1}{\kappa}\frac{\arg(\zeta_1 + i\zeta_2 - L^{-\pi/\Phi})}{\pi} + \frac{1}{\kappa}\frac{\arg(\zeta_1 + i\zeta_2)}{\pi} \tag{3.69}$$

where the arg is defined over the branch $[-\pi/2, 3\pi/2]$. But since θ would only range from 0 to Φ, the argument would lie within $[0, \pi]$. Hence, we could replace the argument function with Arg that uses the principal branch $(-\pi, \pi]$. Upon changing the angle back $\theta \to \Phi - \theta$, we can simplify the expression into

$$w(r, \theta) = 2 - \frac{\theta}{\Phi} - \frac{Arg\left(-r^{\frac{\pi}{\Phi}}\exp\left(-\frac{i\pi\theta}{\Phi}\right) - L_w^{\frac{\pi}{\Phi}}\right) - Arg\left(-r^{\frac{\pi}{\Phi}}\exp\left(-\frac{i\pi\theta}{\Phi}\right) - L_w^{-\frac{\pi}{\Phi}}\right)}{\kappa\pi} \tag{3.70}$$

With all the right ingredients for $v_{a,o}$, we now work towards solving for $v_{a,e}$ in the even

problem in Equation (3.19). First we write down explicitly the boundary condition $T_{d,e}$

$$T_{d,e} = \frac{1}{\kappa}(\mu(1/r)T_d(r) + \mu(r)T_d(1/r)) \tag{3.71}$$

$$= \frac{1}{\kappa}\begin{cases} -\frac{\nu_1/\nu_2}{L_w}e^s + \nu_1/\nu_2, & s < -\log(L_w) \\ -\frac{\nu_1/\nu_2}{L_w}e^s + \nu_1/\nu_2 - \frac{1}{L_w}e^{-s} + 1, & -\log(L_w) < s < 0 \\ -\frac{1}{L_w}e^s + 1 - \frac{\nu_1/\nu_2}{L_w}e^{-s} + \nu_1/\nu_2, & 0 < s < \log(L_w) \\ -\frac{\nu_1/\nu_2}{L_w}e^{-s} + \nu_1/\nu_2, & s > \log(L_w) \end{cases} \tag{3.72}$$

where $s = \log r$. The problem again occurs at $\log(r) = \pm\infty$. To counteract the issue, we shall subtract out the constants from the boundary conditions of $v_{a,e}$ via defining $\tilde{v}_{a,e}$ that

$$\tilde{v}_{a,e} = v_{a,e} - \frac{\nu_1/\nu_2}{\kappa}\frac{\theta}{\Phi} \tag{3.73}$$

Then $\tilde{v}_{a,e}$ satisfies

$$\Delta\tilde{v}_e = 0 \tag{3.74}$$

$$\theta = 0 : \tilde{v}_e = 0 \tag{3.75}$$

$$\theta = \Phi : \tilde{v}_e = \tilde{T}_{d,e} = \frac{1}{\kappa}\begin{cases} -\frac{\nu_1/\nu_2}{L_w}r, & r < \frac{1}{L_w} \\ -\frac{\nu_1/\nu_2}{L_w}r - \frac{1}{L_w}\frac{1}{r} + 1, & \frac{1}{L_w} < r < 1 \\ -\frac{1}{L_w}r + 1 - \frac{\nu_1/\nu_2}{L_w}\frac{1}{r}, & 1 < r < L_w \\ -\frac{\nu_1/\nu_2}{L_w}\frac{1}{r}, & r > L_w \end{cases} \tag{3.76}$$

$$= \frac{1}{\kappa}\begin{cases} -\frac{\nu_1/\nu_2}{L_w}e^s, & s < -\log(L_w) \\ -\frac{\nu_1/\nu_2}{L_w}e^s - \frac{1}{L_w}e^{-s} + 1, & -\log(L_w) < s < 0 \\ -\frac{1}{L_w}e^s - \frac{\nu_1/\nu_2}{L_w}e^{-s} + 1, & 0 < s < \log(L_w) \\ -\frac{\nu_1/\nu_2}{L_w}e^{-s}, & s > \log(L_w) \end{cases} \tag{3.77}$$

where $s = \log r$ as before. Using equation (3.21), we can write the Fourier coefficient of $\tilde{v}_{a,e}$ as

$$\hat{\tilde{v}}_{a,e} = \frac{1}{2\pi \sinh(\alpha\Phi)} \int_{-\infty}^{\infty} \cos(\alpha \log(r)) T_{d,e}(r,\theta) d(\log(r)) \tag{3.78}$$

$$= \frac{1}{\kappa\pi \sinh(\alpha\Phi)} \int_{0}^{\log L_w} \cos(\alpha s) \left(-\frac{1}{L_w} e^s - \frac{\nu_1/\nu_2}{L_w} e^{-s} + 1 \right) ds$$
$$+ \frac{1}{\kappa\pi \sinh(\alpha\Phi)} \int_{\log L_w}^{\infty} \cos(\alpha s) \left(-\frac{\nu_1/\nu_2}{L_w} e^{-s} \right) ds \tag{3.79}$$

$$= \frac{1}{\kappa\pi \sinh(\alpha\Phi)} \int_{0}^{\log L_w} \cos(\alpha s) \left(-\frac{1}{L_w} e^s + 1 \right) ds$$
$$+ \frac{1}{\kappa\pi \sinh(\alpha\Phi)} \int_{0}^{\infty} \cos(\alpha s) \left(-\frac{\nu_1/\nu_2}{L_w} e^{-s} \right) ds \tag{3.80}$$

$$= \frac{-1}{\kappa\pi L_w \sinh(\alpha\Phi)} \int_{0}^{\log L_w} \cos(\alpha s) e^s ds + \frac{1}{\kappa\pi \sinh(\alpha\Phi)} \int_{0}^{\log L_w} \cos(\alpha s) ds$$
$$- \frac{1}{\kappa\pi \sinh(\alpha\Phi)} \frac{\nu_1/\nu_2}{L_w} \int_{0}^{\infty} \cos(\alpha s) e^{-s} ds \tag{3.81}$$

We now compute the three integrals

$$\int_{0}^{\log L_w} e^s \cos(\alpha s) ds = Re \left(\int_{0}^{\log L_w} \exp((1+i\alpha)s) ds \right) \tag{3.82}$$

$$= Re \left(\frac{\exp((1+i\alpha)\log L_w) - 1}{1 + i\alpha} \right) \tag{3.83}$$

$$= \left(\frac{L_w \cos(\alpha \log L_w) + L_w \alpha \sin(\alpha \log L_w)}{1 + \alpha^2} - \frac{1}{1 + \alpha^2} \right) \tag{3.84}$$

$$\int_{0}^{\log L_w} \cos(\alpha s) ds = \frac{\sin(\alpha \log L_w)}{\alpha} \tag{3.85}$$

$$\int_{0}^{\infty} \cos(\alpha s) e^{-s} ds = Re \left(\int_{0}^{\infty} \exp((i\alpha - 1)s) ds \right) \tag{3.86}$$

$$= -Re \left(\frac{1}{i\alpha - 1} \right) \tag{3.87}$$

$$= \frac{1}{1 + \alpha^2} \tag{3.88}$$

$$\hat{\tilde{v}}_{a,e} = \frac{-1}{\kappa\pi\sinh(\alpha\Phi)} \left(\frac{\cos(\alpha\log L_w) + \alpha\sin(\alpha\log L_w)}{1+\alpha^2} - \frac{1}{1+\alpha^2} \right)$$
$$+ \frac{1}{\kappa\pi\sinh(\alpha\Phi)} \frac{\sin(\alpha\log L_w)}{\alpha} - \frac{\nu_1/\nu_2}{\kappa\pi L_w\sinh(\alpha\Phi)} \frac{1}{1+\alpha^2} \tag{3.89}$$

$$= \frac{-1}{\kappa\pi\sinh(\alpha\Phi)} \left(\frac{\cos(\alpha\log L_w) + \alpha\sin(\alpha\log L_w)}{1+\alpha^2} \right)$$
$$+ \frac{1}{\kappa\pi\sinh(\alpha\Phi)} \frac{\sin(\alpha\log L_w)}{\alpha} + \frac{1-\nu_1/\nu_2}{\kappa\pi L_w\sinh(\alpha\Phi)} \frac{1}{1+\alpha^2} \tag{3.90}$$

Now, we can use equation (3.22) to write the solution $\tilde{v}_{a,e}$ as

$$\tilde{v}_{a,e} = \int_{-\infty}^{\infty} \cos(\alpha\log(r))\sinh(\alpha\theta)\hat{\tilde{v}}_{a,e}(\alpha)d\alpha \tag{3.91}$$

$$= \tilde{v}_{a,e}^1 + \tilde{v}_{a,e}^2 + \tilde{v}_{a,e}^3 + \tilde{v}_{a,e}^4 \tag{3.92}$$

where

$$\tilde{v}_{a,e}^1 = \frac{-1}{\kappa\pi} \int_{-\infty}^{\infty} \frac{\alpha\sin(\alpha\log L_w)\cos(\alpha\log r)}{1+\alpha^2} \frac{\sinh(\alpha\theta)}{\sinh(\alpha\Phi)}d\alpha \tag{3.93}$$

$$\tilde{v}_{a,e}^2 = \frac{-1}{\kappa\pi} \int_{-\infty}^{\infty} \frac{\cos(\alpha\log L_w)\cos(\alpha\log r)}{(1+\alpha^2)} \frac{\sinh(\alpha\theta)}{\sinh(\alpha\Phi)}d\alpha \tag{3.94}$$

$$\tilde{v}_{a,e}^3 = \frac{1}{\kappa\pi} \int_{-\infty}^{\infty} \frac{\sin(\alpha\log L_w)\cos(\alpha\log r)}{\alpha} \frac{\sinh(\alpha\theta)}{\sinh(\alpha\Phi)}d\alpha \tag{3.95}$$

$$\tilde{v}_{a,e}^4 = \frac{(1-\nu_1/\nu_2)}{\kappa\pi L_w} \int_{-\infty}^{\infty} \frac{\cos(\alpha\log r)}{1+\alpha^2} \frac{\sinh(\alpha\theta)}{\sinh(\alpha\Phi)}d\alpha \tag{3.96}$$

We shall compute these four integrals separately.

First, we use the trigonometric identity $\sin a\cos b = \frac{1}{2}(\sin(a+b) + \sin(a-b))$ to write

$$\tilde{v}_{a,e}^1 = \frac{-1}{\kappa\pi} \int_{-\infty}^{\infty} \frac{\alpha\sin(\alpha\log L_w)\cos(\alpha\log r)}{1+\alpha^2} \frac{\sinh(\alpha\theta)}{\sinh(\alpha\Phi)}d\alpha \tag{3.97}$$

$$= \frac{-1}{2\kappa\pi} \int_{-\infty}^{\infty} \frac{\alpha\sin(\alpha\log L_w r) + \alpha\sin(\alpha\log(L_w/r))}{1+\alpha^2} \frac{\sinh(\alpha\theta)}{\sinh(\alpha\Phi)}d\alpha \tag{3.98}$$

$$= \tilde{v}_{a,e}^{1,1} + \tilde{v}_{a,e}^{1,1} \tag{3.99}$$

$$\tilde{v}_{a,e}^{1,1} = \frac{-1}{2\kappa\pi} \int_{-\infty}^{\infty} \frac{\alpha\sin(\alpha\log rL_w)}{1+\alpha^2} \frac{\sinh(\alpha\theta)}{\sinh(\alpha\Phi)}d\alpha \tag{3.100}$$

$$\tilde{v}_{a,e}^{1,2} = \frac{-1}{2\kappa\pi} \int_{-\infty}^{\infty} \frac{\alpha\sin(\alpha\log(L_w/r))}{1+\alpha^2} \frac{\sinh(\alpha\theta)}{\sinh(\alpha\Phi)}d\alpha \tag{3.101}$$

Using the complex integral techniques demonstrated in calculating $\tilde{v}_{a,o}^{1,1}$ in Equation (3.57), we can compute $\tilde{v}_{a,e}^{1,1}$ and $\tilde{v}_{a,e}^{1,2}$ and obtain

$$\tilde{v}_{a,e}^{1,1} = \frac{-1}{\kappa} \begin{cases} \frac{1}{2}\frac{\sin(\theta)}{\sin(\Phi)}(rL_w)^{-1} + \sum\limits_{n=1}^{\infty} \frac{(-1)^n n\pi(rL_w)^{-\frac{n\pi}{\Phi}}\sin\left(\frac{n\pi\theta}{\Phi}\right)}{\Phi^2\left(\frac{n^2\pi^2}{\Phi^2}-1\right)} & r > 1/L_w \\[3mm] -\frac{1}{2}\frac{\sin(\theta)}{\sin(\Phi)}rL_w - \sum\limits_{n=1}^{\infty} \frac{(-1)^n n\pi(rL_w)^{\frac{n\pi}{\Phi}}\sin\left(\frac{n\pi\theta}{\Phi}\right)}{\Phi^2\left(\frac{n^2\pi^2}{\Phi^2}-1\right)} & r < 1/L_w \end{cases} \tag{3.102}$$

$$\tilde{v}_{a,e}^{1,2} = \frac{-1}{\kappa} \begin{cases} \frac{1}{2}\frac{\sin(\theta)}{\sin(\Phi)}(L_w/r)^{-1} + \sum\limits_{n=1}^{\infty} \frac{(-1)^n n\pi(L_w/r)^{-\frac{n\pi}{\Phi}}\sin\left(\frac{n\pi\theta}{\Phi}\right)}{\Phi^2\left(\frac{n^2\pi^2}{\Phi^2}-1\right)} & r < L_w \\[3mm] -\frac{1}{2}\frac{\sin(\theta)}{\sin(\Phi)}(L_w/r) - \sum\limits_{n=1}^{\infty} \frac{(-1)^n n\pi(L_w/r)^{\frac{n\pi}{\Phi}}\sin\left(\frac{n\pi\theta}{\Phi}\right)}{\Phi^2\left(\frac{n^2\pi^2}{\Phi^2}-1\right)} & r > L_w \end{cases} \tag{3.103}$$

Secondly, we use the same line of calculation as for $\tilde{v}_{a,e}^1$ to calculate $\tilde{v}_{a,e}^2$ in Equation (3.94) as

$$\tilde{v}_{a,e}^2 = \tilde{v}_{a,e}^{2,1} + \tilde{v}_{a,e}^{2,2} \tag{3.104}$$

where

$$\tilde{v}_{a,e}^{2,1} = \frac{-1}{\kappa} \begin{cases} \frac{1}{2}\frac{\sin\theta}{\sin\Phi}(L_w/r)^{-1} + \sum\limits_{n=1}^{\infty} \frac{(-1)^n (L_w/r)^{-\frac{n\pi}{\Phi}}\sin\left(\frac{n\pi\theta}{\Phi}\right)}{\Phi\left(\frac{n^2\pi^2}{\Phi}-1\right)}, & r < L_w \\[3mm] \frac{1}{2}\frac{\sin\theta}{\sin\Phi}(L_w/r) + \sum\limits_{n=1}^{\infty} \frac{(-1)^n (L_w/r)^{\frac{n\pi}{\Phi}}\sin\left(\frac{n\pi\theta}{\Phi}\right)}{\Phi\left(\frac{n^2\pi^2}{\Phi}-1\right)}, & r > L_w \end{cases} \tag{3.105}$$

$$\tilde{v}_{a,e}^{2,2} = \frac{-1}{\kappa} \begin{cases} \frac{1}{2}\frac{\sin\theta}{\sin\Phi}(rL_w)^{-1} + \sum\limits_{n=1}^{\infty} \frac{(-1)^n (rL_w)^{-\frac{n\pi}{\Phi}}\sin\left(\frac{n\pi\theta}{\Phi}\right)}{\Phi\left(\frac{n^2\pi^2}{\Phi}-1\right)}, & r > 1/L_w \\[3mm] \frac{1}{2}\frac{\sin\theta}{\sin\Phi}(rL_w) + \sum\limits_{n=1}^{\infty} \frac{(-1)^n (rL_w)^{\frac{n\pi}{\Phi}}\sin\left(\frac{n\pi\theta}{\Phi}\right)}{\Phi\left(\frac{n^2\pi^2}{\Phi}-1\right)}, & r < 1/L_w \end{cases} \tag{3.106}$$

Thirdly, we can simplify $\tilde{v}_{a,e}^3$ into

$$\tilde{v}_{a,e}^3 = \tilde{v}_{a,e}^{3,1} + \tilde{v}_{a,e}^{3,2} \tag{3.107}$$

where

$$v_{a,e}^{3,1} = \frac{1}{2\kappa\pi i} \int_{-\infty}^{\infty} \frac{\exp(i\alpha\log(L_w r))}{\alpha} \frac{\sinh(\alpha\theta)}{\sinh(\alpha\Phi)} d\alpha \tag{3.108}$$

$$v_{a,e}^{3,2} = \frac{1}{2\kappa\pi i} \int_{-\infty}^{\infty} \frac{\exp(i\alpha\log(L_w/r))}{\alpha} \frac{\sinh(\alpha\theta)}{\sinh(\alpha\Phi)} d\alpha \tag{3.109}$$

60

Here, we shall use a contour integral with an $\epsilon-$size bump around the original before we let $\epsilon \to 0$. We "loop up" in the complex domain if the argument of the complex exponential is positive; otherwise we "loop down". The results are

$$
v_{a,e}^{3,1} = \frac{1}{2\kappa\pi}
\begin{cases}
\pi\frac{\theta}{\Phi} + 2\pi \sum_{n=1}^{\infty} \frac{(-1)^n (L_w r)^{-\frac{n\pi}{\Phi}} \sin\left(\frac{n\pi\theta}{\Phi}\right)}{n\pi}, & r > 1/L_w \\
-\pi\frac{\theta}{\Phi} - 2\pi \sum_{n=1}^{\infty} \frac{(-1)^n (L_w r)^{\frac{n\pi}{\Phi}} \sin\left(\frac{n\pi\theta}{\Phi}\right)}{n\pi}, & r < 1/L_w
\end{cases}
\tag{3.110}
$$

$$
v_{a,e}^{3,2} = \frac{1}{2\kappa\pi}
\begin{cases}
\pi\frac{\theta}{\Phi} + 2\pi \sum_{n=1}^{\infty} \frac{(-1)^n (L_w/r)^{-\frac{n\pi}{\Phi}} \sin\left(\frac{n\pi\theta}{\Phi}\right)}{n\pi}, & r < L_w \\
-\pi\frac{\theta}{\Phi} - 2\pi \sum_{n=1}^{\infty} \frac{(-1)^n (L_w/r)^{\frac{n\pi}{\Phi}} \sin\left(\frac{n\pi\theta}{\Phi}\right)}{n\pi}, & r > L_w
\end{cases}
\tag{3.111}
$$

Lastly, we can compute $\tilde{v}_{a,e}^4$ using the same complex integral techniques as before

$$
\tilde{v}_{a,e}^4 = \frac{(1 - \nu_1/\nu_2)}{\kappa\pi L_w} \int_{-\infty}^{\infty} \frac{\exp(i\alpha \log r)}{1 + \alpha^2} \frac{\sinh(\alpha\theta)}{\sinh(\alpha\Phi)} d\alpha
\tag{3.112}
$$

$$
= \frac{2(1 - \nu_1/\nu_2)}{\kappa L_w}
\begin{cases}
\frac{1}{2}\frac{\sin(\theta)}{\sin(\Phi)} r^{-1} + \sum_{n=1}^{\infty} \frac{(-1)^n \sin\left(\frac{n\pi\theta}{\Phi}\right)}{\Phi\left(\frac{n^2\pi^2}{\Phi^2} - 1\right)} r^{-\frac{n\pi}{\Phi}}, & r > 1 \\
\frac{1}{2}\frac{\sin(\theta)}{\sin(\Phi)} r + \sum_{n=1}^{\infty} \frac{(-1)^n \sin\left(\frac{n\pi\theta}{\Phi}\right)}{\Phi\left(\frac{n^2\pi^2}{\Phi^2} - 1\right)} r^{\frac{n\pi}{\Phi}}, & r < 1
\end{cases}
\tag{3.113}
$$

Finally, let us put all the puzzle pieces together. According Equation (3.20), $v_a = v_{a,e} + \mu(r)v_{a,o}$, which can be rewritten according to $v_{a,o}$ in Equation (3.31) and $v_{a,e}$ in Equation (3.73) as

$$
v_a = \tilde{v}_e(r,\theta) + \frac{\nu_1/\nu_2}{\kappa}\frac{\theta}{\Phi} + \mu(r)(\tilde{v}_{a,o}(r,\theta) - w)
\tag{3.114}
$$

which can be further broken down into

$$
v_a = \tilde{v}_{a,e}^{1,1} + \tilde{v}_{a,e}^{1,2} + \tilde{v}_{a,e}^{2,1} + \tilde{v}_{a,e}^{2,2} + \tilde{v}_{a,e}^{3,1} + v_{a,e}^{3,2} + \tilde{v}_{a,e}^4
$$
$$
+ \mu(\tilde{v}_{a,o}^{1,1} + \tilde{v}_{a,o}^{1,2} + \tilde{v}_{a,o}^{2,1} + \tilde{v}_{a,o}^{2,2} - w) + \frac{\nu_1/\nu_2}{\kappa}\frac{\theta}{\Phi}
\tag{3.115}
$$

for $\tilde{v}_{a,e}^{1,1}$ in Equation (3.102), $\tilde{v}_{a,e}^{1,2}$ in Equation (3.103), $\tilde{v}_{a,e}^{2,1}$ in Equation (3.105), $\tilde{v}_{a,e}^{2,2}$ in Equation (3.106), $\tilde{v}_{a,e}^{3,1}$ in Equation (3.110), $\tilde{v}_{a,e}^{3,2}$ in Equation (3.111), $\tilde{v}_{a,e}^4$ in Equation (3.112), $\tilde{v}_{a,o}^{1,1}$ in Equation (3.57), $\tilde{v}_{a,o}^{1,2}$ in Equation (3.58), $\tilde{v}_{a,o}^{2,1}$ in Equation (3.60), $\tilde{v}_{a,o}^{2,2}$ in Equation

(3.61), and w in Equation (3.70)

Simplifying the terms for v_a in Equation (3.115) requires some of the nastiest algebra I've ever encountered in my life, so nasty that I want to take a shower. But after all of that, we find that v_a is given by:

$$v_a(r,\theta) =$$

$$
\begin{cases}
-\dfrac{\sin(\theta)}{\sin(\Phi)}\dfrac{r}{L_w} + \dfrac{\nu_1/\nu_2}{\kappa}\dfrac{\theta}{\Phi} - w + \dfrac{2}{\kappa}\left(-\displaystyle\sum_{n=1}^{\infty}\dfrac{(-1)^n(n\pi+\Phi)(r/L_w)^{\frac{n\pi}{\Phi}}\sin\left(\frac{n\pi\theta}{\Phi}\right)}{\Phi^2\left(\frac{n^2\pi^2}{\Phi^2}-1\right)}\right) \\
\quad +\dfrac{1}{\kappa\pi}\left(\displaystyle\sum_{n=1}^{\infty}\dfrac{(-1)^n((r/L_w)^{\frac{n\pi}{\Phi}}-(rL)^{\frac{n\pi}{\Phi}})\sin\left(\frac{n\pi\theta}{\Phi}\right)}{n}\right) + \dfrac{2(1-\nu_1/\nu_2)}{\kappa L_w}\left(\displaystyle\sum_{n=1}^{\infty}\dfrac{(-1)^n\sin\left(\frac{n\pi\theta}{\Phi}\right)}{\Phi\left(\frac{n^2\pi^2}{\Phi^2}-1\right)}r^{\frac{n\pi}{\Phi}}\right) \\
\qquad \text{for } \left[0,\frac{1}{L_w}\right], \\[4pt]
-\dfrac{\sin\theta}{\sin\Phi}\dfrac{r}{L_w} + \dfrac{\theta}{\Phi} - w + \dfrac{2}{\kappa}\left(-\displaystyle\sum_{n=1}^{\infty}\dfrac{(-1)^n(n\pi+\Phi)(r/L_w)^{\frac{n\pi}{\Phi}}\sin\left(\frac{n\pi\theta}{\Phi}\right)}{\Phi^2\left(\frac{n^2\pi^2}{\Phi^2}-1\right)}\right) \\
\quad +\dfrac{1}{\kappa}\left(\displaystyle\sum_{n=1}^{\infty}\dfrac{(-1)^n((L_w r)^{-\frac{n\pi}{\Phi}}+(r/L_w)^{\frac{n\pi}{\Phi}})\sin\left(\frac{n\pi\theta}{\Phi}\right)}{n\pi}\right) + \dfrac{2(1-\nu_1/\nu_2)}{\kappa L_w}\left(\displaystyle\sum_{n=1}^{\infty}\dfrac{(-1)^n\sin\left(\frac{n\pi\theta}{\Phi}\right)}{\Phi\left(\frac{n^2\pi^2}{\Phi^2}-1\right)}r^{\frac{n\pi}{\Phi}}\right) \\
\qquad \text{for } \left[\frac{1}{L_w},1\right], \\[4pt]
-\dfrac{\sin(\theta)}{\sin(\Phi)}\dfrac{r}{L_w} + \dfrac{\theta}{\Phi} - (\nu_1/\nu_2)w + \dfrac{\nu_1/\nu_2-1}{\kappa}\left(\displaystyle\sum_{n=1}^{\infty}\dfrac{(-1)^n(n\pi+\Phi)(rL)^{-\frac{n\pi}{\Phi}}\sin\left(\frac{n\pi\theta}{\Phi}\right)}{\Phi^2\left(\frac{n^2\pi^2}{\Phi^2}-1\right)}\right) \\
\quad +\left(-\displaystyle\sum_{n=1}^{\infty}\dfrac{(-1)^n(n\pi+\Phi)(r/L_w)^{\frac{n\pi}{\Phi}}\sin\left(\frac{n\pi\theta}{\Phi}\right)}{\Phi^2\left(\frac{n^2\pi^2}{\Phi^2}-1\right)}\right) + \dfrac{1}{\kappa}\left(\displaystyle\sum_{n=1}^{\infty}\dfrac{(-1)^n((L_w r)^{-\frac{n\pi}{\Phi}}+(r/L_w)^{\frac{n\pi}{\Phi}})\sin\left(\frac{n\pi\theta}{\Phi}\right)}{n\pi}\right) \\
\quad +\dfrac{2(1-\nu_1/\nu_2)}{\kappa L_w}\left(\displaystyle\sum_{n=1}^{\infty}\dfrac{(-1)^n\sin\left(\frac{n\pi\theta}{\Phi}\right)}{\Phi\left(\frac{n^2\pi^2}{\Phi^2}-1\right)}r^{-\frac{n\pi}{\Phi}}\right) \\
\qquad \text{for } [1,L_w], \\[4pt]
+\dfrac{\nu_1/\nu_2}{\kappa}\dfrac{\theta}{\Phi} - (\nu_1/\nu_2)w + \dfrac{(\nu_1/\nu_2-1)}{\kappa}\left(\displaystyle\sum_{n=1}^{\infty}\dfrac{(-1)^n(n\pi+\Phi)(rL_w)^{-\frac{n\pi}{\Phi}}\sin\left(\frac{n\pi\theta}{\Phi}\right)}{\Phi^2\left(\frac{n^2\pi^2}{\Phi^2}-1\right)}\right) \\
\quad +\left(\displaystyle\sum_{n=1}^{\infty}\dfrac{(-1)^n(n\pi-\Phi)(L_w/r)^{\frac{n\pi}{\Phi}}\sin\left(\frac{n\pi\theta}{\Phi}\right)}{\Phi^2\left(\frac{n^2\pi^2}{\Phi^2}-1\right)}\right) + \dfrac{1}{\kappa}\left(\displaystyle\sum_{n=1}^{\infty}\dfrac{(-1)^n((L_w r)^{-\frac{n\pi}{\Phi}}-(L_w/r)^{\frac{n\pi}{\Phi}})\sin\left(\frac{n\pi\theta}{\Phi}\right)}{n\pi}\right) \\
\quad +\dfrac{2(1-\nu_1/\nu_2)}{\kappa L_w}\left(\displaystyle\sum_{n=1}^{\infty}\dfrac{(-1)^n\sin\left(\frac{n\pi\theta}{\Phi}\right)}{\Phi\left(\frac{n^2\pi^2}{\Phi^2}-1\right)}r^{-\frac{n\pi}{\Phi}}\right) \\
\qquad \text{for } [L_w,\infty).
\end{cases}
$$

$$(3.116)$$

Note that most of the infinite series in the above equation converge geometrically in r, r/L_w, L_w/r, or rL_w. The only caveats exist in the last terms of the solution over $[1/L_w, 1]$ and $[1, L_w]$, which contain the same singularities as the solution to the wedge problem, Equation (2.44), in Section 2.3.3.1. The fix is detailed in Section 2.3.3.2, which, upon applied to v_a in

Equation (3.116), would yield the following answer: $v_a = v_a^{(0)} + v_a^{(1)}$, where $v_a^{(0)}$ contains the dominating terms that give the ballpark value of v_a, while $v_a^{(1)}$ contains all the rest of fast converging series improves on its accuracy with additional terms. First, $v_a^{(0)}$ can be written as

$$
v_a^{(0)}(r,\theta) = \begin{cases}
-\frac{\sin\theta}{\sin(\Phi)}\frac{r}{L_w} + \frac{\nu_1}{\nu_2\kappa}\frac{\theta}{\Phi} - w(r,\theta) + \frac{2(1-\nu_1/\nu_2)\Phi}{\kappa L_w \pi^2}Im\left(Li_2\left(-r^{\frac{n\pi}{\Phi}}e^{\frac{i\pi\theta}{\Phi}}\right)\right) \\
\quad\text{for } 0 \le r \le \frac{1}{L_w}, \\[4pt]
-\frac{\sin\theta}{\sin\Phi}\frac{r}{L_w} + \frac{\theta}{\Phi} - w(r,\theta) + \frac{2(1-\nu_1/\nu_2)\Phi}{\kappa L_w \pi^2}Im\left(Li_2\left(-r^{\frac{n\pi}{\Phi}}e^{\frac{i\pi\theta}{\Phi}}\right)\right) \\
\quad\text{for } \frac{1}{L_w} \le r \le 1, \\[4pt]
-\frac{\sin\theta}{\sin\Phi}\frac{r}{L_w} + \frac{\theta}{\Phi} - \frac{\nu_1}{\nu_2}w(r,\theta) + \frac{2(1-\nu_1/\nu_2)\Phi}{\kappa L_w \pi^2}Im\left(Li_2\left(-r^{-\frac{n\pi}{\Phi}}e^{\frac{i\pi\theta}{\Phi}}\right)\right) \\
\quad\text{for } 1 \le r \le L_w, \\[4pt]
+\frac{\nu_1}{\nu_2\kappa}\frac{\theta}{\Phi} - \frac{\nu_1}{\nu_2}w(r,\theta) + \frac{2(1-\nu_1/\nu_2)\Phi}{\kappa L_w \pi^2}Im\left(Li_2\left(-r^{-\frac{n\pi}{\Phi}}e^{\frac{i\pi\theta}{\Phi}}\right)\right) \\
\quad\text{for } L_w \le r < \infty,
\end{cases}
\tag{3.117}
$$

where $\kappa = 1 + \frac{\nu_1}{\nu_2}$ and $w(r,\theta)$ is defined as

$$
w(r,\theta) = 2 - \frac{\theta}{\Phi} - \frac{Arg\left(-r^{\frac{\pi}{\Phi}}\exp\left(-\frac{i\pi\theta}{\Phi}\right) - L_w^{\frac{\pi}{\Phi}}\right) - Arg\left(-r^{\frac{\pi}{\Phi}}\exp\left(-\frac{i\pi\theta}{\Phi}\right) - L_w^{-\frac{\pi}{\Phi}}\right)}{\kappa\pi}
\tag{3.118}
$$

Here Li_2 is the polylogarithm function of order 2 defined in Equation (2.49) of Chapter 2. Secondly, the fast converging terms of $v_a^{(1)}$ can be written as

$$v_a^{(1)}(r,\theta) =$$

$$
\begin{cases}
+\dfrac{2}{\kappa}\left(-\displaystyle\sum_{n=1}^{\infty}\dfrac{(-1)^n(n\pi+\Phi)(r/L_w)^{\frac{n\pi}{\Phi}}\sin\left(\frac{n\pi\theta}{\Phi}\right)}{\Phi^2\left(\frac{n^2\pi^2}{\Phi^2}-1\right)}\right) \\[4ex]
+\dfrac{1}{\kappa\pi}\left(\displaystyle\sum_{n=1}^{\infty}\dfrac{(-1)^n((r/L_w)^{\frac{n\pi}{\Phi}}-(rL)^{\frac{n\pi}{\Phi}})\sin\left(\frac{n\pi\theta}{\Phi}\right)}{n}\right)+\dfrac{2(1-\nu_1/\nu_2)}{\kappa L_w\Phi}\left(\displaystyle\sum_{n=1}^{\infty}\dfrac{(-1)^n r^{\frac{n\pi}{\Phi}}\sin\left(\frac{n\pi\theta}{\Phi}\right)}{\frac{n^2\pi^2}{\Phi^2}\left(\frac{n^2\pi^2}{\Phi^2}-1\right)}\right) \\[4ex]
\qquad \text{for}\;\; \left[0,\frac{1}{L_w}\right], \\[2ex]
+\dfrac{2}{\kappa}\left(-\displaystyle\sum_{n=1}^{\infty}\dfrac{(-1)^n(n\pi+\Phi)(r/L_w)^{\frac{n\pi}{\Phi}}\sin\left(\frac{n\pi\theta}{\Phi}\right)}{\Phi^2\left(\frac{n^2\pi^2}{\Phi^2}-1\right)}\right) \\[4ex]
+\dfrac{1}{\kappa}\left(\displaystyle\sum_{n=1}^{\infty}\dfrac{(-1)^n((L_wr)^{-\frac{n\pi}{\Phi}}+(r/L_w)^{\frac{n\pi}{\Phi}})\sin\left(\frac{n\pi\theta}{\Phi}\right)}{n\pi}\right)+\dfrac{2(1-\nu_1/\nu_2)}{\kappa L_w\Phi}\left(\displaystyle\sum_{n=1}^{\infty}\dfrac{(-1)^n r^{\frac{n\pi}{\Phi}}\sin\left(\frac{n\pi\theta}{\Phi}\right)}{\frac{n^2\pi^2}{\Phi^2}\left(\frac{n^2\pi^2}{\Phi^2}-1\right)}\right) \\[4ex]
\qquad \text{for}\;\; \left[\frac{1}{L_w},1\right], \\[2ex]
+\dfrac{\nu_1/\nu_2-1}{\kappa}\left(\displaystyle\sum_{n=1}^{\infty}\dfrac{(-1)^n(n\pi+\Phi)(rL)^{-\frac{n\pi}{\Phi}}\sin\left(\frac{n\pi\theta}{\Phi}\right)}{\Phi^2\left(\frac{n^2\pi^2}{\Phi^2}-1\right)}\right) \\[4ex]
+\left(-\displaystyle\sum_{n=1}^{\infty}\dfrac{(-1)^n(n\pi+\Phi)(r/L_w)^{\frac{n\pi}{\Phi}}\sin\left(\frac{n\pi\theta}{\Phi}\right)}{\Phi^2\left(\frac{n^2\pi^2}{\Phi^2}-1\right)}\right)+\dfrac{1}{\kappa}\left(\displaystyle\sum_{n=1}^{\infty}\dfrac{(-1)^n((L_wr)^{-\frac{n\pi}{\Phi}}+(r/L_w)^{\frac{n\pi}{\Phi}})\sin\left(\frac{n\pi\theta}{\Phi}\right)}{n\pi}\right) \\[4ex]
+\dfrac{2(1-\nu_1/\nu_2)}{\kappa L_w\Phi}\left(\displaystyle\sum_{n=1}^{\infty}\dfrac{(-1)^n r^{-\frac{n\pi}{\Phi}}\sin\left(\frac{n\pi\theta}{\Phi}\right)}{\frac{n^2\pi^2}{\Phi^2}\left(\frac{n^2\pi^2}{\Phi^2}-1\right)}\right) \\[4ex]
\qquad \text{for}\;\; [1,L_w], \\[2ex]
+\dfrac{(\nu_1/\nu_2-1)}{\kappa}\left(\displaystyle\sum_{n=1}^{\infty}\dfrac{(-1)^n(n\pi+\Phi)(rL_w)^{-\frac{n\pi}{\Phi}}\sin\left(\frac{n\pi\theta}{\Phi}\right)}{\Phi^2\left(\frac{n^2\pi^2}{\Phi^2}-1\right)}\right) \\[4ex]
+\left(\displaystyle\sum_{n=1}^{\infty}\dfrac{(-1)^n(n\pi-\Phi)(L_w/r)^{\frac{n\pi}{\Phi}}\sin\left(\frac{n\pi\theta}{\Phi}\right)}{\Phi^2\left(\frac{n^2\pi^2}{\Phi^2}-1\right)}\right)+\dfrac{1}{\kappa}\left(\displaystyle\sum_{n=1}^{\infty}\dfrac{(-1)^n((L_wr)^{-\frac{n\pi}{\Phi}}-(L_w/r)^{\frac{n\pi}{\Phi}})\sin\left(\frac{n\pi\theta}{\Phi}\right)}{n\pi}\right) \\[4ex]
+\dfrac{2(1-\nu_1/\nu_2)}{\kappa L_w\Phi}\left(\displaystyle\sum_{n=1}^{\infty}\dfrac{(-1)^n r^{-\frac{n\pi}{\Phi}}\sin\left(\frac{n\pi\theta}{\Phi}\right)}{\frac{n^2\pi^2}{\Phi^2}\left(\frac{n^2\pi^2}{\Phi^2}-1\right)}\right) \\[4ex]
\qquad \text{for}\;\; [L_w,\infty).
\end{cases}
$$

$$\text{(3.119)}$$

Having obtained an expression for v_a, we can use in Equation (3.116) or its singularity-extracted version in Equation (3.117) and (3.119) to construct the solution to the non-dimensionalized steady-state temperature problem with a linearly decreasing boundary profile on $\theta = 0, \Phi$ in Equation (3.10) as

$$T(r,\theta) = v_a(r/a,\theta) + v_a(r/a,\Phi-\theta) \tag{3.120}$$

3.2.2 Concentration Solution

The concentration problem extracted from (3.8) is

$$
\begin{cases}
\Delta C = 0, & r > a \\[4pt]
\frac{\partial C}{\partial \theta} = 0, & \text{on } \theta = 0, \Phi; r < L_w \\[4pt]
C = 0, & \text{on } \theta = 0, \Phi; r > L_w \\[4pt]
C = \beta T + \gamma, & r = a
\end{cases}
\tag{3.121}
$$

Our goal is to solve (3.121) analytically, which will be presented in the following way: first we approach it semi-analytically using series expansion, which we will not fully solve. Rather the insight derived from the semi-analytical approach would guide us to formulate and sanity check the analytical solution. Finally, the analytical solution would require a two-step ansatz, using the known properties of the Dirichlet-to-Neumann mapping and Riemann-Hilbert problems.

3.2.2.1 The Semi-Analytical Method (I): Driving Analytical Insight

The first step is to perform a conformal mapping on the region $r > a$. We define

$$
\xi + i\zeta = \pi + i\frac{\pi}{\Phi} \log\left(\frac{r}{a} e^{i(\Phi-\theta)}\right)
\tag{3.122}
$$

where

$$
\xi = \frac{\pi}{\Phi}\theta
\tag{3.123}
$$

$$
\zeta = \frac{\pi}{\Phi} \log\left(\frac{r}{a}\right)
\tag{3.124}
$$

Consequently, the equations can be solved in the domain $\Omega_{\xi,\zeta} := \{(\xi,\zeta)|0 \leq \xi \leq \pi, \zeta > 0\}$ (see Figure B-9b). Define $\zeta_L = \frac{\pi}{\Phi} \log\left(\frac{L_w}{a}\right)$ and let

$$
g(\xi) = \beta T(r = a, \theta(\xi)) + \gamma
\tag{3.125}
$$

where either $T \equiv 0$ in the case of constant temperature or it can be evaluated using (3.120).

Hence the equation in the conformally transformed coordinate is

$$
\begin{cases}
\Delta C = 0, & (\xi, \zeta) \in \Omega_{\xi, \zeta} \\
\frac{\partial C}{\partial \xi} = 0, & \text{on } \xi = 0, \pi \; ; \; \zeta < \zeta_L \\
C = 0, & \text{on } \xi = 0, \pi \; ; \; \zeta > \zeta_L \\
C = g(\xi), & \text{on } \zeta = 0
\end{cases}
\tag{3.126}
$$

On the first try, we can use the eigenfunction bases of the Laplace operator to write the solution to Equation (3.126) as follows

$$
\begin{cases}
C(\xi, \zeta) = e_0 - b\zeta + \sum\limits_{n=1}^{\infty} (e_n \cosh(n\zeta) + b_n \sinh(n\zeta)) \cos(n\xi), & \zeta < \zeta_L \\
C(\xi, \zeta) = \sum\limits_{n=1}^{\infty} d_n e^{-n\zeta} \sin(n\xi), & \zeta > \zeta_L
\end{cases}
\tag{3.127}
$$

where $\{b_n\}_{n=0}^{\infty}$, $\{d_n\}_{n=0}^{\infty}$ are unknown coefficients and $\{e_n\}_{n=0}^{\infty}$ are coefficients from the cosine expansion of $g(\xi)$

$$
g(\xi) = \sum_{n=0}^{\infty} e_n \cos(\xi).
\tag{3.128}
$$

To solve for the unknown coefficients, we need to impose the following "gluing conditions" at $\zeta = \zeta_L$

$$
[C] = [C]_{\zeta} = 0
\tag{3.129}
$$

The process is algebraically involved and not our ultimate goal anyway. Therefore, we will not solve it fully. Later in Section 3.2.2.8 we will specifically solve for b_0 as a sanity check for the analytical solution. For now, we make the observation that if we try to compute the non-dimensional, total material flux $\mathscr{F}_T$ across the interface $r = a$ (or $\zeta = \zeta_L$) using

Equation (3.127) for $\zeta < \zeta_L$, we obtain

$$\mathscr{F}_T \propto \int_0^\Phi \frac{\partial C}{\partial r}\Big|_{r=a} d\theta \propto \int_0^\pi \frac{\partial C}{\partial \zeta}\Big|_{\zeta=\zeta_L} d\zeta \tag{3.130}$$

$$= -b\pi + \sum_{n=1}^\infty (e_n n \sinh(n\zeta) + b_n n \cosh(n\zeta) \int_0^\pi \cos(n\xi) d\xi \tag{3.131}$$

$$= -b\pi \tag{3.132}$$

where $\int_0^\infty \cos(n\xi) d\xi \equiv 0$ for all n. Later in Section 3.2.2.6, we will derive the precise expression for $\mathscr{F}_T$

> *Hence the only term that contributes to the material flux*
>
> *across the interface in the solution to Equation (3.126) is $-b\zeta$,* $\tag{3.133}$
>
> *which is logarithmic in r*

The insight of (3.133) would aid our search of analytical solution in the sections to follow.

3.2.2.2 Searching for Analytical Solution: a Second Conformal Mapping

The main approach towards an analytical solution is via a series of arguments in complex analysis. To do so, we perform yet another conformal transformation to a new complex coordinate $\hat{z}$ via the mapping[8]

$$\hat{z} = \hat{x} + i\hat{y} = \hat{r}e^{i\hat{\theta}} = \left(\frac{r}{a}\right)^{-\frac{\pi}{\Phi}} \exp\left(\frac{i\pi\theta}{\Phi}\right) \tag{3.134}$$

so that $\hat{r} = \left(\frac{r}{a}\right)^{-\frac{\pi}{\Phi}}$ and $\hat{\theta} = \frac{\pi\theta}{\Phi}$. Note the following connection between the two conformal transformations in Equation (3.122) and (3.134):

$$\hat{\theta} = \xi \tag{3.135}$$

$$\hat{r} = \exp(-\zeta) \tag{3.136}$$

In the coordinate of $\hat{z}$, the domain $\{(r,\theta)|r > a, 0 \le \theta \le \Phi\}$ becomes an upper semi-circle, $\{(\hat{r},\hat{\theta})|\hat{r} < 1, 0 \le \hat{\theta} \le \pi\}$ (See Figure B-9c). The interface $r = a$ becomes $\hat{r} = 1$, while

---

[8]Once again the hat notation has nothing to do with the Fourier transforms defined in the earlier sections. Too bad we aren't using Cyrillic, Arabic, or Hebrew letters. Even Chinese characters would help...

the length of wedge L_w becomes $\hat{L}_w = \left(\frac{L_w}{a}\right)^{-\frac{\pi}{\Phi}}$. Let $\hat{\Delta}$ be the Laplace operator in the new coordinate and define $g\left(\hat{\theta}\right)$ to be the value of C at the interface $\hat{r} = 1$, so that $g\left(\hat{\theta}\right) = \beta T\left(r = a, \theta = \frac{\hat{\theta}\Phi}{\pi}\right) + \gamma$ (same as Equation (3.125)). In this way, the equation of concentration can be rewritten as

$$
\begin{cases}
\hat{\Delta} C = 0, & \hat{r} < 1, \hat{y} > 0 \\
\frac{\partial \hat{C}}{\partial \hat{\theta}} = 0, & \text{on } \hat{y} = 0, \hat{L}_w < \hat{r} < 1 \\
\hat{C} = 0, & \text{on } \hat{y} = 0, \hat{r} < \hat{L}_w \\
C = g\left(\hat{\theta}\right), & \hat{r} = 1
\end{cases}
\tag{3.137}
$$

In the coordinate of $\hat{z}$, we seek a function $F(\hat{z})$ such that[9]

$$
C = Re(F(\hat{z})) \tag{3.138}
$$

Here F is analytic in the upper unit disk and satisfies the following properties

1. $Re(F(\hat{z})) = g\left(\hat{\theta}\right)$ for $\hat{z} = e^{i\hat{\theta}}$

2. The imaginary part of F is constant on each of the intervals along the real axis: $\hat{z} = \hat{x}$ either $-1 < \hat{x} < -\hat{L}_w$ or $\hat{L}_w < \hat{x} < 1$. Note that the constants on the two interval pieces may not necessarily be identical.

Here is a short proof of Item 2 of the above list

Proof. The homogeneous Neumann boundary $\left(\frac{\partial \hat{C}}{\partial \hat{\theta}} = 0\right)$ condition on $\hat{y} = 0, \hat{L}_w < \hat{r} < 1$ translates to a vanishing normal derivative of $\hat{C} = Re(F)$ along the real axis on $-1 < \hat{x} < -\hat{L}_w$ and $\hat{L}_w < \hat{x} < 1$. By Cauchy-Riemann equation, this is equivalent to the vanishing of the tangential derivative of the imaginary part of F. Hence, along the real axis over those two intervals, F is separately constant. $\square$

Now because of the insight derived in (3.133), we are motivated to split F into two parts: $F = F_1 + F_2$, where F_1 contributes to the overall material flux proportional to $b_0 \pi$ as shown in Equation (3.130) and F_2 that does not contribute to the flux.

The next two sections detail the ansatzs for F_1 and F_2.

---

[9]Here Re stands for the real part of a function, not the notation for Reynolds number which will be used in Chapter 4

3.2.2.3 Forming Ansatz for F_1 : Dirichlet-to-Neumann Map and Branch Cut of Square Root

We present the ansatz on F_1. First we realize that the switch from Neumann to Dirichlet boundary condition at $\hat{r} = \hat{L}_w, \hat{y} = 0$ must trigger a singularity in the solution. We surmise that the nature of the singularity is the branch point of a complex square root. This is because the complex square root experiences a multiplicative factor of $e^{i\pi/2} = i$ when going across a branch point. This factor would make what used to be real for F imaginary and what was imaginary real. It would also naturally explain the shift in the boundary from constant imaginary to zero real as $\hat{r}$ transitions from smaller larger than 1 to smaller than 1. This leads to the ansatz that part of the solution must contain $\sqrt{\hat{z}^2 - \hat{L}_w^2}$. Secondly, we leverage the insight derived from (3.133) that there must be a term that looks like the log of a function of r and equivalently in $\hat{r}$, since such function would contribute to the overall material flux across the interface. As a result, F_1 must look like the $\log(something)$ where the *something* involves $\sqrt{\hat{z}^2 - \hat{L}_w^2}$. This *something* must also satisfy (i) being real for $\hat{z} > \hat{L}_w$, (ii) $|something| = 1$ for $-\hat{L}_w < \hat{z} < \hat{L}_w$, and (iii) has a constant argument for $\hat{z} < \hat{L}_w$. After many trials and errors, we reach the ansatz that F_1 is

$$F_1 = b \log \left(\frac{\hat{z} + \sqrt{\hat{z}^2 - \hat{L}_w^2}}{\hat{L}_w} \right) \tag{3.139}$$

where b is a real constant to be determined. Here we use the branch cut that the logarithm is real and positive for $\hat{z} > \hat{L}_w$. We immediately observe the following properties of F_1.

- F_1 is analytic in the upper unit disk

- F_1 is real and positive for $\hat{z}$ real and $\hat{z} > \hat{L}_w$. Hence $Im(F_1) = 0$ (constant) on the real interval $\hat{L}_w < \hat{z} < 1$

- $F_1 = b\pi$ for $\hat{z} < -\hat{L}_w$ real due to the jump in the branch point. Thus $Im(F_1)$ is constant on the real interval $\hat{z} < -\hat{L}_w$

Note that computationally, in order to have the right jump at the branch points, we should evaluate $\sqrt{\hat{z}^2 - \hat{L}_w^2} = \sqrt{\hat{z} - \hat{L}_w}\sqrt{\hat{z} + \hat{L}_w}$ and use principal values for the square roots and the logarithm.

3.2.2.4   Forming Ansatz for F_2: Double Singularities

We now present the ansatz on F_2. As argued before, the switch from Neumann to Dirichlet boundary conditions must trigger a singularity whose underlying nature is the branch point of a complex square root. Hence F_2 must contain $\sqrt{\hat{z}^2 - \hat{L}_w^2}$. In addition, we observe the semi-analytical expansion of C in Equation (3.127): except for the term linear in ζ that contributes to the overall flux, the rest does not and therefore should correspond to F_2. The solution that satisfies the data at $\zeta = \zeta_L$ and Neumann all the way to $\zeta = 0$ should not have any singularities. The solution that satisfies the data at $\zeta = \zeta_L$ and allow the transition to Dirichlet beyond $\zeta = \zeta_L$ should demonstrate some singular behavior. Since Equation (3.127) shows that this part of the solution consists of sine series, it should correspond to a component in F_2 of the form $\sum (some\ coefficients)(\hat{z}^n - \hat{z}^{-n})$. Hence, F_2 needs a singularity not only at $\hat{z} = \pm\hat{L}_w$, but also $\hat{z} = \pm 1/\hat{L}_w$. This leads to the ansatz that $F_2 \propto \sqrt{\hat{z}^2 - \hat{L}_w^2}\sqrt{\hat{z}^{-2} - \hat{L}_w^2}$. We let that proportionality quantity be $G(\hat{z})$, whence

$$F_2 = G(\hat{z})\sqrt{\left(\hat{z}^2 - \hat{L}_w^2\right)\left(\hat{z}^{-2} - \hat{L}_w^2\right)} = G(\hat{z})S(\hat{z}) \tag{3.140}$$

where G is analytic in the upper unit disk $S(\hat{z}) = \sqrt{\left(\hat{z}^2 - \hat{L}_w^2\right)\left(\hat{z}^{-2} - \hat{L}_w^2\right)}$. Moreover,

$$We\ impose\ the\ following\ conditions\ on\ G\ and\ S \tag{3.141}$$

1. We place the branch cuts for S in the lower half plane and select the branch so that, for $\hat{z}$ real, $S(\hat{z}) > 0$ for $\hat{L}_w < S(\hat{z}) < 1/\hat{L}_w$. Then S is purely positive imaginary for $0 < \hat{z} < \hat{L}_w$, purely negative imaginary for $-\hat{L}_w < \hat{z} < 0$, and $S(\hat{z}) > 0$ for $-1/\hat{L}_w < \hat{z} < -\hat{L}_w$

2. $G(\hat{z})$ is real along the real axis;

3. $G(0) = 0$. This condition is necessary to cancel out the simple pole that S has at the origin.

3.2.2.5   Solving for b and $G(\hat{z})$: a Riemann-Hilbert Problem

We are going to solve for b in F_1 of Equation (3.139) and $G(\hat{z})$ in Equation (3.140). For note that if we define the values the real part of $F_1(\hat{z})$ and $F_2(\hat{z})$ on the perimeter of the

upper semi-circle $\hat{z} = e^{i\hat{\theta}}$ as g_1 and g_2, respectively, such that

$$g_1\left(\hat{\theta}\right) = Re\left(F_1\left(e^{i\hat{\theta}}\right)\right) = b\log\left|\frac{e^{i\hat{\theta}} + \sqrt{e^{2i\hat{\theta}} - \hat{L}_w^2}}{\hat{L}_w}\right| \tag{3.142}$$

$$g_2\left(\hat{\theta}\right) = Re\left(G(\hat{z})\right)s(\hat{\theta}) \tag{3.143}$$

where $s(\hat{\theta}) = \sqrt{1 - 2\hat{L}_w^2\cos\left(2\hat{\theta}\right) + \hat{L}_w^4}$. We note that since $C = Re(F_1 + F_2)$, it must be that

$$g = g_1 + g_2 \tag{3.144}$$

for g is the boundary condition of C at $\hat{r} = 1$.

Now if we extend g_2 to the entire circle, even in $\hat{\theta}$, Equation (3.143) yields a classical Riemann-Hilbert problem on the unit circle for G. As a result, the expression for G becomes

$$G\left(\hat{z}\right) = \frac{1}{2\pi i}\oint\frac{\eta + \hat{z}}{\eta - \hat{z}}\frac{g_2(\phi)}{s(\phi)}d\phi + i\alpha \tag{3.145}$$

where $\eta = e^{i\phi}$, $\hat{z} = re^{i\phi}$ and α is some real constant. To prove Equation (3.145), we use the following calculation

Proof. Let $g_2(\hat{\theta})/s(\hat{\theta})$ have the following Fourier expansion: $g_2(\hat{\theta})/s(\hat{\theta}) = \sum\limits_{n=-\infty}^{\infty} f_{2,n}e^{in\hat{\theta}}$, where

$$f_{2,n} = \frac{1}{2\pi}\int_0^{2\pi}\frac{g_2(\eta)}{s(\eta)}e^{-in\eta}d\eta \tag{3.146}$$

However, since g_2 is real, the complex conjugate of $g_{2,n}$ must be $g_{2,-n}$, whence

$$g_2(\hat{\theta})/s(\hat{\theta}) = f_{2,0} + 2Re\left(\sum_{n=1}^{\infty}f_{2,n}e^{in\hat{\theta}}\right) \tag{3.147}$$

where $f_{2,0} = \frac{1}{2\pi}\int_0^{2\pi}\frac{g_2(\eta)}{s(\eta)}d\eta$ is real. Hence, by inspection we can write define $G(\hat{z})$ as

$$G(\hat{z}) = f_{2,0} + 2\sum_{n=1}^{\infty}f_{2,n}\hat{z}^n + i\alpha \tag{3.148}$$

for any $\alpha \in \mathbb{R}$. In this way, $Re(G(\hat{z}))|_{\hat{z}=e^{i\hat{\theta}}} = g_2(\hat{\theta})/s(\hat{\theta})$ defined in Equation (3.147). Finally, we clean up the expression of G by plugging Equation (3.146) into Equation (3.148)

$$G(\hat{z}) = f_{2,0} + 2\sum_{n=1}^{\infty} \hat{z}^n \frac{1}{2\pi} \int_0^{2\pi} \frac{g_2(\eta)}{s(\eta)} e^{-in\eta} d\eta + i\alpha \tag{3.149}$$

$$= \frac{1}{\pi} \int_0^{2\pi} \frac{g_2(\eta)}{s(\eta)} \left(\sum_{n=1}^{\infty} \hat{z}^n e^{-in\eta} + \frac{1}{2} \right) d\eta + i\alpha \tag{3.150}$$

$$= \frac{1}{\pi} \int_0^{2\pi} \frac{g_2(\eta)}{s(\eta)} \left(\frac{1}{1 - \hat{z}e^{-in\eta}} + \frac{1}{2} \right) d\eta + i\alpha \tag{3.151}$$

$$= \frac{1}{2\pi} \int_0^{2\pi} \frac{g_2(\eta)}{s(\eta)} \frac{e^{in\eta} + \hat{z}}{e^{in\eta} - \hat{z}} d\eta + i\alpha \tag{3.152}$$

which completes the proof $\qquad\qquad\square$

Now because of Item 3 of Condition (3.141), $G(0) = 0$, which means that (i) $\alpha = 0$ and (ii)

$$\int_{-\pi}^{\pi} \frac{g_2(\phi)}{s(\phi)} d\phi = 0 \tag{3.153}$$

Substituting $g_2 = g - g_1$ as in Equation (3.144), we have that

$$\int_{-\pi}^{\pi} \frac{g(\phi) - g_1(\phi)}{s(\phi)} d\phi = 0 \tag{3.154}$$

from which we can finally find an expression for b by plugging in Equation (3.142)

$$0 = \int_{-\pi}^{\pi} \frac{g(\phi) - b\log\left|\frac{e^{i\phi}+\sqrt{e^{2i\phi}-\hat{L}_w^2}}{\hat{L}_w}\right|}{s(\phi)} d\phi \tag{3.155}$$

$$b = \frac{\int_{-\pi}^{\pi} \frac{g(\phi)}{s(\phi)} d\phi}{\int_{-\pi}^{\pi} \frac{1}{s(\phi)} \log\left|\frac{e^{i\phi}+\sqrt{e^{2i\phi}-\hat{L}_w^2}}{\hat{L}_w}\right| d\phi} \tag{3.156}$$

Equation (3.156) and (3.145) complete the expressions for F_1 and F_2 in Equation (3.139) and (3.140), which solves completely analytically the main non-dimensionalized concentration equation in (3.121) and its conformally transformed equivalent (3.137).

In the next two sections, we will leverage these exact solutions to calculate the normal flux along the interface and total integrated flux throughout the interface. The radial flux

72

determines the amount of liquid vaporized per unit of time at every point along the liquid-vapor interface, while the total flux is the total amount of vaporized liquid along the entire interface. These two quantities are of high interest for various engineering applications, and will aid our calculation of lifetime later in Section 3.3.

3.2.2.6 Calculation of Total Flux Across the Interface: a Simple Exercise in Complex Analysis

In this section we show how to compute the total material flux, which happens to be easier than calculating the normal flux at each point along the interface. Let $\tilde{F}_T$ be the dimensional total material flux across the interface[10] located at $\tilde{r} = \tilde{a}$. Then $\tilde{F}_T$ can be written as

$$\tilde{\mathscr{F}}_T = \int_0^\Phi \frac{\partial \tilde{C}}{\partial \tilde{r}} \Big|_{\tilde{r}=\tilde{a}} \tilde{a} d\theta \tag{3.157}$$

Using the nondimensionalization of $\tilde{C}$, $\tilde{r}$, and $\tilde{a}$ in Equation (3.4)-(3.7), we can write down the non-dimensional total flux, $\mathscr{F}_T$, such that

$$\tilde{\mathscr{F}}_T = DC_c\mathscr{F}_T \tag{3.158}$$

and

$$\mathscr{F}_T = \int_0^\Phi \frac{\partial C}{\partial r} \Big|_{r=a} a d\theta \tag{3.159}$$

We are interested in computing both $\mathscr{F}_T$ and $\frac{\partial C}{\partial r}$.

First, we note that computing $\mathscr{F}_T$ is much easier than $\frac{\partial C}{\partial r}$. This is because we can use the property of function F in Equation (3.138) to simplify the integral as

$$\mathscr{F}_T = \int_0^\Phi \frac{\partial C}{\partial r} \Big|_{r=a} a d\theta \tag{3.160}$$

$$= \int_0^\pi \frac{\partial}{\partial \hat{r}} Re\left(F\right) \Big|_{\hat{r}=1} a d\hat{\theta} \tag{3.161}$$

where the hat notations indicate the conformally transformed coordinate introduced in Equa-

---

[10]Recall that variables with tildes carry physical units

tion (3.134). But once again, by the Cauchy-Riemann condition, $\frac{\partial Re(F)}{\partial \hat{r}} = \frac{\partial Im(F)}{\partial \hat{\theta}}$. Hence,

$$\mathcal{F}_T = -\int_0^\pi \frac{\partial Im(F)}{\partial \hat{\theta}}\Big|_{\hat{r}=1} d\hat{\theta} \tag{3.162}$$

$$= -\left(Im(F)|_{\hat{\theta}=\pi,\hat{r}=1} - Im(F)|_{\hat{\theta}=0,\hat{r}=1}\right) \tag{3.163}$$

$$= -b\pi \tag{3.164}$$

which agrees with the semi-analytical solution in Equation (3.132). Here b is defined in Equation (3.156)

3.2.2.7 Calculation of Normal Flux: Computational Shortcut of G and G' via Fourier Series

The dimensionless normal flux along the interface is defined as the radial derivative of concentration, $\frac{\partial C}{\partial r}$. This computation requires the differentiation of F_1 and F_2, which, in particular, would require the evaluation of $G(\hat{z})$ and $G'(\hat{z})$. Equation (3.145) provides an explicit but computationally inconvenient formula for G. Instead we leverage the Fourier series of $G(\hat{z})$, first shown in Equation (3.148) in the presentation of the Riemann-Hilbert problem solution:

$$G(\hat{z}) = f_{2,0} + 2\sum_{n=1}^\infty f_{2,n}\hat{z}^n \tag{3.165}$$

where we recall that $\alpha = 0$ and $f_{2,n}$ are the Fourier coefficients of g_2/s_2 defined in Equation (3.146). Hence, we can compute G' as

$$G(\hat{z}) = 2\sum_{n=1}^\infty nf_{2,n}\hat{z}^{n-1} \tag{3.166}$$

Now to compute $\frac{\partial C}{\partial r}$, we just have to crank through some nasty but straightforward algebra based on the analytical expression of C. In the end, we get

$$\frac{\partial C(r,\theta)}{\partial r} = \frac{-\pi}{a\Phi}\left(\frac{r}{a}\right)^{-\frac{\pi}{\Phi}-1} Re\left(\frac{\partial F_1}{\partial \hat{r}} + \frac{\partial F_2}{\partial \hat{r}}\right) \tag{3.167}$$

where using the formula for F_1 in Equation (3.139), we obtain

$$\frac{\partial F_1}{\partial \hat{r}} = b \frac{1 + (\hat{z}^2 - \hat{L}_w^2)^{-1/2} \hat{z}}{\hat{z} + \sqrt{\hat{z}^2 - \hat{L}_w^2}} \tag{3.168}$$

and where we use the formula for F_2 in Equation (3.140) to obtain

$$\frac{\partial F_2}{\partial \hat{r}} = G(\hat{z}) S'(\hat{z}) + G'(\hat{z}) S(\hat{z}) \tag{3.169}$$

Now the final piece is to properly compute S and S' that respect the choice of branch cuts made in Item 1 of (3.141). Some calculations show that using the principal values of the complex square root would render the following formula compliant to the branch choice

$$S(\hat{z}) = \sqrt{\hat{z} - \hat{L}_w} \sqrt{\hat{z} + \hat{L}_w} \sqrt{\hat{z}^{-1} + \hat{L}_w} \sqrt{\hat{z}^{-1} - \hat{L}_w} \tag{3.170}$$

Hence, if we define $h(\eta) := \sqrt{\eta}$ as the complex square root using the principal value and $h'(\eta) = \frac{1}{2} \eta^{-1/2}$ as its derivative, we can compute S as

$$\begin{aligned}
S'(\hat{z}) = & \ h'\left(\hat{z} - \hat{L}_w\right) h\left(\hat{z} + \hat{L}_w\right) h\left(\hat{z}^{-1} - \hat{L}_w\right) h\left(\hat{z}^{-1} + \hat{L}_w\right) \\
& + h\left(\hat{z} - \hat{L}_w\right) h'\left(\hat{z} + \hat{L}_w\right) h\left(\hat{z}^{-1} - \hat{L}_w\right) h\left(\hat{z}^{-1} + \hat{L}_w\right) \\
& + \frac{-1}{\hat{z}^2} h\left(\hat{z} - \hat{L}_w\right) h\left(\hat{z} + \hat{L}_w\right) h'\left(\hat{z}^{-1} - \hat{L}_w\right) h\left(\hat{z}^{-1} + \hat{L}_w\right) \\
& + \frac{-1}{\hat{z}^2} h\left(\hat{z} - \hat{L}_w\right) h\left(\hat{z} + \hat{L}_w\right) h\left(\hat{z}^{-1} - \hat{L}_w\right) h'\left(\hat{z}^{-1} + \hat{L}_w\right)
\end{aligned} \tag{3.171}$$

3.2.2.8 Sanity Check Using a Semi-Analytical Method

Here we perform a quick sanity check on the analytical solution by comparing the analytically computed b in Equation (3.156) with the one in the semi-analytical infinite series solution in Equation (3.127). To do that, we first set up a framework for computing b semi-analytically.

On the first try, we are tempted to work directly with Equation (3.129). The calculation is way too involved. To simplify the calculation, we introduce $C^{(n)}(\xi, \zeta)$, where $n = 0, 1, 2, 3...$, which is almost identical to Equation (3.126) except that at $\zeta = 0$, it satisfies $\cos(n\xi)$. In other words, we are solving Equation (3.126) for each harmonic of $g(\xi)$. Then b should be a linear combination of the corresponding coefficient in the solution of

each harmonic. Specifically, we define $C^{(n)}$, where $n = 0, 1, 2, ...$, as

$$\begin{cases} \Delta C^{(n)} = 0, & 0 \le \xi \le \pi, \zeta > 0 \\ \frac{\partial C^{(n)}}{\partial \xi} = 0, & \text{on } \xi = 0, \pi \; ; \; \zeta < \zeta_L \\ C^{(n)} = 0, & \text{on } \xi = 0, \pi \; ; \; \zeta > \zeta_L \\ C^{(n)} = \cos(n\xi), & \text{on } \zeta = 0 \end{cases} \tag{3.172}$$

where we impose the condition on $C^{(n)}$ at $\zeta = 0$ with $\cos(n\xi)$, where $n = 0, 1, 2, 3$. Then by the same token, we can write down the solution to Equation (3.172) as

$$\begin{cases} C^{(n)}(\xi, \zeta) = \cosh(n\zeta)\cos(n\xi) - b^{(n)}\zeta + \sum\limits_{m=1}^{\infty} b_m^{(n)}\sinh(m\zeta)\cos(m\xi), & \zeta < \zeta_L \\ C^{(n)}(\xi, \zeta) = \sum\limits_{m=1}^{\infty} d_m^{(n)}e^{-m\zeta}\sin(m\xi), & \zeta > \zeta_L \end{cases} \tag{3.173}$$

Then b can be computed as

$$b = \sum_{n=0}^{\infty} e_n b^{(n)} \tag{3.174}$$

where e_n is the Fourier cosine coefficients of g defined in Equation (3.128).

Secondly, we are now tempted to apply the gluing condition $\left[C^{(n)} \right] = \left[C^{(n)} \right]_\zeta = 0$ on Equation (3.173) to solve for $b^{(n)}$. However, doing so would render the problem numerically ill-conditioned. This is because the terms $\cos(nx)\sinh(ny)$ grow exponentially from $\zeta = 0$ to $\zeta = \zeta_L$ and therefore a very small change in b_n would cause huge changes in the product for m large. To fix the issue, we need to encode into the system the fact that b_n decays faster than $\sinh(n\zeta)$ grows. This leads us to the following modified solution

$$C^{(n)}(\xi, \zeta) = \begin{cases} -\frac{1}{\zeta_L} B_0^{(n)}e^{-n\zeta_L}\zeta + e^{-n\zeta}\cos(n\xi) + \sum\limits_{m=1}^{\infty} A_m^{(n)} \frac{\sinh(m\zeta)}{\sinh(m\zeta_L)}\cos(m\xi)e^{-n\zeta_L}, & \zeta < \zeta_L \\ \sum\limits_{k=1}^{\infty} D_k^{(n)}\sin(k\xi)e^{-k(\zeta-\zeta_L)-n\zeta_L}, & \zeta > \zeta_L \end{cases}$$

$$\tag{3.175}$$

and so once we solve for B_0, we can write as $b^{(n)}$

$$b^{(n)} = \frac{1}{\zeta_L} B_0 e^{-n\zeta_L} \tag{3.176}$$

One last step before we can apply the gluing condition to Equation (3.175) is to change basis of the sine series. We let

$$\sin(k\xi) = \frac{2}{\pi} \sum_{m=0}^{\infty} \chi_{km} \cos(m\xi) \tag{3.177}$$

where $\chi_{km} = \frac{\pi}{2} \int_0^\pi \sin(k\xi) \cos(m\xi)$. Some straightforward calculation can show that

$$\chi_{km} = \begin{cases} 0, & k+m \text{ is even} \\ 1/k, & k \text{ is odd and } m = 0 \\ 2m/(k^2 - m^2), & k+m \text{ is odd and } m \neq 0 \end{cases} \tag{3.178}$$

Hence, if we now apply $[C^{(n)}]_{\zeta=\zeta_L} = 0$ and $[C_\zeta^{(n)}]_{\zeta=\zeta_L} = 0$, we obtain

$$-B_0^{(n)} + \cos(n\xi) + \sum_{m=1}^{\infty} A_m^{(n)} \cos(m\xi) = \sum_{m=0}^{\infty} \sum_{k=1}^{\infty} D_k^{(n)} \frac{2}{\pi} \chi_{km} \cos(m\xi) \tag{3.179}$$

$$-\frac{1}{\zeta_L} B_0^{(n)} - n\cos(n\xi) + \sum_{m=1}^{\infty} A_m^{(n)} m \coth(m\zeta_L) \cos(m\xi) = \sum_{m=0}^{\infty} \sum_{k=1}^{\infty} D_k^{(n)} \frac{2}{\pi} (-k) \chi_{km} \cos(m\xi) \tag{3.180}$$

Matching the same order of m, we have that for $m = 0$,

$$-B_0^{(n)} + \delta_{n0} = \sum_{k=1}^{\infty} D_k^{(n)} \frac{2}{\pi} \chi_{k0} \tag{3.181}$$

$$-\frac{1}{\zeta_L} B_0^{(n)} = \sum_{k=1}^{\infty} D_k^{(n)} \frac{2}{\pi} (-k) \chi_{k0} \tag{3.182}$$

$$\tag{3.183}$$

where δ_{nm} represents the Kronecker delta. If we multiply the first equation by $-1/\zeta_L$ before

77

adding to the second equation, we get that

$$\sum_{k=1}^{\infty} D_k^{(n)} \frac{2}{\pi} \left(-k - \frac{1}{\zeta_L} \right) \chi_{k0} = -\frac{1}{\zeta_L} \delta_{n0} \tag{3.184}$$

$$\sum_{k=1}^{\infty} D_k^{(n)} \frac{2}{\pi} \left(k + \frac{1}{\zeta_L} \right) \chi_{k0} = \frac{1}{\zeta_L} \delta_{n0} \tag{3.185}$$

and for $m > 0$, we have that

$$A_m^{(n)} + \delta_{nm} = \sum_{k=1}^{\infty} D_k^{(n)} \frac{2}{\pi} \chi_{km} \tag{3.186}$$

$$A_m^{(n)} m \coth(m\zeta_L) - n\delta_{nm} = \sum_{k=1}^{\infty} D_k^{(n)} \frac{2}{\pi} \chi_{km}(-k) \tag{3.187}$$

If we multiply the first equation by $-m \coth(m\zeta_L)$ before adding to the second equation, we get that

$$\delta_{nm}(n + m \coth(m\zeta_L)) = \sum_{k=1}^{\infty} D_k^{(n)} \frac{2}{\pi} \chi_{km}(k + m \coth(m\zeta_L)) \tag{3.188}$$

So here we shall define the matrix $A^{(n)}$, vector $\vec{D}^{(n)}$, and vector $\vec{l}^{(n)}$ such that

$$A_{mk}^{(n)} = \begin{cases} \frac{2}{\pi} \left(k + \frac{1}{\zeta_L} \right) \chi_{k0}, & m = 0 \\ \frac{2}{\pi} \chi_{km}(k + m \coth(m\zeta_L)), & m > 0 \end{cases} \tag{3.189}$$

$$\vec{l}^{(n)} = \begin{cases} \frac{1}{\zeta_L} \delta_{n0}, & m = 0 \\ \delta_{nm}(n + m \coth(m\zeta_L)), & m > 0 \end{cases} \tag{3.190}$$

$$\vec{D}^{(n)} = (D_1^{(n)}, D_2^{(n)}, ..., D_k^{(n)}, ...)^T \tag{3.191}$$

Hence, the matrix $\vec{D}^{(n)}$ can be expressed as

$$\vec{D}^{(n)} = \left(A^{(n)} \right)^{-1} \vec{l}^{(n)} \tag{3.192}$$

Using the above expression for $D^{(n)}$, we can leverage Equation (3.181) to write $B_0^{(n)}$ as

$$B_0^{(n)} = \delta_{n0} - \sum_{k=1}^{\infty} \vec{D}_k^{(n)} \frac{2}{\pi} \chi_{k0} \tag{3.193}$$

78

and so according to Equation (3.176), we can write $b^{(n)}$

$$b^{(n)} = \frac{\delta_{n0}e^{-n\zeta_L}}{\zeta_L} - \frac{e^{-n\zeta_L}}{\zeta_L}\sum_{k=1}^{\infty}\vec{D}_k^{(n)}\frac{2}{\pi}\chi_{k0} \tag{3.194}$$

which, coupled with Equation (3.174), enables us to write an infinite series expression for b

$$b = \sum_{n=0}^{\infty}e_n\frac{e^{-n\zeta_L}}{\zeta_L}\left(\delta_{n0} - \sum_{k=1}^{\infty}\vec{D}_k^{(n)}\frac{2}{\pi}\chi_{k0}\right) \tag{3.195}$$

$$\approx \sum_{n=0}^{N}e_n\frac{e^{-n\zeta_L}}{\zeta_L}\left(\delta_{n0} - \sum_{k=1}^{\infty}\vec{D}_k^{(n)}\frac{2}{\pi}\chi_{k0}\right) := b_N \tag{3.196}$$

for some integer cutoff N. We compare the semi-analytical form of b_N in Equation (3.196) with the analytical form of b in Equation (3.156) for each N via the following error norm

$$err_b(N) = |b_N - b| \tag{3.197}$$

3.3 Lifetime of Evaporating Liquid

With the analytical form of vapor concentration, we can derivative the evaporation time analytically as well. To do so, we first write down the relation between flux and loss of mass over an increment of time $d\tilde{t}$[11]:

$$\int_0^{\Phi}D\frac{d\tilde{C}}{d\tilde{r}}|_{\tilde{r}=\tilde{a}}\tilde{a}d\theta d\tilde{t} = \rho_1\tilde{a}\Phi d\tilde{a} \tag{3.198}$$

from which we can derive the expression for the lifetime of the liquid channel:

$$\tilde{t} = \rho_1\Phi a_0\int_0^1\frac{da}{D\int_0^{\Phi}\frac{\partial\tilde{C}}{\partial\tilde{r}}|_{\tilde{r}=\tilde{a}}d\theta} \tag{3.199}$$

Finally, recalling the rescaling of evaporation time in (3.7), we can write down the evaporation of time in terms of its dimensionless quantity t as

$$\tilde{t} = \frac{\rho_1 a_0^2}{DC_{\infty}}t \tag{3.200}$$

---

[11]Recall that all variables with tildes ($\sim$) carry physical units

where

$$t = \frac{\Phi C_\infty}{\pi(C_{sat}(T_0) - HC_\infty)} \int_0^1 \frac{a}{b} da \qquad (3.201)$$

Here b is the analytically derived expression in Equation (3.156).

3.3.1 Parameter Choice

Unless explicitly stated or varied, all parameters are chosen from Table A.1. We use water as the liquid to fill the channel with air above.

3.4 Discussion

3.4.1 Temperature Profiles

We present the solution (3.12) to the temperature problem of a linearly decreasing boundary in Equation (3.10) in Figure B-10. Here we take the height of the liquid to be $a = 1$ and $\nu_2/\nu_1 = 1000$. The ratio represents an extreme and unphysical limit only to exacerbate the singularity at $r = a$ and demonstrate the power of the PSM. Figure B-10a shows the heat map. Temperature decreases as r gets large, which is consistent with the imposed, linearly decreasing boundary condition. Also, for a fixed radius, temperature is higher closer to the boundary walls than towards the center. This contributes to the higher material flux near the boundary, which we will discuss later. On the other hand, Figure B-10b plots temperature against radius for various values of Φ's. Despite that the temperature expressions in Equation (3.116) and equivalently the singularity-extracted form in Equation (3.117) are piece-wise defined in between $r = 1/L_w, r = 1, r = L_w$, there is no discontinuity at $r = 1/L_w$ or $r = L_w$. The only discontinuity, as expected, occurs at the liquid-vapor interface $r = a = 1$ where materials of two different properties intersect.

3.4.2 Convergence of the Analytical and Semi-Analytical Concentration Solutions

As a sanity check on the analytical solution, we leverage the semi-analytical computation of the parameter b in Equation(3.196) with an integer cutoff N and study its deviation from the analytical form in Equation (3.156) via the error norm defined in Equation (3.197). Fig-

ure B-11 plots $err_b(N)$ vs N on a log-log scale for both the constant and varied temperature scenarios. As one can see, the semi-analytical solution converges to the analytical solution, though the rate is slow and sub-linear. Since the semi-analytical solution is obtained via a completely different process, the fact that it converges to the analytical one reassures us of the correctness of the analytical solution.

3.4.3   Radial Fluxes and Total Fluxes

Figure B-12a shows the radial flux, $\frac{\partial C}{\partial r}$, which is defined in Equation (3.167). In particular, we see that there is higher amount of flux around the edges of the interface than the center. This is consistent with the profile of higher temperature closer to the wedge sides. In Figure B-12b and B-12c, we plot the total flux, defined in Equation (3.162) as a function of the interface height for different humidity levels and wedge angles. Overall, the total flux increases as the interface height increases due to the growing surface area exposed to the vapor region. In particular, Figure B-12b shows that as the air gets more humid, the amount of vaporizing liquid reduces and does so sharply as H gets close to 1. Similarly, in Figure B-12c, we see that as the angle increases, the surface area of the liquid grows, leading to a greater flux. This explains the upward shift of the curves as the angle gets larger. However, a bigger angle that results in more flux does not necessarily lead to a shorter lifetime. This will be elaborated in the next section.

3.4.4   Evaporation Times

Figure B-13a and Figure B-13b show the plots of dimensionless evaporation times in Equation (3.201) against the variations of the temperature gradient, humidity, wedge size, and wedge angle. Here we non-dimensionalize the measure of temperature gradient as the maximum temperature difference in the system relative to T_∞, namely $\Delta T_{max}/T_\infty$, where $\Delta T_{max} = T_0 - T_\infty$.

We see that in Figure B-13a, evaporation time increases as humidity increases across all levels of thermal gradients. This agrees with the physical intuition that the more humid the air, the harder it is to "dry out". Note that for constant temperature ($\Delta T_{max}/T_\infty = 0$), as H gets close to 1, lifetime approaches infinity. Indeed, examining the analytical expression (3.200) for lifetime, when $T_0 = T_\infty$ and $H = 1$, $t = \infty$. In the absence of external thermal drive, when vapor gets saturated in the air, the evaporation process stops. On a different

note, we plot lifetime against the thermal gradient for different humidity levels in Figure B-13b. We observe that the liquid takes less time to evaporate as temperature gradient increases, which also agrees with the physical intuition that heat accelerates evaporation. It is interesting to note that the impact of an increasing thermal gradient on lifetime is enhanced as humidity increases. As the air becomes more humid, thermal driving plays a bigger role in accelerating the evaporation of liquid. If we take the percentage change in lifetime between $\Delta T_{max}/T_\infty = 0$ and $\Delta T_{max}/T_\infty = 0.01$ in Figure B-13b) for each humidity level and plot the percentage against H, we uncover Figure B-13c: for a completely dry air ($H = 0$), an increase in $\Delta T_{max}/T_\infty$ from 0 to 0.01 results in only a 10% reduction in lifetime, whereas for $H = 0.95$, turning up the knob of $\Delta T_{max}/T_\infty$ by the same amount reduces the liquid's lifetime by more than 70%.

On the other hand, Figure B-13d and B-13e show how the geometry of the wedge affects lifetime. In B-13d, lifetime increases as the size of the wedge increase. Other things being equal, a larger wedge implies a higher temperature at the V-tip, which leads to a greater flux at the interface that reduces the lifetime. On the other hand, an larger wedge also moves the ambient atmosphere saturated with vapor away from the liquid, which elongates the lifetime. From the simulation, the effect of elongation dominates that of reduction on the evaporation of the liquid. Similarly, in B-13e, we note that lifetime increases as the wedge angle gets wider. A larger angle implies a greater material flux that consequently accelerates the evaporation. At the same time, for the same interface height, a bigger angle means more liquid mass, which increases linearly as the angle gets large. The fact that lifetime is positively linearly growing with the angle means that the effect of mass increase dominates that of flux increase as a result of widening the angle.

3.5   Conclusion

We analytically study the problem of 2D evaporation of a liquid bridge within a long V-shaped channel. The liquid bridge forms a 90° contact angle with the wedge sides. Slow quasi-static evaporation is assumed after thermal equilibrium is reached, so that the temperature is not affected by the latent heat released. To accommodate the $2D$ nature of the problem, we use an infinite wedge as our domain and transform what would be far-field conditions in 3D, to boundary conditions along the wedge sides. This series of assumptions

renders the concentration-temperature coupled equations in (3.3), which can be rescaled into the system (3.8). The solution for the temperature is found using a new analytical method, the Parity Split Method (PSM). The PSM explores the symmetry of the wedge geometry and splits the problem into sub-problems that do not contain the internal boundary conditions at the liquid-vapor interface. The temperature solution is then used as an input into the equation satisfied by the vapor concentration, and the resulting problem is solved using complex variable techniques.

After obtaining the solutions for the temperature and concentration analytically, we compute two quantities that are of significant interest in applications: the vapor flux at the interface, and the evaporation lifetime for the liquid. In particular, we study the behavior of the lifetime versus both: environmental variables (applied thermal gradient and ambient humidity), and wedge-geometric variables (wedge angle and wedge depth). A higher humidity increases lifetime, while a higher temperature lowers lifetime. Moreover, the lifetime reduction by the thermal effect increases as humidity gets larger. At the same time, the lifetime grows with both wedge angle and size.

Quite clearly, the model used here has several limitations. First, the artificial boundary conditions on both the temperature and concentration beyond the wedge sides ($\tilde{r} > \tilde{L}_w$) add some non-physical effects when the interface is too close to the end of the wedge. This can be seen in the temperature heat map in Figure B-10a, where the contour lines for $r > L_w := 2$ bend around the artificial extension of the wedge sides. This bending of the temperature contour lines inevitably causes a larger evaporative flux when the liquid-vapor interface gets too close to the top of the wedge. To avoid this problem, we keep the ratio a/L_w below 0.7. The second limitation arises because the contact angle must be 90° for the Parity Split Method to be applicable. Small corrections to this value would seem possible by the use of perturbation techniques. We are keen on exploring such perturbations.

Chapter 4

Preliminary Results on the Biharmonic Equation

4.1 Stokes Equations with Internal Boundary Boundary Conditions: Challenges and Opportunities

4.1.1 The Stokes Equation

The Stokes equations govern fluid flow when inertial forces can be neglected, so that the motion occurs as the balance between pressure, viscous, and body forces. Small-scale devices almost always operate in the Stokes flow regime, which is characterized by a small Reynolds number, $R_e \ll 1$, where: $R_e = \rho_0 \, U \, L / \nu_0$, ρ_0 is a typical density, U is a typical flow speed, L is a typical length scale, and ν_0 is a typical dynamic viscosity. The (dimensionless, constant density) Stokes flow equations, in the absence of body forces, are

$$\nabla p = \nu \, \Delta \vec{u} \quad \text{and} \quad \nabla \cdot \vec{u} = 0, \tag{4.1}$$

where $\nu = \tilde{\nu}/\nu_0$ is the dynamic viscosity, p is the pressure, and $\vec{u}$ is the flow velocity — all adimensional quantities. Note: because we will consider more than one fluid, we cannot use "the density" or "the viscosity" to produce adimensional quantities. Thus the equations above are valid in each fluid, with appropriate jump conditions across the interfaces — e.g.: continuity of the normal velocity and matching of stresses.

4.1.2 Axi-symmetric and 2D Stokes: Stream function Formulation

The Stokes equations allow 3D axi-symmetric solutions, which can written in terms of a stream function that satisfies a $2D$ problem. Using spherical coordinates [†] (r, θ, ϕ), these solutions (on any simply connected domain) can be written in the form

$$\vec{u} = \nabla \times \left(\Psi(r,\theta)\hat{\phi} \right), \tag{4.2}$$

where $\hat{\phi}$ denotes [†] the azimuthal unit vector, Ψ satisfies $\qquad E^2\,\Psi(r,\theta) = 0, \tag{4.3}$

and E is the operator $E\,f = \Delta f - \frac{1}{r^2\sin^2\theta}\,f$. Here Δ is the Laplacian restricted to functions of (r,θ), that is: $\Delta\,f = \frac{1}{r^2}(r^2 f_r)_r + \frac{1}{r^2\sin\theta}(\sin\theta\,f_\theta)_\theta$.

Note: (4.3) *is equivalent to stating that* $\Phi = \Psi\,\cos(\phi + \phi_0)$

satisfies the 3D biharmonic equation $\qquad\qquad\qquad \Delta^2\,\Phi = 0, \tag{4.4}$

for any constant ϕ_0.

[†]Note: in spherical coordinates: $0 \leq r$ is the radial distance, $0 \leq \theta \leq \pi$ is the polar angle,

and $0 \leq \phi \leq 2\,\pi$ is the azimuthal angle. In cartesian coordinates: $\hat{\phi} = (-\sin\phi,\,\cos\phi,\,0)$.

Similarly, the equations allow $2D$ solutions, where (in cartesian coordinates $(x,\,y,\,z)$) the solution depends only on $(x,\,y)$, and $u \cdot \hat{z} = 0$ ($\hat{z}$ is the unit vector along z-axis). Then $u = \nabla \times (\Psi(x,\,y)\hat{z})$, where $\qquad \Delta^2\psi = 0, \tag{4.5}$

and $\Delta = \partial_x^2 + \partial_y^2$ is the Laplacian in 2D. That is: ψ satisfies the biharmonic equation. Again: a simply connected domain is needed, so that the pressure can be recovered by solving the first equation in (4.1), once the flow velocity is known.

4.1.3 Motivation: *Dynamics of a Janus drop in an External Flow*

As stated in section 1.3, the initial motivation for the work in this thesis was to produce "simple" analytical solutions for the response of a Janus drop to an applied thermal gradient. And our intention was to use, as the starting point for the analysis, the work by Shklyaev, et. al [49, 8, 50, 9]. In particular, *Dynamics of a Janus Drop in an External Flow* [49]. Thus we studied this last paper with the aim of extending its approach to suit our purposes. Unfortunately, we run into difficulties when trying to understand the method proposed in [49]. The attempt to resolve these difficulties lead to the PSM.

For the purpose of completeness, next we summarize the results in [49], and document the issues that worried us — some of which we have not yet managed to fully resolve/understand.

In this paper, the authors consider a fixed shape spherical[1] Janus drop in an external uniform flow ($u \to u_\infty = $ constant as $r \to \infty$); see Figure B-14. In adimensional variables: (i) the drop has unit radius and it is centered at the origin; (ii) the dynamic viscosity is ν_1 in the upper hemisphere (region Ω_1), ν_2 in the lower hemisphere (region Ω_2), and $\nu_0 = 1$ in the surrounding liquid (region Ω_0). Furthermore: at the interfaces the flow velocity is continuous, with zero normal component, and the normal stresses match as well.

Here we summarize the axi-symmetric case only, when the drop's axis is aligned with the external flow: $u_\infty = -U\hat{z}$ ($\beta = 0$ in Figure B-14). Roughly the first half of [49] is dedicated to this situation. Then the governing equations, which can be written using a stream function formulation (4.2–4.3), are[2]

$$E^2 \Psi = 0, \text{ in each region } \Omega_j \ (j = 0,\, 1,\, 2), \text{ with b.c.:} \tag{4.6}$$

$$\Psi = 0, \ \ [\partial_r \Psi] = [\nu \partial_r^2 \Psi] = 0, \quad \text{for } r = 1. \tag{4.7}$$

$$\Psi = 0, \ \ [\partial_\theta \Psi] = [\nu \partial_\theta^2 \Psi] = 0, \quad \text{for } \theta = \pi/2. \tag{4.8}$$

$$\Psi \sim -\frac{r}{2}\sin\theta, \qquad\qquad \text{for } r \gg 1. \tag{4.9}$$

Here, as usual, the brackets indicate the jumps in the enclosed quantities across an interface, thus: $[f]|_{r=1} = f_{r=1^+} - f_{r=1^-}$ and $[f]|_{\theta=\pi/2} = f_{\theta=(\pi/2)^+} - f_{\theta=(\pi/2)^-}$.

Note 4.8. (Notation) Ψ is continuous, but not smooth, at the interfaces. Thus denote by $\Psi^{(j)}$ the solution in Ω_j (then $\Psi^{(j)}$ is smooth *inside* Ω_j). Further, *define piece-wise constant functions* for $r \leq 1$ (ν, $\nu^{\#}$, and σ) by: $\nu = \nu_p$, $\nu^{\#} = \nu_{3-p}$, and $\sigma = (-1)^{p+1}$ in Ω_p ($p = 1,\, 2$). We can think of these as (step-functions) that depend on $\xi = \cos\theta$ only: $\sigma(\xi) = \text{sign}(\xi)$, $\nu(\xi) = \nu_2 + (\nu_1 - \nu_2)H(\xi)$ ($H = $ Heaviside function), and $\nu^{\#}(\xi) = \nu(-\xi)$. ♣

The authors in [49] propose that the solution to (4.6–4.9) can be written in the form

$$\Psi^{(0)} = \sum_{n=1}^{\infty} \frac{A_n P_n^1(\xi)}{r^{n+1}}(1 - r^2) + \frac{1}{4}\left(3 - \frac{1}{r^2} - 2r\right)\sin\theta, \tag{4.10}$$

$$\Psi^{(p)} = \nu^{\#}\sum_{n=1}^{\infty}(B_n T_n(\xi) + \sigma\, C_n r R_n(\xi))r^{2n+1} + \sum_{n=1}^{\infty} D_n P_{2n}^1(\xi)r^{2n}(1 - r^2). \tag{4.11}$$

Here: $p = 1$ or $p = 2$, the (A_n, B_n, D_n) are constants to be found, P_n^1 is the nth degree first

---

[1]Surface tension is large enough that deformations of the interfaces can be ignored.
[2]These correspond to Equations (9a–9d) in [49].

order associated Legendre polynomial, $Q_n = \xi P_n' - n(n+1)P_n$,

$$T_n = \frac{P_{2n+1}^1(\xi)}{P_{2n+1}^1(0)} - \frac{P_{2n-1}^1(\xi)}{P_{2n-1}^1(0)}, \quad \text{and} \quad R_n = \frac{P_{2n+2}^1(\xi)}{Q_{2n+2}(0)} - \frac{P_{2n}^1(\xi)}{Q_{2n}(0)}. \qquad (4.12)$$

These expressions, substituted into (4.7), yield a system of infinite linear equations that should determine the (A_n, B_n, D_n). By construction

(4.10) satisfies (4.9). In addition: $\qquad$ (4.11) *satisfies, term-by-term,* (4.8). $\quad$ (4.13)

Note 4.9. *At this point we stop to ask a few questions.*

Q1 While the modes used to expand the solution for $r > 1$ (i.e.: $\Psi^{(0)}$) are standard for the Stokes equations, the modes in the expansion for $r < 1$ are not. Clearly they satisfy the problem for $r < 1$, but: is this the result of some clever manipulation/trick that works for this problem only, or *is there some general principle at work here from which these non-smooth modes follow?*

Q2 Follow up on **Q1**: *Are the modes in* (4.11) *linearly independent, and form a complete set?* Else, how can we be sure that the solution can be expanded as in (4.11)?

Q3 If the series defining $\Psi^{(1)}$ and $\Psi^{(2)}$ converge, then they converge everywhere for $r < 1$. This means that *both $\Psi^{(1)}$ and $\Psi^{(2)}$ can be extended as smooth solutions to* (4.3) *over the whole sphere $r < 1$, beyond the boundary at $\theta = \pi/2$.* This is rather unusual for elliptic problems. If true, there must be a reason for it, *what is this reason?*

Q4 We expect the solution to (4.6–4.9) to be singular at the triple point $r = 1$, $\theta = \pi/2$. Thus, for $r = 1$, the convergence rate for (4.10–4.11) must be quite poor. Hence the calculation of important quantities is likely almost impossible to do accurately — specially those requiring high order derivatives, like the drag.[3] Hence, *series convergence acceleration is a "must", but: is this possible without a-priori knowledge of the coefficients (A_n, B_n, D_n)?*

Q5 Finally, we observe that the factor $\nu^{\#}$ in (4.11) can also be written in the form $\frac{\nu_1 \nu_2}{\nu}$. This is significant to connect (4.11) with the theoretical development in §4.3.

*We have been able to get answers to **Q1-Q3**, but (unfortunately) not for **Q4**.* $\qquad$ ♣

Note 4.10. Below we require the scalar products $\qquad \langle P_k^1, P_\ell^1 \rangle_I = \int_I P_k^1(\xi)\, P_\ell^1(\xi)d\xi$, where $I = [-1, 1]$, $[-1, 0]$, or $[0, 1]$; and k, ℓ are

---

[3]Note that, a very important motivation for a calculation like this is to get quantities such as the drop velocity when a force (e.g.: gravity) is applied. This requires computing the drag.

natural numbers. For $I = [-1, 1]$
$$\langle P_k^1, P_\ell^1 \rangle_{[-1,1]} = \frac{2(l+1)l}{2l+1} \delta_{k,\ell},$$

by orthogonality of the associated Legendre polynomials.

For analytic expressions when $I = [0, 1]$ see Appendix C.

The case $I = [-1, 0]$ follows by symmetry. ♣

Next we substitute (4.10–4.11) *into* (4.7), *to obtain equations for the* (A_n, B_n, D_n).

First. The condition $\Psi^{(p)} \equiv 0$ $(p = 1, 2)$, at $r = 1$ yields

$$0 = \nu^\# \sum_{n=1}^{\infty} (B_n T_n + \sigma C_n R_n) \quad \text{for} \quad -1 < \xi < 1. \tag{4.14}$$

We transform this functional equation into an equivalent discrete system system by projecting it on the orthogonal basis $\{P_k^1\}_{k=1}^{\infty}$. This yields the equations:

$$0 = \sum_{n=1}^{n} B_n \left\langle \nu^\# T_n, P_k^1 \right\rangle + C_n \left\langle \nu^\# \sigma R_n, P_k^1 \right\rangle, \quad \text{for} \quad k = 1, 2, 3, \ldots, \tag{4.15}$$

where $\langle f, g \rangle = \int_{-1}^{1} f(\xi) g(\xi) \, d\xi$ is the standard inner product in $[-1, 1]$.

Note 4.11. We have
$$\left\langle \nu^\# T_n, P_k^1 \right\rangle = \nu_1 \left\langle T_n, P_k^1 \right\rangle_{[-1, 0]} + \nu_2 \left\langle T_n, P_k^1 \right\rangle_{[0, 1]},$$
and
$$\left\langle \nu^\# \sigma R_n, P_k^1 \right\rangle = -\nu_1 \left\langle R_n, P_k^1 \right\rangle_{[-1, 0]} + \nu_2 \left\langle R_n, P_k^1 \right\rangle_{[0, 1]}.$$
Thus, using (4.12) and note **4.10**, the coefficients in (4.15) can be computed explicitly. ♣

Finally, we write (4.15) in matrix form
$$\begin{bmatrix} \Pi^{(1)} & \Pi^{(2)} \end{bmatrix} \begin{bmatrix} \vec{B} \\ \vec{C} \end{bmatrix} = 0, \tag{4.16}$$
where: (i) $\vec{B}$ and $\vec{C}$ are the infinite vectors

with components B_n and C_n, respectively; and (ii) $\Pi^{(1)}$ and $\Pi^{(2)}$ are the infinite matrices with entries

$$\{\Pi^{(1)}\}_{kn} = \left\langle \nu^\# T_n, P_k^1 \right\rangle \quad \text{and} \quad \{\Pi^{(2)}\}_{kn} = \left\langle \nu^\# \sigma R_n, P_k^1 \right\rangle \tag{4.17}$$

Second. To implement $[\partial_r \Psi]_{r=1} = 0$ follow the same procedure: (4.10–4.11) yield

$$-2 \sum_{n=1}^{\infty} A_n P_n^1 = \nu^\# \sum_{n=1}^{\infty} ((2n+1) B_n T_n + (2n+2) C_n \sigma R_n) - 2 \sum_{n=1}^{\infty} D_n P_{2n}^1, \tag{4.18}$$

for $-1 < \xi < 1$. Next project this equality onto the basis $\{P_k^1\}_{k=1}^{\infty}$, and obtain:

$$-\frac{4(k+1)k}{2k+1} A_k = \sum_{n=1}^{\infty} \left((2n+1) \left\langle \nu^\# T_n, P_k^1 \right\rangle B_n + (2n+2) \left\langle \nu^\# \sigma R_n, P_k^1 \right\rangle C_n \right.$$
$$\left. - \frac{4(k+1)k}{2k+1} \delta_{k, 2n} D_n \right), \quad \text{for} \quad k = 1, 2, 3, \ldots$$

In matrix form this is (4.19), where:

(i) $\vec{D} = \{D_n\}$ and $\vec{A} = \{A_n\}$ are infinite vectors; and (ii) $\Lambda^{(1)}$ through $\Lambda^{(4)}$ are the infinite matrices with entries

$$\begin{bmatrix} \Lambda^{(1)} & \Lambda^{(2)} & \Lambda^{(3)} & \Lambda^{(4)} \end{bmatrix} \begin{bmatrix} \vec{B} \\ \vec{C} \\ \vec{D} \\ \vec{A} \end{bmatrix} = 0, \qquad (4.19)$$

$$\left.\begin{array}{ll} \Lambda^{(1)}_{kn} = (2\,n+1)\,\langle \nu^{\#}\,T_n,\,P_k^1\rangle, & \Lambda^{(2)}_{kn} = (2\,n+2)\,\langle \nu^{\#}\,\sigma\,R_n,\,P_k^1\rangle, \\[2mm] \Lambda^{(3)}_{kn} = -\frac{4(k+1)\,k}{2\,k+1}\,\delta_{k,\,2n}, & \text{and} \quad \Lambda^{(4)}_{kn} = +\frac{4(k+1)\,k}{2\,k+1}\,\delta_{k,\,n}. \end{array}\right\} \qquad (4.20)$$

Third. Next we implement the condition $[\nu\,\partial_r^2\Psi]_{r=1} = 0$. From (4.10–4.11) we obtain:

$$-\frac{3}{2}\sin\theta + \sum_{n=1}^{\infty} A_n\,(4n+2)\,P_n^1 \;=\; \nu_1\nu_2 \sum_{n=1}^{\infty}\Big((4\,n^2+2\,n)\,B_n\,T_n + (4\,n^2+6\,n+2)\,C_n\,\sigma\,R_n)\Big)$$

$$-\nu\sum_{n=1}^{\infty}(8\,n+2)\,D_n\,P_{2n}^1. \qquad (4.21)$$

Again, we project this equality onto the basis $\{P_k^1\}_{k=1}^{\infty}$, and obtain:

$$-\frac{3}{2}\left\langle\sqrt{1-\xi^2},\,P_k^1\right\rangle + 4\,(k+1)\,k\,A_k \;=\; \nu_1\nu_2\sum_{n=1}^{\infty}(4\,n^2+2\,n)\langle T_n,\,P_k^1\rangle\,B_n +$$

$$\nu_1\nu_2\sum_{n=1}^{\infty}(4\,n^2+6\,n+2)\langle\sigma\,R_n,\,P_k^1\rangle\,C_n \;-\; \sum_{n=1}^{\infty}(8\,n+2)\,\langle\nu\,P_{2n}^1,\,P_k^1\rangle\,D_n, \qquad (4.22)$$

for $k = 1, 2, 3, \ldots$ In matrix form this is (4.23), where: $\Gamma^{(j)}$ are the matrices with the entries in (4.24), and $\vec{V}$ is the vector with entries $V_k = -\frac{3}{2}\left\langle\sqrt{1-\xi^2},\,P_k\right\rangle$.

$$\begin{bmatrix} \Gamma^{(1)} & \Gamma^{(2)} & \Gamma^{(3)} & \Gamma^{(4)} \end{bmatrix} \begin{bmatrix} \vec{B} \\ \vec{C} \\ \vec{D} \\ \vec{A} \end{bmatrix} = \vec{V}, \qquad (4.23)$$

$$\left.\begin{array}{ll} \Gamma^{(1)}_{kn} = \nu_1\,\nu_2\,(4\,n^2+2\,n)\,\langle T_n,\,P_k^1\rangle, & \Gamma^{(2)}_{kn} = \nu_1\,\nu_2\,(4\,n^2+6\,n+2)\,\langle\sigma\,R_n,\,P_k^1\rangle, \\[2mm] \Gamma^{(3)}_{kn} = -(8\,n+2)\,\langle\nu\,P_{2n}^1,\,P_k^1\rangle, & \Gamma^{(4)}_{kn} = -4\,(k+1)\,k\,\delta_{k,\,n}. \end{array}\right\} \qquad (4.24)$$

Fourth. Finally, combine (4.16), (4.19), and (4.23), to obtain $\qquad M\vec{x} = \vec{b}.$ (4.25)

Here $\qquad M = \begin{bmatrix} \Pi^{(1)} & \Pi^{(2)} & 0 \\ \Theta^{(1)} & \Theta^{(2)} & \Theta^{(3)} \end{bmatrix}, \quad \vec{x} = \begin{bmatrix} \vec{B} \\ \vec{C} \\ \vec{D} \end{bmatrix}, \quad \vec{b} = \begin{bmatrix} 0 \\ \mathcal{D}\vec{V} \end{bmatrix}, \quad \Theta^{(j)} = \mathcal{D}\,\Gamma^{(j)} + \Lambda^{(j)},$ (4.26)

and $\mathcal{D} = \mathrm{diag}\left(\frac{1}{2\,k+1}\right)$ — a diagonal matrix. Note: $\Lambda^{(4)}$ and $\Gamma^{(4)}$ are diagonal, and $\Theta^{(4)} = 0$. Thus $\vec{A}$ drops out from these equations. Once $\vec{B}$, $\vec{C}$, and $\vec{D}$ are obtained from (4.25–4.26), $\vec{A}$ follows from (4.19).

90

Specifically, from
$$\Lambda^{(4)}\vec{A} = -\Lambda^{(1)}\vec{B} - \Lambda^{(2)}\vec{C} - \Lambda^{(3)}\vec{D}. \quad (4.27)$$
Easy to solve because $\Lambda^{(4)}$ is diagonal.

4.1.4 Solving the equations: reduction to a finite system

The system of equations in (4.25–4.27) is linear, discrete, and infinite. In order to actually compute the solution (or a suitable approximation) we need to reduce it (by truncation or other means) to a finite system. The crucial step is to reduce the infinite matrix M in (4.26) to finite size. The authors in [49] report that they reduced the matrix, for their calculations, to one of size $5N \times 5N$ — where N is some (large) integer. But they do not explain how, nor do they exhibit the reduced matrix. Hence we had to develop our own reduction, which produced a matrix of size $4N \times 3N$. We have no way of knowing if our reduction is better or worse than theirs — e.g.: in terms of the conditioning.[4] However, note that our reduction is over-determined (so we solve it in the least squares sense), while the reduction in [49] yields a square matrix. Our reduction is explained below.

First: intuitive explanation. Let us go back to (4.10–4.11), and truncate the infinite series so the resulting sums all have the same level of approximation (for $r = 1$, since there is where the jump conditions apply). This means that each of the sums must involve the same range of P_n^1 — or as close as possible: an exact match cannot be done. Thus keep: (i) the first N for B_n, C_n, and D_n; and (ii) the first $2N$ for A_n. Thus each of the truncated sums involves P_n^1 with n up to either $2N + 1$ or $2N$. However, the jump conditions involve linear relations between $r = 1 - dr$ (inside) and $r = 1 + dr$ (outside), and the inside "vectors" $(\vec{B}, \vec{C}, \vec{D})$ are now length N, while the outside vector $\vec{A}$ is length $2N$. Hence the jump conditions must be written in terms of $2N \times N$ matrices. This leads to two sets of size $2N \times 3N$ problems when $\vec{A}$ is eliminated from the equations. That is, M size $4N \times 3N$.

A more precise description relies on the scalar products $\langle P_n^1, P_m^1 \rangle$ that appear in the construction of (4.25–4.27). The idea is to truncate the various matrices by keeping only terms where n and m are below some threshold. It is then easy to see that this produces reduced sub-matrices $\Pi^{(j)}$, $\Theta^{(j)}$, and $\Lambda^{(j)}$ of size $2N \times N$ (for some positive integer cutoff N). This then reduces the matrix M to size $4N \times 3N$ matrix.

Unfortunately, the condition number for the reduced matrix M grows like $\sim N^3$ — see

---

[4]We wrote to the authors in [49], to request the details of the reduction, but they were not provided. We also asked if their reduction exhibited too fast a growth of the condition number with N (like ours does), and we did not get an answer to this either.

Figure B-15. This, coupled with the slow convergence of the series defining the solution (see item **Q4** in note **4.9**), creates a serious problem: a fairly large N is needed for accuracy, which is hard to obtain because of the large condition number.[5] The *solutions also exhibit a fairly strong Gibbs' phenomenon, which makes the situation worse.* For example: Figure B-16 shows various aspects of the solution for $N = 200$ (note that then the condition number exceeds 10^7). In this figure: *Panel* (a) shows the streamlines in and near the drop; the picture is visually similar to FIG. 4 of [49]. *Panel* (b) is intended to check how well the condition $\Psi^{1,2} = 0$ for $r = 1$ is satisfied. While oscillations are clearly visible, their amplitude is small $O(10^{-3})$. *Panel* (c) checks the condition $[\partial_r \Psi] = 0$ for $r = 1$ in (4.7). The errors here are size ~ 1.5, with fairly large oscillations everywhere. Finally, *Panel* (d) checks the condition $[\nu \, \partial_r^2 \Psi] = 0$ in (4.7). The situation is similar to that in panel (c) but the errors are 25 times bigger.

The errors sizes mentioned above are in the L^∞ norm, but it is easy to see from the plots that the L^1 and L^2 errors are not small either. So, if this solution converges, it may not be close to its actual value for $N \sim 200$. It also means that attempting to compute the drag using it is pointless. This is a very unsatisfactory situation, which points to a general lack of understanding of the Stokes equation with internal boundary conditions. We neither understand how the internal solution in Equation (4.10) is obtained nor know how to deal with the intractable growth of the condition number of the M matrix in Equation (4.26). In order to resolve these difficulties (as well as the other ones mentioned in note **4.9**) in the next few sections we examine a similar, but simpler, problem: a Stokes problem in $2D$, involving a circle with an internal boundary.

4.2 General Results for the Biharmonic Equation

In this section, we present general properties of biharmonic functions, to lay the theoretical framework needed for the construction of solutions to biharmonic problems with internal interfaces in §4.3. We begin with a general description of the solutions to the 2D biharmonic equation, using complex analysis, in §4.2.1. Then we introduce some properties of the solutions near a hyper-plane in § 4.2.2 and 4.2.3.

---

[5]Not to mention the fact that the whole point of an analytic solution is, mostly, to obtain "simple" and compact expressions that yield either intuition, or can be used as building blocks for more complicated problems. Without this a full numerical simulation is likely preferable.

4.2.1   Representation via Complex Analysis (2D)

As shown in §4.1.2, the 2D Stokes equation collapses into the biharmonic equation for the stream function $\Psi = \Psi(x, y)$, $\Delta^2\Psi = 0$, where $\Delta = \partial_x^2 + \partial_y^2$ is the Laplace operator — in polar coordinates: $\Psi = \Psi(r, \theta)$ and $\Delta = \partial_r^2 + \frac{1}{r}\partial_r + \frac{1}{r^2}\partial_\theta^2$. Below we use complex analysis to represent biharmonic functions (solutions of the biharmonic equation) in 2D.

Theorem 4.2. Let Ψ be a biharmonic function defined in a simply connected open set. Then

$$\Psi = r^2\Psi_1 + \Psi_2. \quad (4.28)$$

where Ψ_1 and Ψ_2 are harmonic. Further, Ψ_1 and Ψ_2 are unique up to transformations of the form[†]

$$\Psi_1 \to \Psi_1 + \tfrac{1}{r^2}\,L \ \text{ and } \ \Psi_2 \to \Psi_2 - L,$$

where L is a linear function: $L = c_1\,x + c_2\,y$.

Equivalently, in terms of the complex variable $\zeta = x + i\,y$ (and its conjugate $\bar\zeta = x - i\,y$),

$$\Psi = \text{Real}\left(\bar\zeta\,f_1(\zeta) + f_2(\zeta)\right). \quad (4.29)$$

Here f_1 and f_2 are analytic functions, unique up to transformations of the form[†]

$$f_1 \to f_1 + i\,a\,\zeta + c \ \text{ and } \ f_2 \to f_2 - \bar c\,\zeta + i\,b,$$

with constants: a and b real and $c = c_1 + i\,c_2$ complex (c_1 and c_2 are as above). Then

$$\Psi_1 = \text{Real}(f_1/\zeta) \ \text{ and } \ \Psi_2 = \text{Real}(f_2).$$

Note that *if $\zeta = 0$ is in the domain, then the complex constant c is uniquely determined by the requirement $f_1(0) = 0$.*

[†] *Transformation invariance.* ♣

Proof. $\Delta\Psi$ is harmonic. Thus $\Delta\Psi = \text{Real}(h(\zeta))$, where h is analytic (see #1). Let $f_1(\zeta)$ be the analytic function defined by $f_1' = h$ (see #2). Then $\Psi - \text{Real}(\bar\zeta\,f_1(\zeta))$ is harmonic. Hence $\Psi - \text{Real}(\bar\zeta\,f_1(\zeta)) = \text{Real}(f_2(\zeta))$, where f_2 is analytic (see #3). This proves (4.29).

    #1 Note that h is unique up to the transformations: $h \to h + i\,a$, with a a real constant.

    #2 Clearly f_1 is unique up to the transformations: $f_1 \to f_1 + i\,a\,\zeta + c$, with c a complex constant.

    #3 Clearly f_2 is unique up to the transformations: $f_2 \to f_2 - \bar c\,\zeta + i\,b$, with b a real constant.

Finally, (4.28) follows from $\Psi_1 = \text{Real}(f_1/\zeta)$ and $\Psi_2 = \text{Real}(f_2)$. □

What happens if the domain in theorem 4.2 is not simply connected? (4.30)
In this case *the Ψ_j (and f_j) can be multiple valued:* following them along a closed loop may return them not to the original value, but one that differs by a transformation invariance, as the following **example** shows:

Take $f_1 = (a_1\,\zeta + a_2)\log\zeta \ \text{ and } \ f_2 = a_2\,\zeta\log\zeta$, with the a_j real constants. This leads to

the (single valued) biharmonic function (on $r > 1$) $\Psi = a_1 r^2 \ln r + 2 a_2 x \ln r$. However,

$\Psi_1 = a_1 \ln r + a_2 r^{-2}(x \ln r + y \theta)$ and $\Psi_2 = a_2 (x \ln r - y \theta)$ are multiple valued. ♣

Expansions for biharmonic functions in the unit disk. (4.31)

Let Ψ be a biharmonic function defined on the unit disk $r < 1$. Then we can use (4.28–4.29)

to write
$$\Psi = r^2 \sum_{n=-\infty}^{\infty} \psi_{1,n}\, r^{|n|}\, e^{i n \theta} + \sum_{n=-\infty}^{\infty} \psi_{2,n}\, r^{|n|} e^{i n \theta}, \tag{4.32}$$

for some expansion coefficients $\psi_{1,n}$ and $\psi_{2,n}$, with the *series radius of convergency being at least* 1. In terms of sines and cosines this is

$$\begin{aligned} \Psi \;=\;& a_0 + r\,(a_1 \cos\theta + b_1 \sin\theta) + r^2\,(a_2 \cos(2\theta) + b_2 \sin(2\theta) + c_2) + \\ & \sum_{n=3}^{\infty} r^n \left(a_n \cos(n\theta) + b_n \sin(n\theta) + c_n \cos((n-2)\theta) + d_n \sin((n-2)\theta) \right), \end{aligned} \tag{4.33}$$

for constants a_n, b_n, c_n, and d_n. Alternatively:

$$\Psi = \sum_{n=0}^{\infty} \left(\tilde{a}_n + \tilde{b}_n\, r^2 \right) r^n \cos(n\theta) + \sum_{n=0}^{\infty} \left(\tilde{c}_n + \tilde{d}_n\, r^2 \right) r^n \sin(n\theta). \tag{4.34}$$

for constants $\tilde{a}_n$, $\tilde{b}_n$, $\tilde{c}_n$, and $\tilde{d}_n$.

What happens in dimension $d > 2$? (4.35)

It is easy to see, through direct calculation, that Ψ *as defined by* (4.28), *is biharmonic if the* Ψ_j *are harmonic. This is true in any dimension.*

We do not know if the the converse (biharmonic functions in simply connected open sets can be written as in (4.28)) is true for $d > 2$. However it can be shown that *the converse is valid on "radial sets".* The proof employs a variation of the technique used in §4.2.2.

Note. We *define a radial set* as the portion of a solid angle characterized by $R_1 < r < R_2$, where the R_j are functions of the angle variables suc that $0 < R_1 < r_0 < R_2$, where r_0 is a constant. Thus every point in the set is connected, by a radial line, to a single point in the sphere of radius r_0.

4.2.2 Hyperplane based representation

Here we will prove a result analogous to that in theorem **4.2**, but for a plane geometry (instead of spherical).[6] Here we *no longer assume 2D.*

---

[6]Note that, while the result in theorem **4.2** is well known, the one in theorem **4.3** is less known.

Theorem 4.3. Let Ψ be a biharmonic function defined on a region Ω with the properties listed below. Then

$$\Psi = u + z\,v, \quad (4.36)$$

where u and v are harmonic functions. Conversely: any function of the form in (**4.3**) is biharmonic. The properties of Ω are:

p1 Ω is associated with a hyperplane $\mathcal{P}$. Without loss of generality label the Cartesian coordinates as $(x_1, ..., x_n, z) = (\vec{x}, z)$, and assume that $\mathcal{P}$ is the hyperplane $z = 0$.

p2 Let $\mathcal{R}$ be a region within $\mathcal{P}$. Assume that the Poisson problem: $\Delta_\perp w = f$ in $\mathcal{R}$, has solutions.[7] Here $\Delta_\perp$ is the Laplace operator in terms of $\vec{x}$, and $f = \Delta(\Psi)_z|_{z=0}$.

p3 Ω is the set of points such that $\vec{x} \in \mathcal{R}$ and $Z_d(\vec{x}) < z < Z_u(\vec{x})$, where Z_d and Z_u are "nice" functions such that $Z_d \leq 0 \leq Z_u$ and $Z_d < Z_u$. ♣

Figure B-20 shows an example region Ω.

Proof. If $\Psi = u + z\,v$ then $\Delta\Psi = \Delta u + z\,\Delta v + 2\,v_z$. Hence, if u and v are harmonic, Ψ is biharmonic (as then v_z is also harmonic). Viceversa, let Ψ be biharmonic and suppose there is a v harmonic such that $2\,v_z = \Delta\Psi$. Then $u = \Psi - z\,v$ is harmonic. Thus, to complete the proof we need only show that $2\,v_z = \Delta\Psi$ has an harmonic solution, given a biharmonic Ψ. However, $2\,v_z = \Delta\Psi$ is an ode along each line $\vec{x} = $ constant, and completely determines v in Ω given $v_0 = v_0(\vec{x}) = v|_{z=0}$ for $\vec{x} \in \mathcal{R}$. Furthermore: $2\,(\Delta v)_z = 0$. Thus v is harmonic if $\Delta v = 0$ for $z = 0$. But $\Delta v = v_{zz} + \Delta_\perp v = \frac{1}{2}(\Delta\Psi)_z + \Delta_\perp v$. Hence v is harmonic if we select v_0 to be a solution to the Poisson equation $\Delta_\perp v_0 = -\left(\frac{1}{2}(\Delta\Psi)_z\right)|_{z=0}$. ☐

4.2.3 Continuation Across a Hyperplane

In §4.3, to solve a biharmonic problem with an internal interface, the solutions on each side of the interface are extended to the other side. This must be justified: in general extending elliptic functions outside their domain of definition is an ill-posed problem [46]. The results below provide this justification.

Note: In both theorems below $Z_d = 0$. Hence the assumption in **p2** of theorem **4.3** applies.

Theorem 4.4. Let Ψ be a biharmonic function defined in Ω (Ω is as in theorem **4.3**, with $Z_d \equiv 0$). Further

$$\Psi|_{z=0} = \partial_z \Psi|_{z=0} = 0. \quad (4.37)$$

Then Ψ can be extended as a biharmonic function to the symmetrized region $-Z_u(\vec{x}) < z < Z_u(\vec{x})$. ♣

---

[7]This is only needed for the converse part of the theorem. An issue when (in **p3**) either $Z_d = 0$ or $Z_u = 0$, because the boundary values of harmonic functions need not be nice.

Theorem 4.5. Let Ψ be a biharmonic function defined in Ω (Ω is as in theorem **4.3**, with $Z_d \equiv 0$). Further

$$\Psi|_{z=0} = \partial_z^2 \Psi|_{z=0} = 0. \quad (4.38)$$

Then Ψ can be extended as an odd biharmonic function to the symmetrized region $-Z_u(\vec{x}) < z < Z_u(\vec{x})$. ♣

Proof. From theorem **4.3** we can write $\Psi = u + z\, v$.

Then, when (4.37) applies it follows that: $u|_{z=0} = 0$ and $(u_z + v)|_{z=0} = 0$. Now, since both u and $w_1 = u_z + v$ are harmonic functions, they can be extended as odd harmonic functions to $|z| < Z_u(\vec{x})$. Thus $\Psi = u + z\,(w_1 - u_z)$ is extended as a biharmonic function to $|z| < Z_u(\vec{x})$. Note also that $\Psi_o = u - z\,u_z$ is odd part of the extension, while $\Psi_e = z\,w_1$ is even part.

On the other hand, when (4.38) applies $u|_{z=0} = 0$ and $(u_{zz} + 2\,v_z)|_{z=0} = 0$. Now, since both u and $w_2 = u_z + 2\,v$ are harmonic functions, they can be extended as harmonic functions to $|z| < Z_u(\vec{x})$ — with u odd and w_2 even. Thus $\Psi = u + \frac{1}{2}\,z\,(w_2 - u_z)$ is extended as an odd biharmonic function to $|z| < Z_u(\vec{x})$. □

4.3 Biharmonic Equation with an Internal Interface: PSM

In this section we present an extension of the Parity Split Method (PSM) for the biharmonic equation with an internal interface. Specifically we will consider a 2D "Janus cylinder" problem, and show how the PSM developed earlier for the Laplace equation can be extended to this problem. We point out that the extension has some drawbacks relative to the Laplace case. For example: the boundary conditions cannot be split a-priori. Thus an explicit solution is not possible, and we must resort to a semi-analytical approach involving the solution of an infinite matrix system, with a condition number that grows too rapidly. On the other hand, the approach resolves questions **Q1-Q3** in note **4.9**. Further work is needed to resolve question **Q4**.

Important note: *While the presentation here is for the 2D case, the results in §4.3.1 have a straightforward generalization to a sphere in any number of dimensions.*

4.3.1 The mathematical problem to be solved, and main results

We consider the biharmonic equation in the unit circle, with interface along a diameter. Thus, in cartesian [8] (x, z) and polar coordinates ($x = r\cos\theta$ and $z = r\sin\theta$, the main

---

[8]We use (x, z), instead of (x, y), to be consistent with the notation in §4.2.

domain is: Ω = disk $r < 1$. The subdomains are: Ω_1 = upper half disk ($r < 1$ and $z > 0$) and Ω_2 = lower half disk ($r < 1$ and $z < 0$), with interface along $z = 0$. The problem to be solved is then

$$\begin{cases} \Delta^2 \Psi = 0 & \text{for } r < 1 \text{ and } z \neq 0, \\ \Psi = [\partial_z \Psi] = [\nu \partial_z^2 \Psi] = 0 & \text{on } z = 0, \\ \Psi = f \text{ and } \Psi_r = g & \text{on } r = 1, \end{cases} \qquad (4.39)$$

where: (i) As usual $[w] = w|_{z=0^+} - w|_{z=0^-}$ indicates the jump across the interface of the enclosed quantity; (ii) $\nu = \nu(x, z)$ is defined by $\nu = \nu_j$ in Ω_j, where the ν_j are positive constants. (iii) $f = f(\theta)$ and $g = g(\theta)$ are given functions. *This problem is a 2D version (the "Janus cylinder") of the one in* (4.8), *were we eliminate the "outside" region, and replace it by boundary conditions at $r = 1$* (prescribing the flow velocity there). This allows us to concentrate exclusively on how to deal with the internal interface.

Note 4.12. Our aim is that of methods to obtain explicit solutions. Thus, to avoid being embroiled in mathematical subtleties, *we assume that: f and g in* (4.39) *are such that:*

(a) The solutions exist and are unique.

(b) The limits at the interface, from each side, of the solution and its derivatives (up to third order) are nice and well defined[9] for $|x| < 1$. ♣

The main results of this section are the following two theorems

Theorem 4.6. (First parity split).

The solution to (4.39) can be written in the form $\qquad \Psi = \Psi_1 + \dfrac{1}{\nu} \Psi_2, \quad (4.40)$

where:

(1) Ψ_1 is odd and Ψ_2 is even (relative to z).

(2) Ψ_1 is the solution to $\qquad\qquad\qquad\qquad\qquad\qquad \Delta^2 \Psi_1 = 0, \quad (4.41)$

with $\Psi_1 = f_1$ and $\partial_r \Psi_1 = g_1$ at $r = 1$.

(3) Ψ_2 is the solution to $\qquad\qquad\qquad\qquad\qquad\qquad \Delta^2 \Psi_2 = 0, \quad (4.42)$

with $\Psi_2 = f_2$ and $\partial_r \Psi_2 = g_2$ at $r = 1$,

and interface conditions at $z = 0$ $\qquad\qquad\qquad \Psi_2 = \partial_z \Psi_2 = [\partial_z^2 \Psi_2] = 0.$

(4) $\qquad\qquad f_1 = \mathcal{O} f, \quad g_1 = \mathcal{O} g, \quad f_2 = \mathcal{E} f, \quad \text{and} \quad g_2 = \mathcal{E} g, \qquad (4.43)$

where $\mathcal{O}$ and $\mathcal{E}$ are defined below.

---

[9] In general we expect singularities at $x = \pm 1$.

(5) The transformation $(\Psi_1 \text{ odd}, \Psi_2 \text{ even}) \longrightarrow \Psi = \Psi_1 + \frac{1}{\nu}\Psi_2$ in (4.40) is a bijection, with

inverse

$$\Psi_1 = \frac{1}{\kappa}\left(\frac{1}{\nu^{\#}}\Psi - \frac{1}{\nu}\Psi^{\#}\right) = \mathcal{O}\Psi \text{ and } \Psi_2 = \frac{1}{\kappa}\left(\Psi + \Psi^{\#}\right) = \mathcal{E}\Psi \qquad (4.44)$$

where $\kappa = 1/\nu_1 + 1/\nu_2$, and we use $^{\#}$ to indicate the reflection across $z = 0$ of a

function: $G^{\#}(x, z) = G(x, -z)$. This is consistent with $\nu^{\#}$ defined in note **4.8**.   ♣

The key point to notice here is that *there is no interface in the problem for* Ψ_1. *Hence it*

can be solved by "standard" methods, e.g.: using (4.31). The interface conditions for Ψ_2 have

been simplified, but not removed (this is done in the next theorem). In addition:

(a) f_1 and g_1 are odd (guarantees odd solution to (4.41)),

(b) f_2 and g_2 are even (guarantees even solution to (4.42)),

(c) The PSM here is similar to that in §2.2, with the even and odd roles reversed.

The proof for this theorem follows after the statement of the next theorem.

Note that the jump conditions for Ψ_2 guarantee that Ψ_2 is C^2 across the interface, but $\partial_z^3 \Psi_2$

may not be continuous. Hence a further split is needed:

Theorem 4.7. (Second parity split). The even biharmonic, Ψ_2, in the first parity split

of theorem **4.6**, can be written in the form

$$\Psi_2 = \Psi_{2,e} + \sigma\Psi_{2,o}, \qquad (4.45)$$

where: (i) $\sigma = \text{sign}(z)$; (ii) $\Psi_{2,e}$ and $\Psi_{2,o}$ are biharmonic functions in Ω (no interface);

(iii) $\Psi_{2,e}$ is even (relative to z) and $\Psi_{2,e}|_{z=0} = 0$; (iv) $\Psi_{2,o}$ is odd (relative to z) and

$\partial_z\Psi_{2,o}|_{z=0} = 0$; (v) $\Psi_{2,e}$ and $\Psi_{2,o}$ are uniquely determined by Ψ_2. (vi) Any function of the

form (4.45) satisfies the interface jump conditions for Ψ_2 in (4.42).   ♣

This second split finally *removes, completely, the interface from the solution of* (4.39), *and*

expresses the solution as a linear combination of four biharmonic functions defined in the

whole domain Ω — this addresses the "puzzle" in **Q3** of note **4.9**.

Important point.   (4.46)

Unfortunately, the proof of the existence of (4.45) is not constructive. In particular, it does

not provide boundary values that can be used to solve for $\Psi_{2,e}$ and $\Psi_{2,o}$. It seems that the

boundary values for $\Psi_{2,e}$ and $\Psi_{2,o}$ depend "globaly" on f_2 and g_2 (there is no analogue to

(4.43)), and cannot be obtained independently of, essentially, solving the whole problem.

The proof of this second theorem is after the proof of the first theorem right below.

Proof of the first parity split.

First we show that if Ψ_1 and Ψ_2 satisfy (4.40–4.41), then Ψ in (4.40) satisfies (4.39):

(i) Statement (5) is trivial. Thus
$$f = f_1 + \frac{1}{\nu} f_2 \quad \text{and} \quad g = g_1 + \frac{1}{\nu} g_2, \quad (4.47)$$
from which the boundary conditions at

$r = 1$ for (4.39) follow. **(ii)** Because Ψ_1 is odd (and smooth) it trivially satisfies the interface jump conditions for (4.39). **(iii)** The interface jump conditions for Ψ_2 are such that $\frac{1}{\nu}\Psi_2$ satisfies the interface jump conditions for (4.39). **(iv)** Finally, because ν is constant in each Ω_j, and the Ψ_j are biharmonic there, Ψ is biharmonic in each Ω_j. **QED**

Next we show that, if Ψ satisfies (4.39), then it can be written as in (4.40).

(v) The Ψ_j are given by (4.44). Thus they satisfy the boundary data in (4.43). Further: they are also bi-harmonic because ν and $\nu^{\#}$ are constant on the Ω_j. **(vi)** Using (4.44) and the interface jump conditions in (4.39), a direct check shows that (on $z = 0$) $\Psi_1 = \partial_z^2 \Psi_1 = 0$ and $\Psi_2 = \partial_z \Psi_2 = [\partial_z^2 \Psi_2] = 0$. **(vii)** Finally, theorem **4.5** shows that Ψ_1 (as defined in Ω_1) can be extended to an odd biharmonic function in Ω (no interface). But Ψ_1 is odd, so it must be its own extension. **QED**

Proof of the second parity split.

We begin by introducing a bit of notation, to emphasize the fact that Ψ_2 is actually two biharmonic functions (one for each subdomain, Ω_1 and Ω_2) linked through the interface jump conditions
$$\Psi_2 = \Psi_2^+ \text{ for } z > 0 \quad \text{and} \quad \Psi_2 = \Psi_2^- \text{ for } z < 0. \quad (4.48)$$

Because of the interface jump conditions for Ψ_2 in (4.42), $\Psi_2^{\pm} = \partial_z \Psi_2^{\pm} = 0$ on $z = 0$. Thus theorem **4.4** allows us to extend these functions to the whole of Ω, as biharmonic functions. Further, because Ψ_2 is even, $\Psi_2^+(x, z) = \Psi_2(x, z) = \Psi_2(x, -z) = \Psi_2^-(x, -z)$ for $z > 0$, and the extensions satisfy
$$\Psi_2^+(x, z) = \Psi_2^-(x, -z), \quad (4.49)$$
for all z. Further
$$\Psi_2 = \begin{cases} \frac{1}{2}\left(\Psi_2^+ + \Psi_2^-\right) + \frac{1}{2}\left(\Psi_2^+ - \Psi_2^-\right) = \Psi_{2,e} + \Psi_{2,o} & \text{for } z > 0, \\ \frac{1}{2}\left(\Psi_2^+ + \Psi_2^-\right) - \frac{1}{2}\left(\Psi_2^+ - \Psi_2^-\right) = \Psi_{2,e} - \Psi_{2,o} & \text{for } z < 0, \end{cases} \quad (4.50)$$

where $\Psi_{2,e}$ and $\Psi_{2,o}$ are defined by the formulas. However, from (4.49), $\Psi_2^- = (\Psi_2^+)^{\#}$. Hence $\Psi_{2,e}$ and $\Psi_{2,o}$ are even and odd, respectively. It is also easy to check that $\Psi_{2,e}|_{z=0} = \partial_z \Psi_{2,o}|_{z=0} = 0$. Thus (4.50) is (4.45).

Uniqueness: Assume now that $\Psi_2 = \tilde{\Psi}_{2,e} + \sigma \tilde{\Psi}_{2,o}$ for some other even-odd pair $\tilde{\Psi}_{2,e}$ and

$\tilde{\Psi}_{2,o}$. Then, for $z > 0$, $\Psi_2^+ = \tilde{\Psi}_{2,e} + \tilde{\Psi}_{2,o}$, from which it follows that $\Psi_2^+ = \tilde{\Psi}_{2,e} + \tilde{\Psi}_{2,o}$ everywhere. Similarly $\Psi_2^- = \tilde{\Psi}_{2,e} - \tilde{\Psi}_{2,o}$. Thus (4.50) yields $\Psi_{2,e} = \tilde{\Psi}_{2,e}$ and $\Psi_{2,o} = \tilde{\Psi}_{2,o}$

Finally, a straightforward calculation shows that if Ψ_2 can be written as in (4.45), then $\Psi_2 = \partial_z \Psi_2 = [\partial_z^2 \Psi_2] = 0$.   **QED**

4.3.2 Solving the Odd Subproblem: a Well Conditioned Problem

First we can write Ψ_1 using the odd basis functions of the form in Equation (4.34). Since the sines are odd, we will set $\tilde{a}_n = \tilde{b}_n = 0$

$$\Psi_1 = \sum_{n=1}^{\infty} \left(\tilde{c}_n + \tilde{d}_n r^2 \right) r^n \sin(n\theta) \tag{4.51}$$

Note that Equation (4.51) already satisfies all conditions at $z = 0$ of Equation (4.41). Satisfying the conditions at $r = 1$ would result in the following

$$f_1 = \sum_{n=1}^{\infty} \left(\tilde{c}_n + \tilde{d}_n \right) \sin(n\theta) \tag{4.52}$$

$$g_1 = \sum_{n=1}^{\infty} \left(n\tilde{c}_n + (n+2)\tilde{d}_n \right) \sin(n\theta) \tag{4.53}$$

which, upon taking the inner product with respect to $\sin(k\theta)$ over $[0, 2\pi]$, for $k = 1, 2, 3, ...$, result in the standard Fourier series problem

$$\langle f_1, \sin k\theta \rangle_{[0,2\pi]} = \sum_{n=1}^{\infty} \left(\tilde{c}_n + \tilde{d}_n \right) \langle \sin(n\theta), \sin(k\theta) \rangle_{[0,2\pi]} \tag{4.54}$$

$$\langle g_1, \sin k\theta \rangle_{[0,2\pi]} = \sum_{n=1}^{\infty} \left(n\tilde{c}_n + (n+2)\tilde{d}_n \right) \langle \sin(k\theta), \sin(n\theta) \rangle_{[0,2\pi]} \tag{4.55}$$

where f_1 and g_1 are defined in (4.43). But since $\langle \sin(k\theta), \sin(n\theta) \rangle_{[0,2\pi]} = \pi\delta_{kn}$, we can conclude that

$$\tilde{c}_k + \tilde{d}_k = \frac{1}{\pi} \langle f_1, \sin k\theta \rangle_{[0,2\pi]} \tag{4.56}$$

$$k\tilde{c}_k + (k+2)\tilde{d}_k = \frac{1}{\pi} \langle g_1, \sin k\theta \rangle_{[0,2\pi]} \tag{4.57}$$

which means that

$$\tilde{d}_k = \frac{1}{2\pi} \left(\langle g_1, \sin k\theta \rangle_{[0,2\pi]} - k \langle f_1, \sin k\theta \rangle_{[0,2\pi]} \right) \tag{4.58}$$

$$\tilde{c}_k = \frac{1}{\pi} \langle f_1, \sin k\theta \rangle_{[0,2\pi]} - \tilde{d}_k \tag{4.59}$$

4.3.3 Solving the Even Subproblem: an Ill Conditioned Problem

We now write down the expressions of Ψ_2 in terms of $\Psi_{2,e}$ and $\Psi_{2,o}$ using the corresponding basis functions in Equation (4.33):

$$\Psi_{2,e} = \sum_{n=1}^{\infty} a_n r^{n+1} (\cos((n+1)\theta) - \cos((n-1)\theta)) \tag{4.60}$$

$$\Psi_{2,o} = \sum_{n=2}^{\infty} b_n r^{n+1} ((n-1)\sin((n+1)\theta) - (n+1)\sin((n-1)\theta)) \tag{4.61}$$

so that

$$\Psi_2 = \Psi_{2,e} + \sigma \Psi_{2,o} \tag{4.62}$$

Note that in the second equation, the index starts at $n = 2$ since the basis function is 0 for $n = 1$. Also note that Ψ_2 defined as such automatically satisfies the boundary conditions at $z = 0$ of Equation (4.42).

Now to satisfy the boundary conditions at $r = 1$, we again use the inner product and the definitions of f_2 and g_2 in (4.43) to write

$$\langle \Psi_2, \cos k\theta \rangle_{[0,2\pi]} = \langle f_2, \cos k\theta \rangle_{[0,2\pi]} \tag{4.63}$$

$$\langle \Psi_{2,r}, \cos k\theta \rangle_{[0,2\pi]} = \langle g_2, \cos k\theta \rangle_{[0,2\pi]} \tag{4.64}$$

Which becomes

$$\langle f_2, \cos k\theta \rangle_{[0,2\pi]} = \sum_{n=1}^{\infty} a_n \left(\langle \cos((n+1)\theta), \cos(k\theta) \rangle_{[0,2\pi]} - \langle \cos((n-1)\theta), \cos(k\theta) \rangle_{[0,2\pi]} \right)$$

$$+ \sum_{n=2}^{\infty} b_n \left((n-1) \langle \sigma(z) \sin((n+1)\theta), \cos(k\theta) \rangle_{[0,2\pi]} \right)$$

$$+ \sum_{n=2}^{\infty} b_n \left(-(n+1) \langle \sigma(z) \sin((n-1)\theta)), \cos(k\theta) \rangle_{[0,2\pi]} \right)$$

$$= \sum_{n=1}^{\infty} a_n A_{kn}^{(1)} + \sum_{n=2}^{\infty} b_n B_{kn}^{(1)}$$

(4.65)

and

$$\langle g_2, \cos(k\theta) \rangle = \sum_{n=1}^{\infty} a_n \left((n+1)(\langle \cos((n+1)\theta), \cos(k\theta) \rangle_{[0,2\pi]} - \langle \cos((n-1)\theta), \cos(k\theta) \rangle_{[0,2\pi]} \right)$$

$$+ \sum_{n=2}^{\infty} b_n \left((n+1)((n-1) \langle \sigma(z) \sin((n+1)\theta), \cos(k\theta) \rangle_{[0,2\pi]} \right)$$

$$+ \sum_{n=2}^{\infty} b_n \left(-(n+1) \langle \sigma(z) \sin((n-1)\theta)), \cos(k\theta) \rangle_{[0,2\pi]} \right)$$

$$= \sum_{n=1}^{\infty} a_n A_{kn}^{(2)} + \sum_{n=2}^{\infty} b_n B_{kn}^{(2)}$$

(4.66)

Here $A_{kn}^{(1)}, B_{kn}^{(1)}, A_{kn}^{(2)}, B_{kn}^{(2)}$ are infinite matrices defined as

$$A_{kn}^{(1)} = \langle \cos((n+1)\theta), \cos(k\theta) \rangle_{[0,2\pi]} - \langle \cos((n-1)\theta), \cos(k\theta) \rangle_{[0,2\pi]}$$

(4.67)

$$B_{kn}^{(1)} = (n-1) \langle \sigma(z) \sin((n+1)\theta), \cos(k\theta) \rangle_{[0,2\pi]}$$

$$- (n+1) \langle \sigma(z) \sin((n-1)\theta)), \cos(k\theta) \rangle_{[0,2\pi]}$$

(4.68)

$$A_{kn}^{(2)} = (n+1)(\langle \cos((n+1)\theta), \cos(k\theta) \rangle_{[0,2\pi]}$$

$$- (n+1) \langle \cos((n-1)\theta), \cos(k\theta) \rangle_{[0,2\pi]}$$

(4.69)

$$B_{kn}^{(2)} = (n+1)((n-1) \langle \sigma(z) \sin((n+1)\theta), \cos(k\theta) \rangle_{[0,2\pi]}$$

$$- (n+1) \langle \sigma(z) \sin((n-1)\theta)), \cos(k\theta) \rangle_{[0,2\pi]}$$

(4.70)

Here we remark that for any integer k, $\langle \sigma(z) \sin(m\theta)), \cos(k\theta) \rangle_{[0,2\pi]}$ can be evaluated as

follows.

$$\langle \sigma(z)\sin(m\theta)), \cos(k\theta)\rangle_{[0,2\pi]} = \int_0^\pi \sin(m\theta)\cos(k\theta)d\theta - \int_\pi^{2\pi} \sin(m\theta)\cos(k\theta)d\theta \quad (4.71)$$

$$= 2\int_0^\pi \sin(m\theta)\cos(k\theta)d\theta \quad (4.72)$$

$$= \pi\chi_{mk} \quad (4.73)$$

where $\chi_{mk} = \frac{2}{\pi}\int_0^\pi \sin(m\theta)\cos(k\theta)d\theta$ was first defined in Equation (3.178) and is now rewritten here as

$$\chi_{mk} = \begin{cases} 0, & k+m \text{ is even} \\ 1/m, & m \text{ is odd and } k=0 \\ 2m/(m^2-k^2), & k+m \text{ is odd and } m \neq 0 \end{cases} \quad (4.74)$$

Lastly, we decide on the cutoff as by presetting a natural number N such that

$$\langle f_2, \cos k\theta\rangle_{[0,2\pi]} = \sum_{n=1}^N a_n A_{kn}^{(1)} + \sum_{n=2}^{N+1} b_n B_{kn}^{(1)} \quad (4.75)$$

$$\langle g_2, \cos(k\theta)\rangle_{[0,2\pi]} = \sum_{n=1}^N a_n A_{kn}^{(2)} + \sum_{n=2}^{N+1} b_n B_{kn}^{(2)} \quad (4.76)$$

and that $0 \leq k \leq N-1$. We form the following three matrices

$$A = \begin{bmatrix} A^{(1)} \\ A^{(2)} \end{bmatrix}, B = \begin{bmatrix} B^{(1)} \\ B^{(2)} \end{bmatrix}, C = \begin{bmatrix} A & B \end{bmatrix} \quad (4.77)$$

Note that

$$A \in \mathbb{R}^{N \times N}, B \in \mathbb{R}^{N \times N}, C \in \mathbb{R}^{2N \times 2N} \quad (4.78)$$

In this way, we can obtain the coefficients a_n and b_n via the following linear system

$$C\vec{v} = \vec{F} \quad (4.79)$$

where

$$\vec{v} = [a_1, a_2, ...a_N, b_2, b_3, ..., b_{N+1}]^T \tag{4.80}$$

$$\vec{F} = \left[\left\{ \langle f_2, \cos k\theta \rangle_{[0,2\pi]} \right\}_{k=1}^N, \left\{ \langle g_2, \cos k\theta \rangle_{[0,2\pi]} \right\}_{k=2}^{N+1} \right]^T \tag{4.81}$$

Now we check the condition number of C. We plot the condition number of the matrix C vs. N on a log-log scale in Figure B-17. As one can see, the condition number grows like $O(N^4)$, rendering the system ill-conditioned. The reason for this seems to elude us.

4.4 Fixing the Condition Number: In Search of a "Natural Basis"

Figure B-17 points to the fact that the ill-conditioned nature of the Stokes problem with internal boundary exists not only in $3D$ but also in $2D$. We surmise that this is because we are not using the most "natural" basis. As an analogy we know that $\sum a_n x^n$ is not the most natural way to express $f(x)$, for $|x| < 1$, due to the resulting ill-conditioned Hilbert matrix. Instead, we must use $P_n(x)$, Legendre polynomials of order n, to expand $f(x)$ to be well-conditioned. Similarly, the basis functions $\cos(n\theta)$ and $\pm \sin(n\theta)$ may also not be natural to the system. We must search for the equivalent of Legendre polynomials for the even subproblem in Equation (4.42).

4.4.1 A Simplification: Biharmonic on Upper Unit Disk with Zero on $z = 0$

Because of the reflection symmetry in the second parity split resulted from Theorem **4.4**, we can simplify the problem by just considering Ψ_2 biharmonic in the upper unit disk with $\Psi_2 = \partial_z \Psi_2 = 0$ along $z = 0$. As before, the solution would be $\Psi_2 = \Psi_{2,e} + \Psi_{2,o}$, where $\Psi_{2,e}$ and $\Psi_{2,o}$ are shown in Equation (4.60), and upon reindexing, can be written as

$$\Psi_{2,e} = \sum_{n=1}^{\infty} a_n r^{n+1} (\cos((n+1)\theta) - \cos((n-1)\theta) \tag{4.82}$$

$$\Psi_{2,o} = \sum_{n=1}^{\infty} b_n r^{n+1} ((n-1)\sin((n+1)\theta) - (n+1)\sin((n-1)\theta)) \tag{4.83}$$

4.4.2 The Candidate Basis: C_n and S_n

We now introduce two new basis functions $\{C_n\}_{n=1}^\infty$ and $\{S_n\}_{n=1}^\infty$ over the upper half unit circle.

$$C_n(\theta) = \cos((n+1)\theta) - \cos((n-1)\theta) \tag{4.84}$$

$$S_n(\theta) = (n-1)\sin((n+1)\theta) - (n+1)\sin((n-1)\theta) \tag{4.85}$$

Then Ψ_2 can be written as

$$\Psi_2 = \sum_{n=1}^\infty r^{n+1}\left(\alpha_n C_n(\theta) + \beta_n S_n(\theta)\right) \tag{4.86}$$

We hypothesize C_n and S_n are the candidate natural basis functions for the system. But first, we must prove that C_n and S_n are complete, orthogonal (with respect to $1/\sin^2\theta$) basis functions in the vector space $L^2([0,\pi])$ with vanishing value and first derivative value at the end points $\theta = 0, \pi$.

To see that C_n is complete in the same L^2 space, we let f be a function with Fourier cosine series such that

$$f = \sum_{n=0}^\infty a_n \cos(n\theta) \tag{4.87}$$

with $\sum|a_n| < \infty$ and $\sum_{n \text{ odd}} a_n = \sum_{n \text{ even}} a_n = 0$. This ensures that $f(\theta) = f'(\theta) = 0$ for $\theta = 0, \pi$. Now we define coefficients α_n such that

$$\alpha_n = -\sum_{l=0}^{(n-1)/2} a_{n-2l-1} \tag{4.88}$$

This ensures that $a_n = \alpha_{n-1} - \alpha_{n+1}$ and that

$$f = \sum_{n=1}^\infty \alpha_n C_n(\theta) = \sum_{n=0}^\infty a_n \cos(n\theta) \tag{4.89}$$

In this way, $\alpha_n \to 0$ as $n \to \infty$. Moreover, we observe that

$$\sum_{n=1}^N \alpha_n C_n = \sum_{n=0}^{N-1} a_n \cos(n\theta) + \alpha_{N-1}\cos(N\theta) + \alpha_N \cos((N+1)\theta) \tag{4.90}$$

As $N \to \infty$, $\sum_{n=1}^{N} \alpha_n C_n \to f$, uniformly.

Now to see that C_n are orthogonal, we first observe that through the trig identity, $\sin(a)\sin(b) = \frac{1}{2}(\cos(a-b) - \cos(a+b))$, we can rewrite C_n as

$$C_n(\theta) = -2\sin\theta\sin(n\theta) \tag{4.91}$$

and hence we can compute that for some integers $k, n > 1$

$$\int_0^\pi C_n C_k \frac{d\theta}{\sin^2\theta} = 2\pi\delta_{kn} \tag{4.92}$$

whence we conclude that C_n are orthogonal with respect to the weight factor $\frac{1}{\sin^2\theta}$.

Next we prove that S_n form a complete orthogonal basis for the same L^2 space. To do that, we write formally that

$$\sum_{n=1}^{\infty} b_n \sin(n\theta) = \sum_{n=2}^{\infty} \beta_n S_n(\theta) \tag{4.93}$$

where we establish the connections between b_n and β_n as

$$b_n = (n-2)\beta_{n-1} - (n+2)\beta_{n+1} \tag{4.94}$$

$$\beta_n = -\sum_{l=0}^{(n-2)/2} \frac{n-2l}{n^2-1} b_{n-2l-1} \tag{4.95}$$

Then following the arguments as before, we can establish the uniform convergence of the S_n series towards f.

Now to see that S_n are orthogonal with respect to the weight factor $1/\sin^2\theta$, we compute

$$\int_0^\pi S_n(\theta)S_k(\theta)\frac{d\theta}{\sin^2\theta} \tag{4.96}$$

To do so, we note that $\left(\frac{\sin(n\theta)}{\sin\theta}\right)' = \frac{S_n(\theta)}{2\sin^2\theta}$ and that $S_n'(\theta) = (n^2-1)C_n(\theta)$. Hence we

perform an integration by parts

$$\int_0^\pi S_n(\theta)S_k(\theta)\frac{d\theta}{\sin^2\theta} = \int_0^\pi \left(\frac{\sin n\theta}{\sin\theta}\right)'(2S_k(\theta))d\theta \tag{4.97}$$

$$= \int_0^\pi \left(\frac{\sin n\theta}{\sin\theta}\right)'(2S_k(\theta))d\theta \tag{4.98}$$

$$= \left(\frac{\sin n\theta}{\sin\theta}\right)\bigg|_{\theta=0}^\pi - 2\int_0^\pi \frac{\sin n\theta}{\sin\theta}\left((k^2-1)C_n(\theta)\right)d\theta \tag{4.99}$$

The first term can be evaluated using L'Hopital's rule to be zero, while the second term can be calculated using Equation (4.91)

$$\int_0^\pi S_n(\theta)S_k(\theta)\frac{d\theta}{\sin^2\theta} = 4\int_0^\pi \sin(n\theta)\sin(k\theta)(k^2-1) \tag{4.100}$$

$$= 2\pi(k^2-1)\delta_{nk} \tag{4.101}$$

Hence, we can take the inner product with respect to $1/\sin^2\theta$ to find the coefficients α_n and β_n in Equation (4.86) at $r=1$, which would look like

$$f_2(\theta) = \sum_{n=1}^\infty \left(\alpha_n C_n(\theta) + \beta_n S_n(\theta)\right) \tag{4.102}$$

$$g_2(\theta) = \sum_{n=1}^\infty (n+1)\left(\alpha_n C_n(\theta) + \beta_n S_n(\theta)\right) \tag{4.103}$$

which, upon taking the inner product, becomes

$$\int_0^\pi f_2(\theta)C_k(\theta)\frac{d\theta}{\sin^2\theta} = \sum_{n=1}^\infty \left(\alpha_n \int_0^\pi C_n(\theta)\frac{d\theta}{\sin^2\theta} + \beta_n \int_0^\pi S_n(\theta)\frac{d\theta}{\sin^2\theta}\right) \tag{4.104}$$

$$\int_0^\pi g_2(\theta)C_n(\theta)\frac{d\theta}{\sin^2\theta} = \sum_{n=1}^\infty (n+1)\left(\alpha_n \int_0^\pi C_n(\theta)\frac{d\theta}{\sin^2\theta} + \beta_n \int_0^\pi S_n(\theta)\frac{d\theta}{\sin^2\theta}\right) \tag{4.105}$$

Hence we now define infinite matrices $C^{(1)}, D^{(1)}, C^{(2)}, D^{(2)}, E$, such that

$$C_{kn}^{(1)} = \int_0^\pi C_n C_k \frac{d\theta}{\sin^2 \theta} \tag{4.106}$$

$$D_{kn}^{(1)} = \int_0^\pi S_n C_k \frac{d\theta}{\sin^2 \theta} \tag{4.107}$$

$$C_{kn}^{(2)} = (n+1) \int_0^\pi C_n C_k \frac{d\theta}{\sin^2 \theta} \tag{4.108}$$

$$D_{kn}^{(2)} = (n+1) \int_0^\pi S_n C_k \frac{d\theta}{\sin^2 \theta} \tag{4.109}$$

$$E = \begin{bmatrix} C^{(1)} & D^{(1)} \\ C^{(2)} & D^{(2)} \end{bmatrix} \tag{4.110}$$

We will make each of the $C^{(1)}, C^{(2)}, D^{(1)}, D^{(2)}$ an $2N \times N$ matrix, rendering E an $N \times 2N$ matrix. Hence, we can recast Equation (4.102) and (4.103) into a matrix-vector equation

$$E\vec{u} = \vec{H} \tag{4.111}$$

where

$$\vec{u} = [\vec{\alpha}, \vec{\beta}]^T = [\alpha_1, ..., \alpha_N, \beta_1, ..., \beta_N]^T \tag{4.112}$$

$$\vec{H} = \left[\vec{H}_1, \vec{H}_2 \right]^T \tag{4.113}$$

$$= \left[\left\{ \int_0^\pi f_2(\theta) C_k(\theta) \frac{d\theta}{\sin^2 \theta} \right\} |_{k=1}^N, \left\{ \int_0^\pi g_2(\theta) C_n(\theta) \frac{d\theta}{\sin^2 \theta} \right\} |_{k=1}^N \right]^T \tag{4.114}$$

4.4.3 Schur-Banachiewicz Blockwise Inversion: Condition Number Reduction

We will solve the matrix equation in (4.111) using the Schur-Banachiewicz blockwise inversion, which effectively reduces the condition number of E to its block matrices. Given the expression of E in Equation (4.110) and the matrix equation (4.111), the Schur-Banachiewicz Blockwise inversion claims that the unknown coefficients $\vec{u}$ satisfies

$$E_{mod}\vec{v} = \vec{H}_{mod} \tag{4.115}$$

where

$$E_{mod} = \begin{bmatrix} \left(I_N - \left(C^{(1)}\right)^{-1} D^{(1)} \left(D^{(2)}\right)^{-1} C^{(1)} \right) \\ \left(I_N - \left(D^{(2)}\right)^{-1} C^{(2)} \left(C^{(1)}\right)^{-1} D^{(1)} \right) \end{bmatrix} \tag{4.116}$$

$$\vec{H}_{mod} = \begin{bmatrix} \left(C^{(1)}\right)^{-1} \vec{H}_1 - \left(C^{(1)}\right)^{-1} D^{(1)} \left(D^{(2)}\right)^{-1} \vec{H}_2 \\ \left(D^{(2)}\right)^{-1} \vec{H}_2 - \left(D^{(2)}\right)^{-1} C^{(2)} \left(C^{(1)}\right)^{-1} \vec{H}_1 \end{bmatrix} \tag{4.117}$$

Here I_N is the identity matrix of dimension N. To prove the Schur-Banachiewicz Block-wise inversion formula, we first multiple out the matrix-vector form in Equation (4.111)

$$C^{(1)}\vec{\alpha} + D^{(1)}\vec{\beta} = \vec{H}_1 \tag{4.118}$$

$$C^{(2)}\vec{\alpha} + D^{(2)}\vec{\beta} = \vec{H}_2 \tag{4.119}$$

We multiply Equation (4.118) by $\left(C^{(1)}\right)^{-1}$ and Equation (4.119) by $\left(D^{(2)}\right)^{-1}$

$$\vec{\alpha} + \left(C^{(1)}\right)^{-1} D^{(1)}\vec{\beta} = \left(C^{(1)}\right)^{-1} \vec{H}_1 \tag{4.120}$$

$$\left(D^{(2)}\right)^{-1} C^{(2)}\vec{\alpha} + \vec{\beta} = \left(D^{(2)}\right)^{-1} \vec{H}_2 \tag{4.121}$$

We then multiply Equation (4.120) by $\left(D^{(2)}\right)^{-1} C^{(2)}$ before subtracting Equation (4.121) from it to obtain

$$\left(I_N - \left(D^{(2)}\right)^{-1} C^{(2)} \left(C^{(1)}\right)^{-1} D^{(1)} \right) \vec{\beta} = \left(D^{(2)}\right)^{-1} \vec{H}_2 - \left(D^{(2)}\right)^{-1} C^{(2)} \left(C^{(1)}\right)^{-1} \vec{H}_1 \tag{4.122}$$

Using the similar Gaussian elimination process, we can compute that

$$\left(I_N - \left(C^{(1)}\right)^{-1} D^{(1)} \left(D^{(2)}\right)^{-1} C^{(1)} \right) \vec{\alpha} = \left(C^{(1)}\right)^{-1} \vec{H}_1 - \left(C^{(1)}\right)^{-1} D^{(1)} \left(D^{(2)}\right)^{-1} \vec{H}_2 \tag{4.123}$$

Equation (4.122) and (4.123) for the entries in the Schur-Banachiewicz Blockwise inversion formula in Equation (4.116).

As shown in Figure B-18, the C_n and S_n basis functions and the Schur-Banachiewicz Blockwise inversion formula stifle the growth of the condition number to $O(N^2)$.

4.5 Conclusion and Future Directions

In this chapter of the dissertation we summarized the results in [49], as well as the various puzzles and issues that this work uncovers, such as: (i) Is there some underlying general principle behind the solution form proposed in [49]? (ii) Is the proposed form a valid representation for solutions (i.e.: are the "modes" complete and independent)? (iii) Is it true that the solutions in each subdomain have extensions to the other subdomain (a rather uncommon phenomena for elliptic equations)? (iv) Can the growth of the condition number for the linear system that needs to be solved be ameliorated? (v) What is the nature of the singularity, and can it be extracted so as to improve the convergence rate?

These questions motivated us to study a simpler analog of the problem, designed so that the same issues arise: the biharmonic equation in $2D$, over a domain that includes a circle with an internal boundary. We then extend the Parity Split Method (PSM) of prior chapters to this second problem; which then allows us to resolve the issues in items (i–iii) above. As in the case of Laplace's, the PSM splits the biharmonic problem into even and odd problems. While the odd problem is easy to solve, the even problem exhibits the type of problem in item (iv) above. However, in this case we find a way to reduce the growth rathe of the condition number via a combination of functional analysis and linear algebra. The issue in item (v) above remains open.

We believe that the $2D$ results reported above can be extended to the $3D$ Janus drop case. In particular, an improved convergence rate might allow then an accurate computation of important physical quantities such as the drag. However, the key issue that remains to be solved is item (v) above. This is the main roadblock that prevents simple and compact approximations to the solution of problems of this type; such approximations are the key to being able to, say, model large arrays of Janus drops. They would also provide intuition as to, for example, how to best control the behavior of Janus drops.

Appendix A

Tables

Table A.1: Unless otherwise explicitly specified, the parameters used to perform the calculations in Section 3.4 are as in this table. The starred quantities are from [11]. The wedge size and angle are typical dimensions for a micro heat pipe [54]. The thermal gradient is such that the maximum temperature and the far-field temperature differ by $\sim 1K$ over $500\mu m$.

Parameter	Description	Values
T_∞	*far-field temperature	$295K$
ρ_1	Density of liquid (water)	$1000 kg/m^3$
ρ_2	Density of Gas (air)	$1 kg/m^3$
$\frac{dC_{sat}}{dT}\big|_{T=T_\infty}$	*an empirical constant	$1.11 * 10^{-3} kg/(m^3 K)$
$C_{sat}(T_\infty)$	*saturation concentration at T_∞	$1.94 * 10^{-2} kg/m^3$
D	*mass diffusivity	$2.46 * 10^{-5} m^2/s$
ν_1	conductivity of liquid (water)	$0.5918 J/(msK)$
ν_2	conductivity of gas (air)	$0.0260 J/(msK)$
a_0	initial height of the interface	$250\mu m$
$\tilde{L}_w$	wedge size	$500\mu m$
Φ	wedge angle	20°
η_T	thermal gradient	$2000 K/m$
$c_{v,1}$	the specific heat capacity of water at T_∞	$4200 J/(kg * K)$
$c_{v,2}$	the specific heat capacity of air at T_∞	$710 J/(kg * K)$

Appendix B

Figures
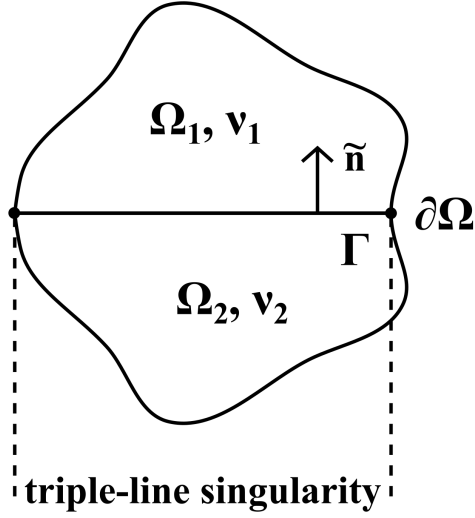
Figure B-1: Example of the type of domain to be considered. Triple-line singularities typically arise at the points where materials of three different properties meet. Plot author: Daniel Bergen, Master in Molecular Biotechnology at Bielefeld University (Bielefeld, German) and PhD in Systems Biology at ETH Zurich (Zurich, Switzerland).


(a) (b)
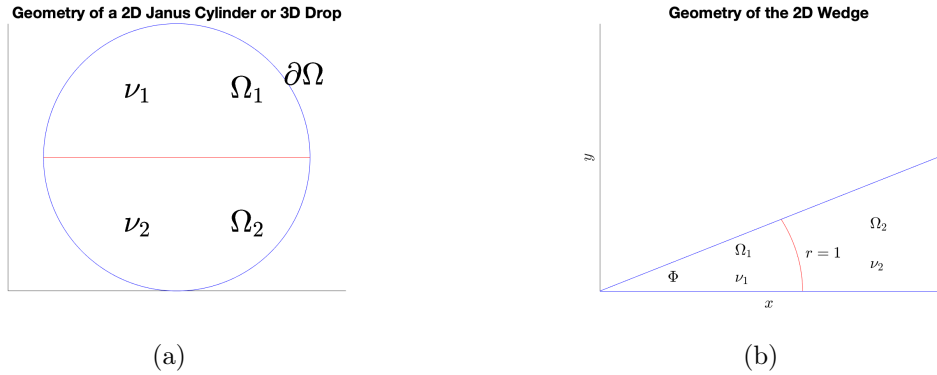
Figure B-2: Example geometries: (a) Sketch for a $2D$ Janus cylinder or a $3D$ Janus drop. The upper and lower hemispheres have different material properties, e.g.: viscosties ν_1 and ν_2, respectively. (b) Infinite wedge, with an interface placed at $r = 1$, and different material properties for $r < 1$ and $r > 1$.
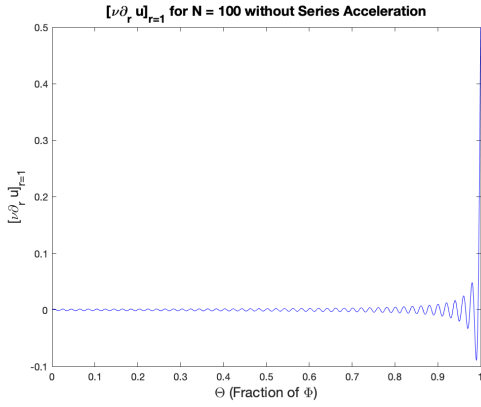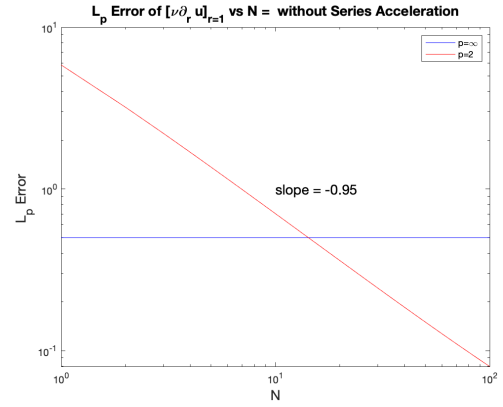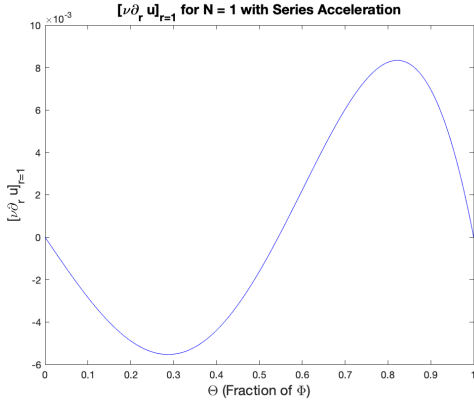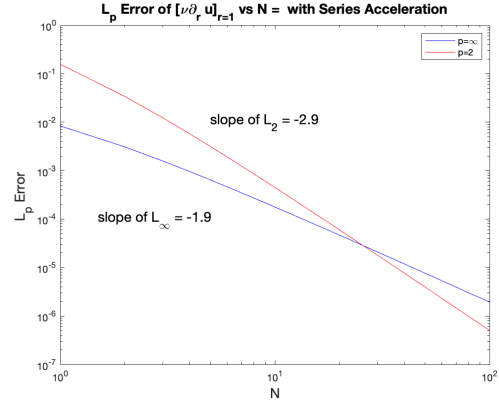
Figure B-3: Comparison of how well the solution, with and without series acceleration, satisfies the boundary condition $[\partial_r u]|_{r=1} = 0$ — see §2.3.3.2. Panels (a) and (b) display results without series acceleration, while panels (c) and (d) correspond to the accelerated series. The difference is dramatic.
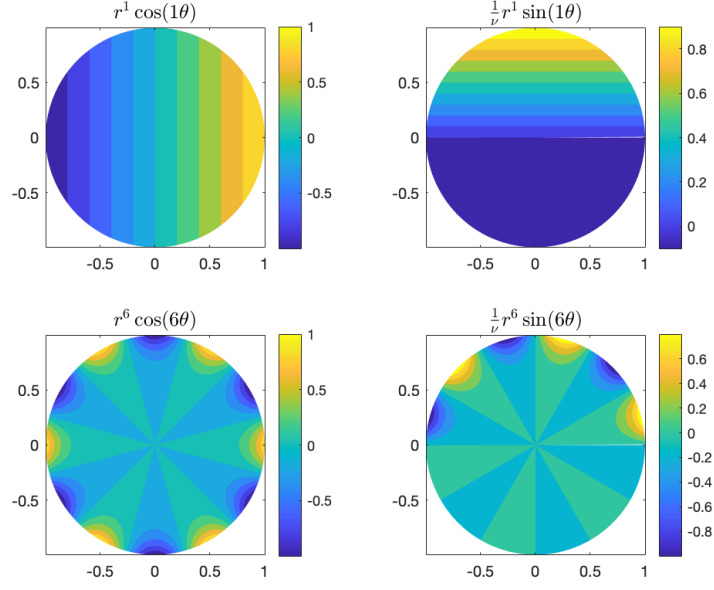
Figure B-4: Eigenmodes in (2.18). $2D$ Janus cylinder with $\nu_1 = 1$ and $\nu_2 = 10$.
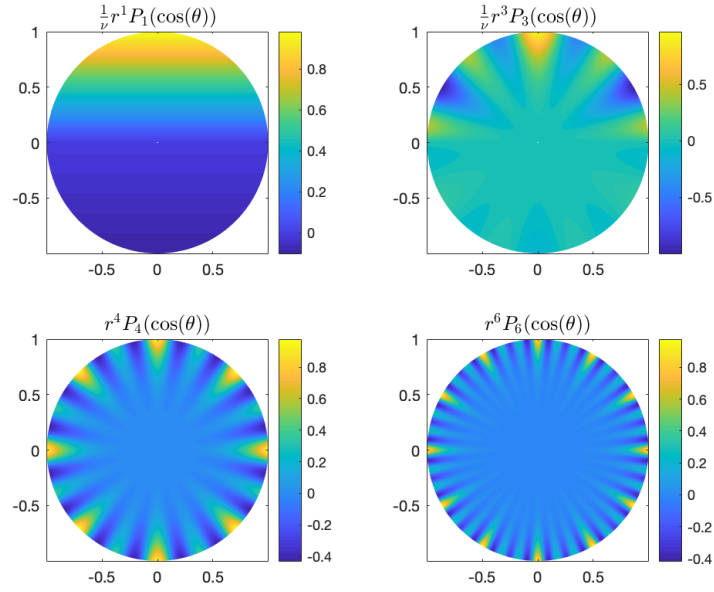
Figure B-5: Eigenmodes in (2.27). $3D$ Janus drop with $\nu_1 = 1$ and $\nu_2 = 10$.
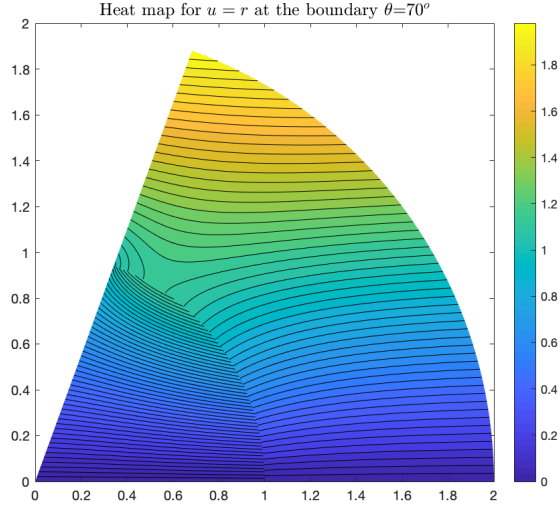
Figure B-6: Heat map for the solution in (2.44), with $\nu_1 = 1$ and $\nu_2 = 10$. The boundary conditions are: $u = 0$ for $\theta = 0$ and $u = r$ for $\theta = \Phi$.
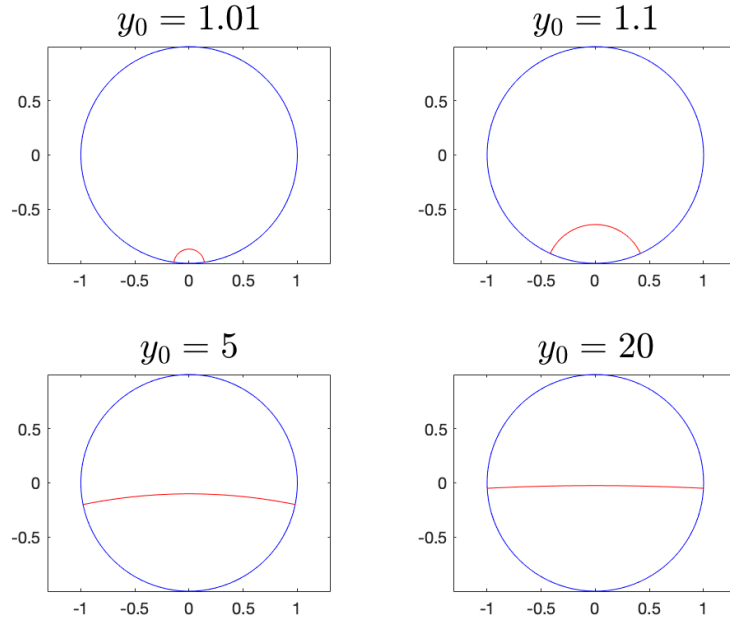
Figure B-7: Acceptable PSM interfaces (in red) for the unit disk — see (2.69). The interfaces are circles of radius $\sqrt{y_0^2 - 1}$ centered at some $-y_0 < 1$, in any Cartesian coordinate system sharing the origin with the disk. As $y_0 \to \infty$, the interface approaches a flat line at $y = 0$.
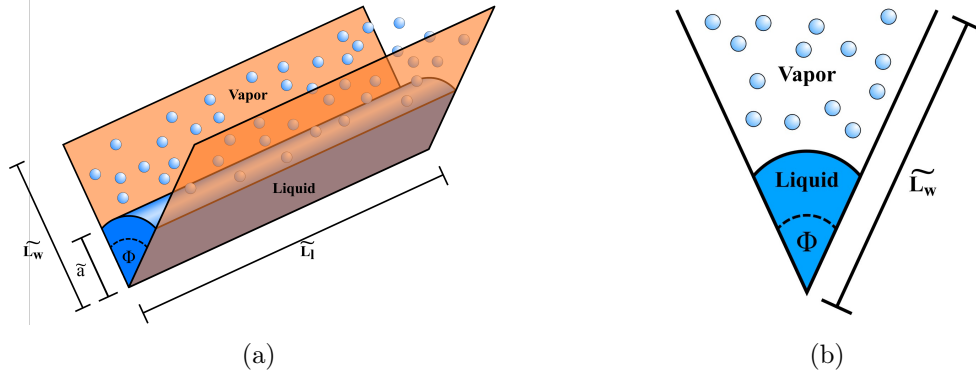
Figure B-8: Schematics for the V-shaped liquid wedge. (a) shows a $3D$ rendition. When $\tilde{L}_l >> \tilde{L}_w$, the long dimension can be ignored, to yield a $2D$ problem — shown in (b). These figures are the product of the generosity and craftsmanship of Daniel Bergen, Master in Molecular Biotechnology at Bielefeld University (Bielefeld, German) and PhD in Systems Biology at ETH Zurich (Zurich, Switzerland).
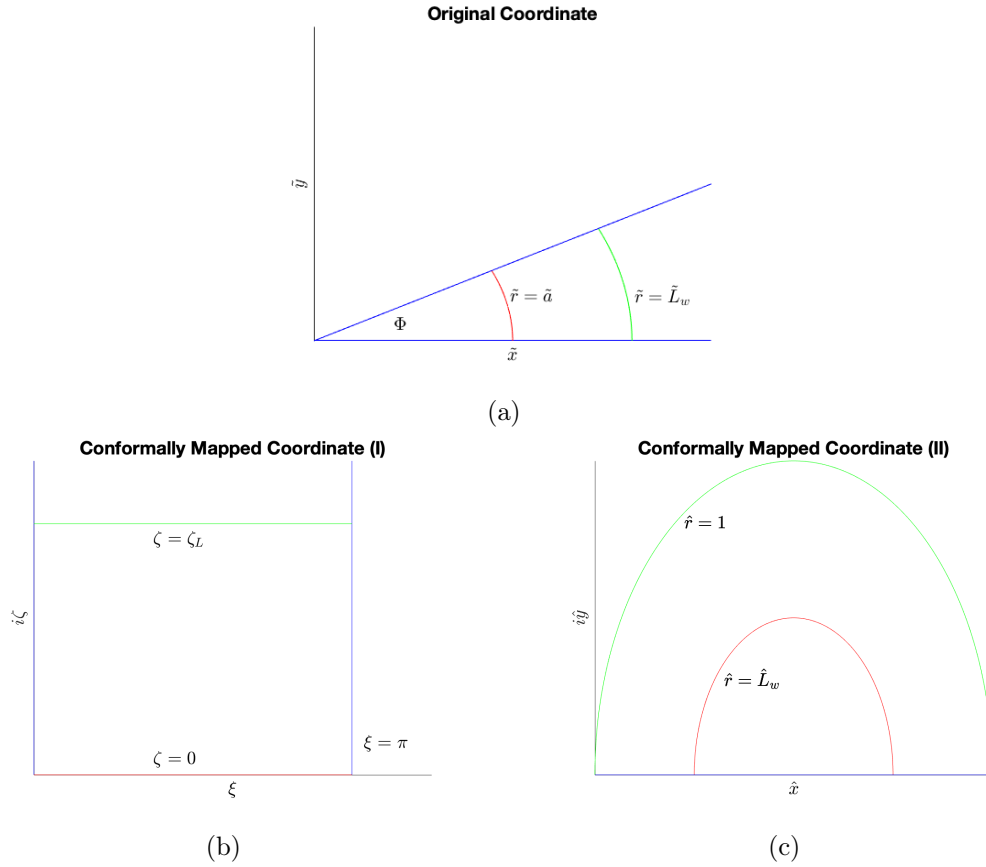
Figure B-9: The coordinates used to solve the Laplace problem. (a) original coordinates, (b) and (c) conformally mapped coordinates in (3.122) and (3.134), respectively. Here curves of the same color map onto each other.

(a)   (b)
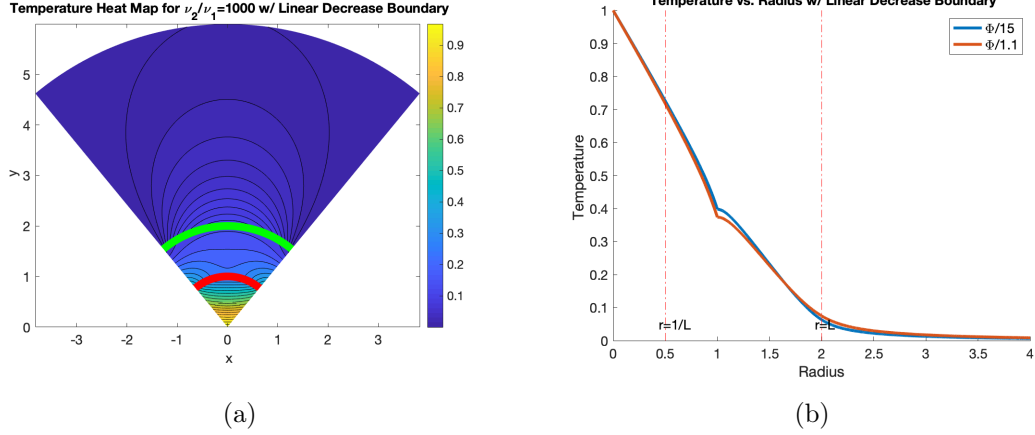
Figure B-10: Solution to the temperature problem with a linearly decreasing boundary temperature (here $\nu_2/\nu_1 = 1000$ and $L_w = 2$). (a) heat map of the temperature — in red the liquid-vapor interface, the green line is at the top of the wedge. (b) temperature vs. radius — the doted lines correspond to $r = L_w$ and $1/L_w$.

(a)   (b)
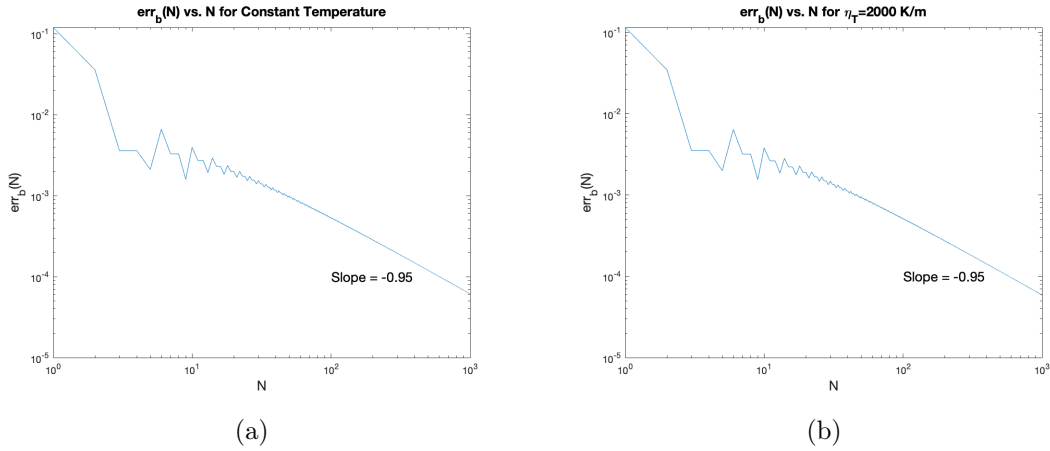
Figure B-11: $err_b(N)$ vs. N plotted on a log-log scale for two temperature wedge-boundary conditions: (a) constant, and (b) piece-wise linear. These plots gauge the convergence of the series solution in (3.127) through the error in the total flux across the interface, as characterized by b in (3.162). This is given by $err_b(N)$ in (3.196–3.197), the absolute value of the difference between the exact value for b in (3.156), and the first N terms in the series in (3.174). In both cases, the series solution converges (slowly) at a sub-linear rate $O(N^{-0.95})$.
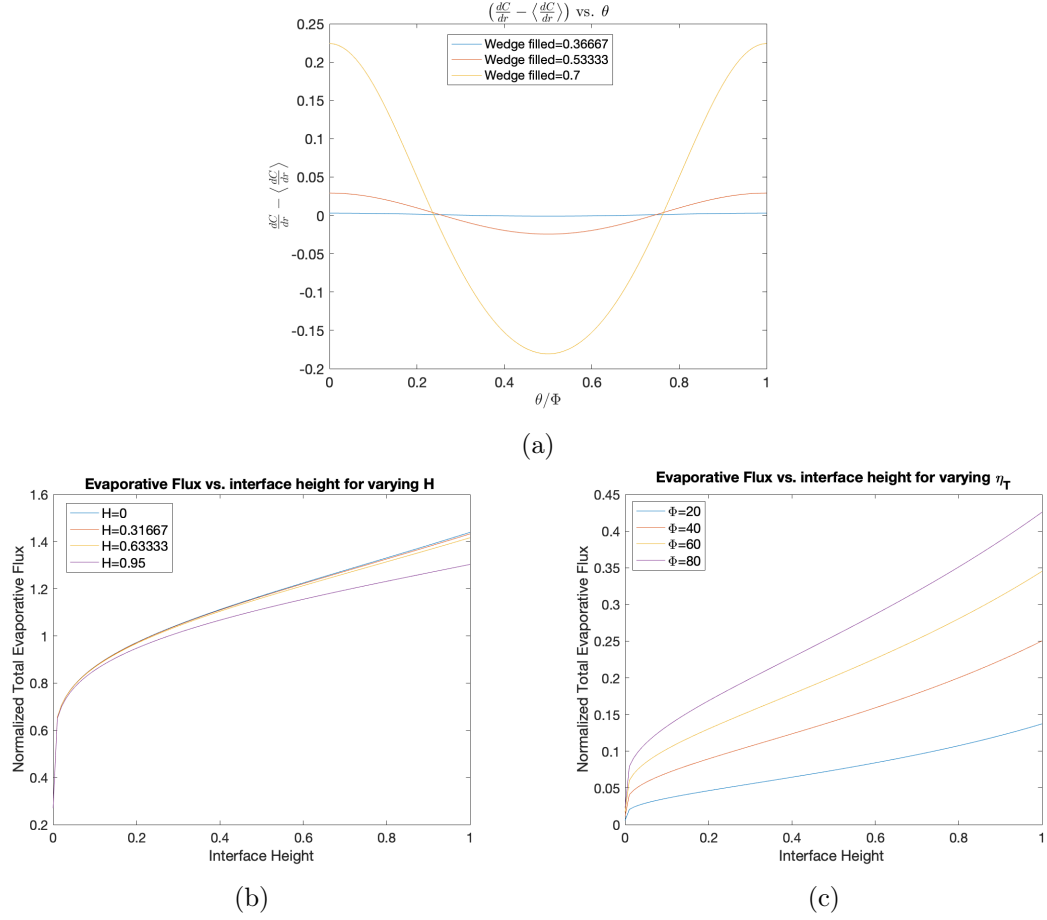
Figure B-12: Plots of the radial flux: (a) Normalized radial flux with the mean subtracted. The flux is larger near the wedge sides $(\theta = 0, \Phi)$, as expected. (b) and (c) Total normalized evaporation flux for different: heights of the liquid vapor interface, humidity levels, and angle sizes. As expected, the flux is smaller for higher humidity or a larger angle.
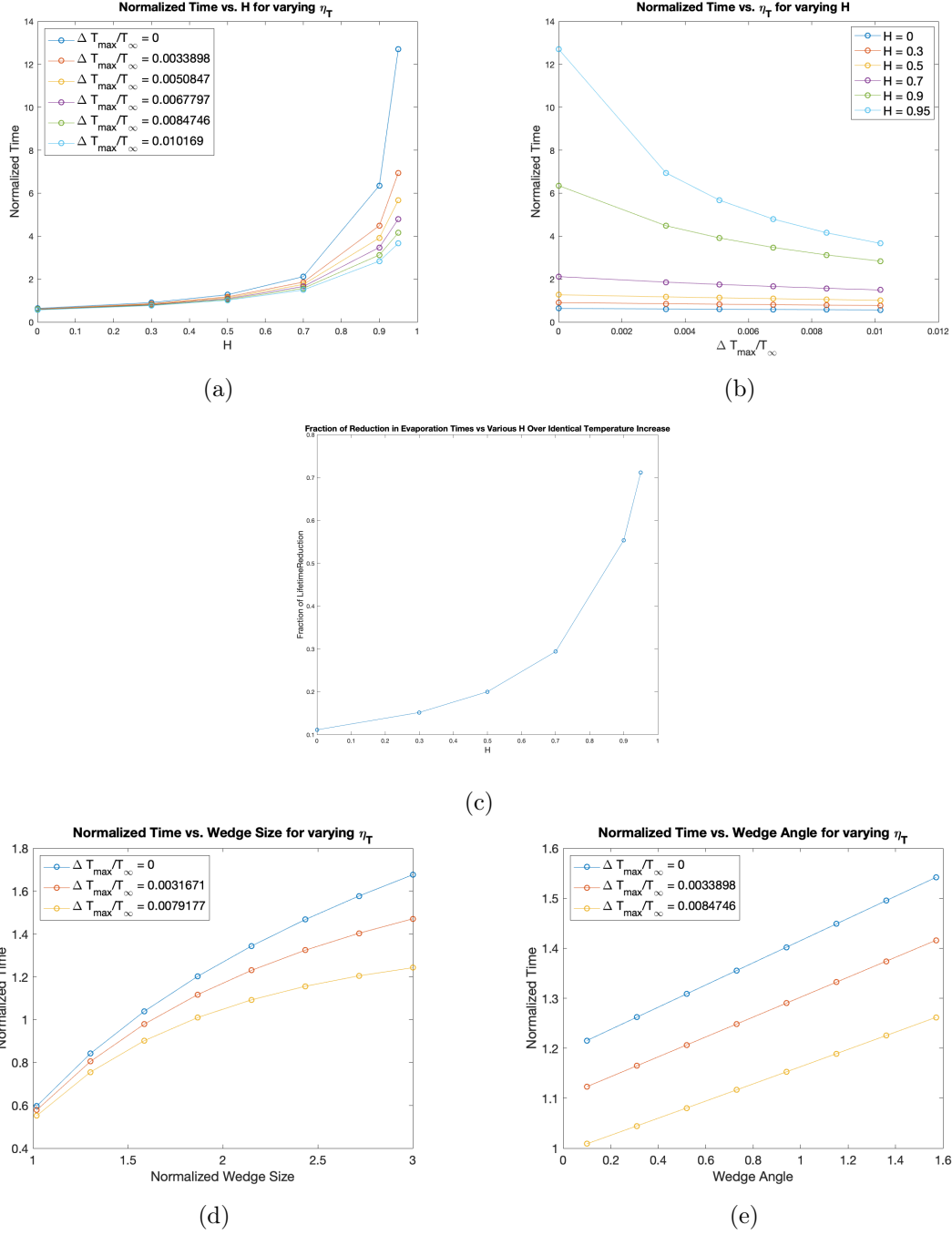
(a)

(b)

(c)

(d)

(e)

Figure B-13: Plots of the normalized lifetime versus temperature, relative humidity, wedge size, and wedge angle. The lifetime increases with the humidity (a), and it decreases with the thermal gradient (b). Note in (c) the enhancement of the thermal gradient by the humidity: the same temperature increment reduces the lifetime by a larger fraction as humidity increases. We further note an increasing trend in lifetime with both wedge size and wedge angle, (d) and (e).
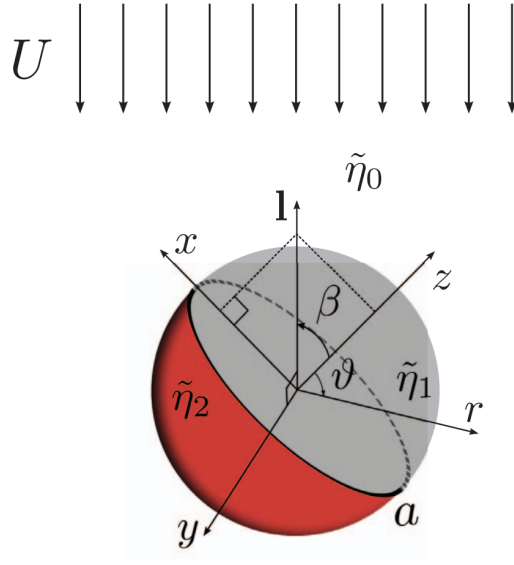
Figure B-14: (From FIG 1 in [49]) Janus drop in an external flow $-U\hat{z}$. The angle β indicates the drop orientation with respect to the flow: $\beta = 0$ corresponds to the internal interface normal to the external flow (axis-symmetric problem). Note that the authors use η, while we use ν, to denote viscosities.
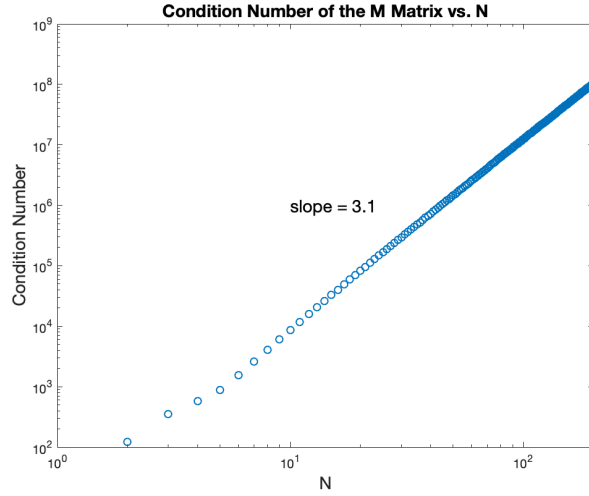

Figure B-15: Condition number for the matrix M in (4.26), truncated to size $4N \times 3N$, versus N, on a log-log scale. Here $\nu_1 = 1$ and $\nu_2 = 0.5$. The condition number grows too rapidly: $O(N^3)$.

(a)

(b)

(c)

(d)
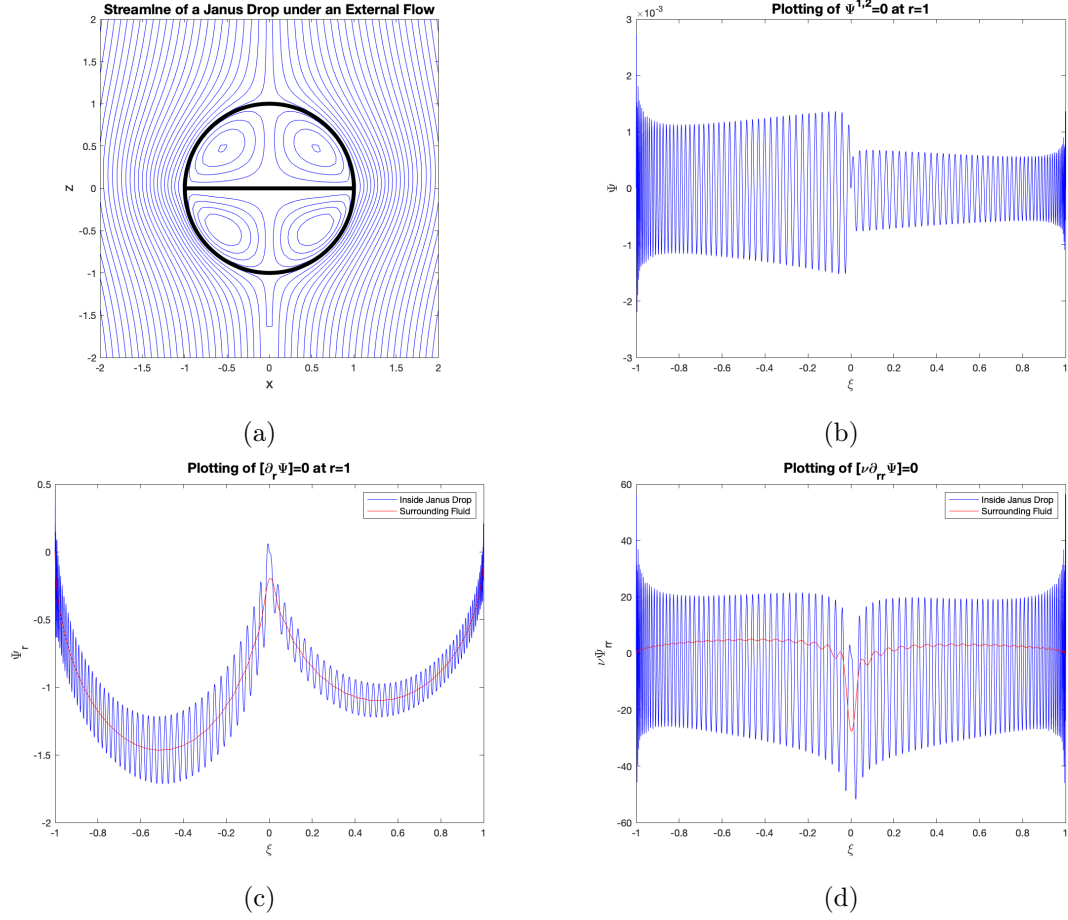
Figure B-16: Solution in (4.10)-(4.11), for $\nu_1 = 1$ and $\nu_2 = 0.5$, with $N = 200$. a) shows the streamlines for the Janus drop under the external flow. This agrees visually with the result in FIG. 4 of [49]. However, the boundary conditions at $r = 1$ are poorly satisfied. While (b) shows acceptable accuracy for $\Psi^{1,2} = 0$ at $r = 1$ (error $O(10^{-3})$), (c) and (d) indicate lack of convergence for the boundary conditions at $r - 1$ involving first and second derivatives of the stream-function. Note the large spurious oscillations
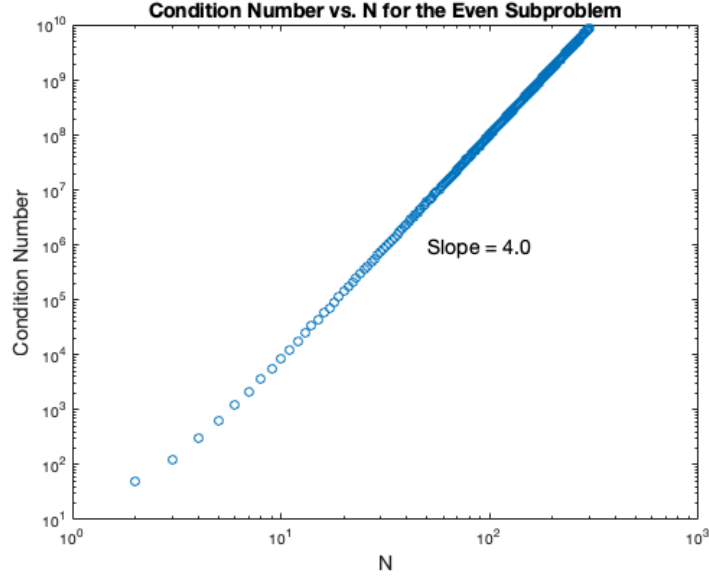
Figure B-17: Condition Number for the matrix C in (4.77), truncated to size $2N \times 2N$, versus N, on a log-log scale. The condition number grows too rapidly, $O(N^4)$. This is the same issue that arises with the matrix M in (4.26), for the $3D$ axisymmetric Stokes equation.
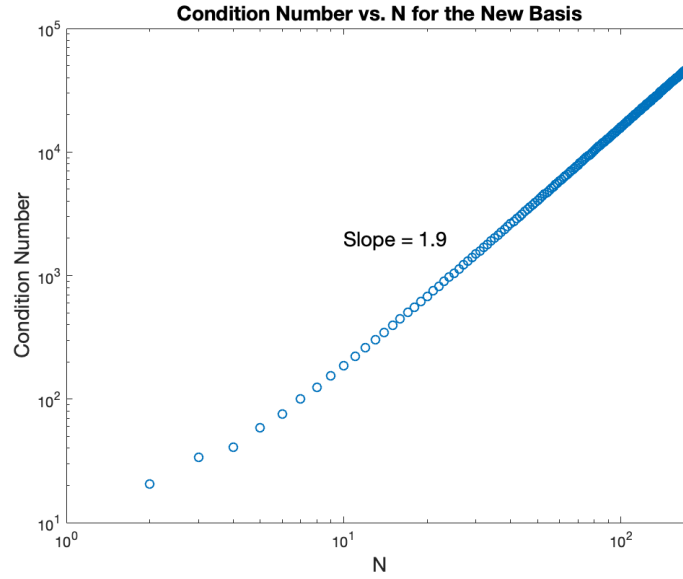

Figure B-18: Condition Number for the matrix E_{mod} in (4.116), obtained with the Schur-Banachiewicz Blockwise Inversion, truncated to size of $2N \times 2N$, versus N on a log-log scale. The condition number here grows slower, $O(N^2)$, than the case shown in Figure B-17.
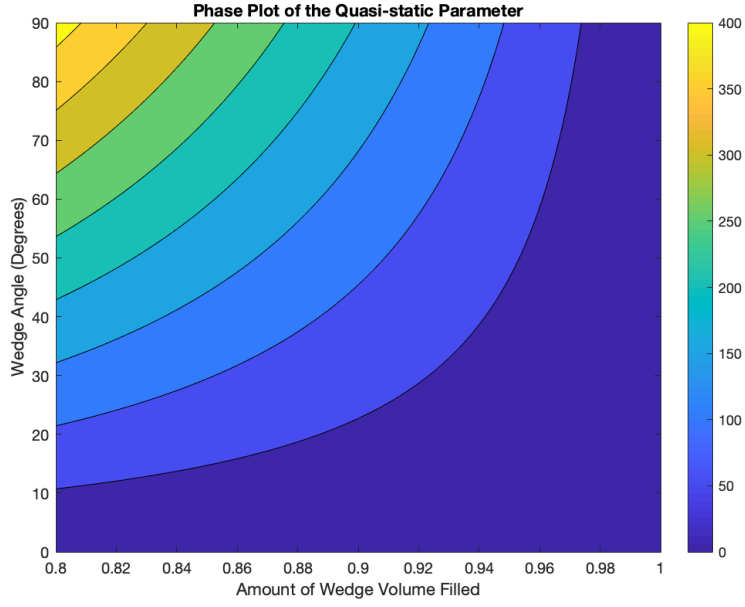
Figure B-19: Heat map for the quasi-static parameter λ in (D.17), with a/L_w on the x-axis and the wedge angle on the y-axis. The quasi-static assumption is valid for a "not too large" wedge angle, and a "not too filled with liquid" wedge.
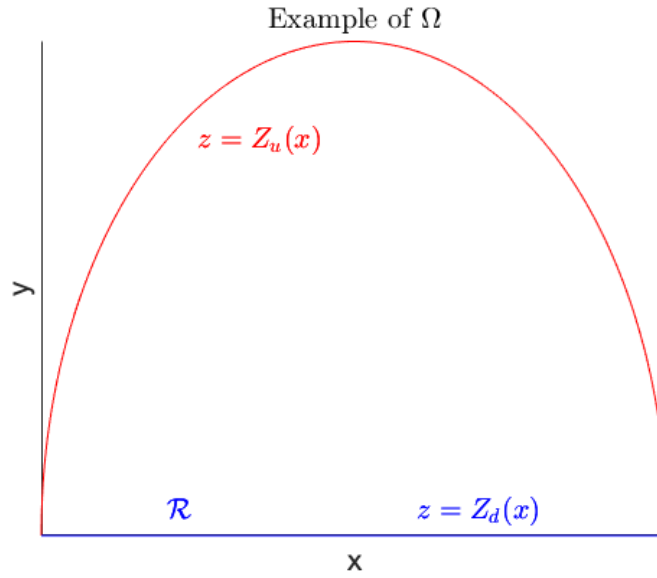

Figure B-20: Example of the region Ω in Section 4.2.2.

Appendix C

Integration of the Associated Legendre Polynomials over a Half Interval

This section concerns the efficient computation of the inner products of associated Legendre polynomials over the half interval $[0, 1]$. For two integers k, l, we would like to compute

$$U_{kl} = \int_0^1 P_k^1(\xi) P_l^1(\xi) d\xi \tag{C.1}$$

The analytical answer of U_{kl} is known to be

$$U_{kl} = \begin{cases} \frac{l(l+1)}{2l+1}, & l = k \\ 0, & l \neq k \\ f_{kl}, & \text{otherwise} \end{cases} \tag{C.2}$$

Here f_{kl} is

$$f_{kl} = \frac{2}{\pi} \left(l(l+1) \frac{\sin\left(\frac{\pi}{2}k\right) \cos\left(\frac{\pi}{2}l\right) A_{kl}}{k(k+1) + l(l+1)} - k(k+1) \frac{\sin\left(\frac{\pi}{2}l\right) \cos\left(\frac{\pi}{2}k\right) A_{lk}}{k(k+1) + l(l+1)} \right) \tag{C.3}$$

where A_{lk} is defined as

$$A_{lk} = \frac{\Gamma\left(\frac{l}{2}+1\right)\Gamma\left(\frac{k}{2}+\frac{1}{2}\right)}{\Gamma\left(\frac{l}{2}+\frac{1}{2}\right)\Gamma\left(\frac{k}{2}+1\right)} \tag{C.4}$$

Here Γ denotes the gamma function. If we directly compute A_{lk}, we would run into the issue of numerical overflows. Therefore, we must massage Equation (C.4). More specifically, we will consider two cases: (i) l even and k odd; (ii) l odd and k even.

For l even and k odd, $l/2$ and $\frac{k}{2}+\frac{1}{2}$ are integers, whence we can simplify that

- $\Gamma\left(\frac{l}{2}+1\right) = \Gamma(integer) = \left(\frac{l}{2}\right)!$

- $\Gamma\left(\frac{l}{2}+1\right) = \sqrt{\pi}\frac{(l-1)!!}{2^{l/2}} = \sqrt{\pi}\frac{l!}{4^{l/2}\left(\frac{l}{2}\right)!}$

- $\Gamma\left(\frac{k}{2}+\frac{1}{2}\right) = \left(\frac{k}{2}+\frac{1}{2}-1\right)! = \left(\frac{k}{2}-\frac{1}{2}\right)! = \left(\frac{k-1}{2}\right)!$

- $\Gamma\left(\frac{k}{2}+1\right) = \Gamma\left(\frac{k}{2}+\frac{1}{2}+\frac{1}{2}\right) = \sqrt{\pi}\frac{(k)!!}{2^{(k+1)/2}} = \sqrt{\pi}\frac{(k+1)!}{4^{(k+1)/2}\left(\frac{k+1}{2}\right)!} = \sqrt{\pi}\frac{k!!}{2^{(k+1)/2}}$

Putting everything together, we can simplify A_{lk} as

$$A_{lk} = \frac{\left(\frac{l}{2}\right)!\left(\frac{k-1}{2}\right)!}{\sqrt{\pi}\frac{(l-1)!!}{2^{l/2}}\sqrt{\pi}\frac{k!!}{2^{(k+1)/2}}} \tag{C.5}$$

$$= \frac{1}{\pi}4^{\frac{l+k+1}{2}}\frac{(l/2)!!(l/2)!}{l!}\frac{\left(\frac{k-1}{2}\right)!\left(\frac{k+1}{2}\right)!}{(k+1)!} \tag{C.6}$$

Hence if we now define the following vectors of size l,

$$v_1 = [1, 2, ..., l/2, (4)(1), (4)(2), ..., (4)(l/2)]^T \tag{C.7}$$

$$w_1 = [1, 2, ..., l]^T \tag{C.8}$$

$$\tag{C.9}$$

Then we can simplify some terms in Equation (C.5)

$$\prod_{j=1}^{l}\left(\frac{v_{1,j}}{w_{1,j}}\right) = 4^{l/2}\frac{(l/2)!(l/2)!}{l!} \tag{C.10}$$

Similarly, if we define the following vectors of size k,

$$v_2 = [1, 2, ..., (k-1)/2, 4(1), 4(2), ..., (4)((k+1)/2)]^T \tag{C.11}$$

$$w_2 = [1, 2, ..., K]^T \tag{C.12}$$

then we can write

$$\frac{1}{k+1} \prod_{j=1}^{l} \left(\frac{v_{2,j}}{w_{2,j}} \right) = 4^{(k+1)/2} \frac{\left(\frac{k-1}{2} \right)! \left(\frac{k+1}{2} \right)!}{(k+1)!} \tag{C.13}$$

As a result, we can rewrite A_{lk} as

$$A_{lk} = \frac{1}{\pi} \frac{1}{k+1} \prod_{j=1}^{l} \left(\frac{v_{1,j}}{w_{1,j}} \right) \prod_{j=1}^{l} \left(\frac{v_{2,j}}{w_{2,j}} \right) \tag{C.14}$$

For l odd and k even, we can follow an almost identical calculation. In the end, we can define the following vectors

$$v_3 = [1, 2, ..., l]^T \tag{C.15}$$

$$w_3 = [1, 2, ..., (l-1)/2, (4)(1), (4)(2), ..., (4)((l+1)/2)]^T \tag{C.16}$$

$$v_4 = [1, 2, ..., k]^T \tag{C.17}$$

$$w_4 = [1, 2, ..., k/2, (4)(1), (4)(2), ..., (4)(k/2)]^T \tag{C.18}$$

so that A_{lk} can be written as

$$A_{lk} = \pi(l+1) \prod_{j=1}^{l} \left(\frac{v_{3,j}}{w_{3,j}} \right) \prod_{j=1}^{l} \left(\frac{v_{4,j}}{w_{4,j}} \right) \tag{C.19}$$

In this way, we avoid having to compute the large gamma functions that breaks the computational limit of a standard computer.

Appendix D

Justification for Quasi-Staticity

The quasi-static assumptions of concentration and temperature in Equation (3.3) and (3.8) will be justified in this section. We first study the characteristic time scales associated with the full time-driven heat and concentration equations. We would simplify the physical and just consider homogeneous boundary conditions over the wedge. Quasi-staticity would be justified if the largest characteristic times is dominated by the lifetime of the liquid bridge. This would ensure that the equations reach equilibrium much sooner than the droplet completely evaporates. Secondly, we calculate the incremental mass loss during the initial transience of the time-dependent concentration evolution. We would want to be sure that the mass loss is small compared with the total remaining mass.

D.1 Comparing Characteristic Times with Lifetime of Liquid Bridge

To estimate the time scale needed by the temperature and the concentration to reach steady state, we solve the time dependent equations with homogeneous boundary conditions, in the domains

$$\Omega_1 = \{(r, \theta) : 0 \leq r < a, 0 \leq \theta \leq \Phi\} \text{ and } \Omega_2 = \{(r, \theta) : a \leq r < \infty, 0 \leq \theta \leq \Phi\}.$$

There are then three characteristic time scales: (i) $t_{T,1}$, the characteristic time for temperature in Ω_1; (ii) $t_{T,2}$, the characteristic time for temperature in Ω_2; (iii) $t_{C,2}$, the characteristic time for concentration in Ω_2. To calculate these time scales, we let $T^{(1)}$ denote temperature in Ω_1, $T^{(2)}$, C denote the temperature and concentration in Ω_2, and solve the PDE below.

Over Ω_1, solve

$$
\begin{cases}
T_t^{(1)} = \dfrac{\nu_1}{\rho_1 c_{v,1}} \Delta T^{(1)} \\[2mm]
T^{(1)} = 0, & \theta = 0, \Phi \\[2mm]
T_r^{(1)} = 0, & r = a
\end{cases}
\tag{D.1}
$$

and over Ω_2, we want to solve

$$
\begin{cases}
T_t^{(2)} = \dfrac{\nu_2}{\rho_2 c_{v,2}} \Delta T^{(2)} \\[2mm]
T^{(2)} = 0, \theta = 0, \Phi \\[2mm]
T_r^{(2)} = 0, r = a
\end{cases}
\quad , \quad
\begin{cases}
C_t = D \Delta C \\[2mm]
C_\theta = 0, \theta = 0, \Phi \\[2mm]
C = 0, r = a
\end{cases}
\tag{D.2}
$$

Here c_v denotes the specific heat capacity. Using separation of variables, we can express the solutions as infinite series

$$
T^{(1)} = \sum_{m=1}^{\infty} \sum_{n=1}^{\infty} A_{mn}^{(1)} \sin\left(\frac{n\pi\theta}{\Phi}\right) J_n\left(\frac{\eta_{m,n} r}{a}\right) e^{-\frac{\eta_{m,n}^2 \nu_1}{\rho_1 c_{v,1} a^2} t}
\tag{D.3}
$$

where J_n are the Bessel's functions of the first kind and order n, and $\eta_{m,n}$ denotes the mth root of the first derivative of J_n. Of all the terms in the infinite series, the most slowly decaying term is for $n = m = 1$. Hence, we can take $t_{T,1}$ to be the largest characteristic time of $n = m = 1$

$$
t_{T,1} = \frac{\rho_1 c_{v,1} a^2}{\eta_{1,1}^2 \nu_1}
\tag{D.4}
$$

Here $\eta_{1,1} \approx 2$. Similarly, we can write down the solutions $T^{(2)}$

$$
T^{(2)}(r, \theta, t) = \sum_{m=1}^{\infty} \sum_{n=1}^{\infty} A_{mn}^{(2)} \sin\left(\frac{n\pi\theta}{\Phi}\right) J_n\left(\frac{\eta_{m,n} r}{a}\right) e^{-\frac{\eta_{m,n}^2 \nu_2}{\rho_2 c_{v,2} a^2} t}
\tag{D.5}
$$

$$
t_{T,2} = \frac{\rho_2 c_{v,2} a^2}{\eta_{1,1}^2 \nu_2}
\tag{D.6}
$$

Finally, we write down the solution to the concentration as

$$C(r, \theta, t) = \sum_{m=1}^{\infty} \sum_{n=0}^{\infty} A_{mn} \cos\left(\frac{n\pi\theta}{\Phi}\right) J_n\left(\frac{\gamma_{m,n}}{a} r\right) e^{-\frac{\gamma_{m,n}^2 D}{a^2} t} \tag{D.7}$$

where $\gamma_{m,n}$ is the mth zero of J_n. Here then, the slowest decaying process would be for $n = 0, m = 1$, which makes the characteristic time of concentration

$$t_{C,2} = \frac{a^2}{\gamma_{1,0}^2 D} \tag{D.8}$$

Here $\gamma_{1,0} \approx 2.25$. The characteristic time t_c chosen to compare with the lifetime would then be

$$t_C = \max\{t_{T,1}, t_{T,2}, t_{C,2}\} \tag{D.9}$$

$$= \max\left\{\frac{a^2}{\gamma_{1,0}^2 D}, \frac{\rho_2 c_{v,2} a^2}{\eta_{1,1}^2 \nu_2}, \frac{\rho_1 c_{v,1} a^2}{\eta_{1,1}^2 \nu_1}\right\} \tag{D.10}$$

Next we compute the lifetime of the liquid bridge. As guided by Equation (3.198), we can set up the following relation of mass loss during a period of time dt at radius r

$$\int_0^{\Phi} D \frac{dC}{dr} r d\theta dt = \rho_1 r \Phi dr \tag{D.11}$$

$$t = \frac{\rho_1 \Phi}{D} \int_0^a \frac{dr}{\int_0^{\Phi} \frac{dC}{dr} d\theta} \tag{D.12}$$

To estimate $\frac{dC}{dr}$, we will shall use the mass flux from the following problem

$$\begin{cases} \Delta C = 0, & a \leq r \leq a_2, 0 \leq \theta \leq \Phi \\ C = C_{sat}, & r = a \\ C = 0, & r = L_w \\ \frac{\partial C}{\partial \theta} = 0, & \theta = 0, \Phi \end{cases} \tag{D.13}$$

$$\frac{dC}{dr} = C_{sat} \frac{1}{r \log\left(\frac{a}{L_w}\right)} \tag{D.14}$$

133

which, upon plugging in to Equation (D.12), renders the quantity of t_e, the evaporative lifetime of the liquid

$$t_e = \frac{\rho_1 \Phi a^2 \log\left(\frac{L_w}{a}\right)}{DC_{sat}} \tag{D.15}$$

The hope is that $t_e >> t_C$ in Equation (D.9). Therefore, we define the dimensionless, quasi-static parameter λ, as

$$\lambda = \frac{t_e}{t_C} \tag{D.16}$$

so that the quasi-static assumptions would hold if $\lambda >> 1$. We plug in the parameters in Table A.1, which we use to perform the calculations in Chapter 3, and simplify it to

$$\lambda \approx -1197\Phi \log\left(\frac{a}{L_w}\right) \tag{D.17}$$

We plot the heat map of λ with a/L_w on the x-axis and the wedge angle on the y-axis in Figure (B-19). As demonstrated, the quasi-static assumption is valid for a "not too large" wedge angles and "not too full" of a filled volume. For our case, with a wedge angle of 20°, the system is quasi-static as long as the height of the liquid stays around 80%-85% of the wedge size.

D.1.1 Estimate of the Mass Loss During the Initial Transience

We would like to estimate the amount of mass loss during the initial transience to steady state, characterized by the time scale $t_{C,2}$ in Equation(ref). In other words, we would like to compute

$$\frac{\Delta m}{m} = \frac{1}{\rho\frac{a^2}{2}\sin\Phi} \int_0^{t_C} \int_0^\Phi D\frac{dC}{dr}|_{r=a}ad\theta dt \tag{D.18}$$

where C satisfies the PDE below

$$
\begin{cases}
C_t = D\Delta C, & r > a \\
C = C_{sat}, & r = a \\
\frac{\partial C}{\partial \theta} = 0, & \theta = 0, \Phi \\
C = 0, & t = 0
\end{cases}
\tag{D.19}
$$

Here C_{sat} is the saturation concentration that has a temperature dependence. The solution to the differential equation above is

$$
C(r, \theta; t) = C_{sat} + \sum_{m=1}^{\infty} \sum_{n=0}^{\infty} A_{mn} \cos\left(\frac{n\pi\theta}{\Phi}\right) J_n\left(\frac{\gamma_{m,n}}{a}r\right) e^{-\frac{\gamma_{m,n}^2 D}{a^2}t}
\tag{D.20}
$$

where A_{mn} is to be determined by the initial condition. Plugging in $t = 0$, we get that

$$
0 = C_{sat} + \sum_{m=1}^{\infty} \sum_{n=0}^{\infty} A_{mn} \cos\left(\frac{n\pi\theta}{\Phi}\right) J_n\left(\frac{\gamma_{m,n}}{a}r\right)
\tag{D.21}
$$

$$
-C_{sat} = \sum_{m=1}^{\infty} \sum_{n=0}^{\infty} A_{mn} \cos\left(\frac{n\pi\theta}{\Phi}\right) J_n\left(\frac{\gamma_{m,n}}{a}r\right)
\tag{D.22}
$$

Upon taking the inner product with respect to the cosine terms for each n, we realize that $A_{mn} = 0$ for all $n \neq 0$, whence,

$$
-C_{sat} = \sum_{m=1}^{\infty} A_{m0} J_0\left(\frac{\gamma_{m,0}}{a}r\right)
\tag{D.23}
$$

Now we use the orthogonality relation that

$$
\int_0^a r J_0\left(\frac{\gamma_{m,0}}{a}r\right) J_0\left(\frac{\gamma_{k,0}}{a}r\right) = \frac{a^2}{2}(J_1(\gamma_{m,0}))^2 \delta_{m,k}
\tag{D.24}
$$

and the integration property of Bessel function

$$
\int_0^a r J_0(r) dr = a J_1(a)
\tag{D.25}
$$

to get that

$$-C_{sat} \int_0^a r J_0 \left(\frac{\gamma_{m,0}}{a} r \right) dr = A_{m0} \frac{a^2}{2} (J_1(\gamma_{m,0}))^2 \tag{D.26}$$

$$-C_{sat} \left(\frac{a}{\gamma_{m,0}} \right)^2 \int_0^{\gamma_{m,0}} r J_0(r) dr = A_{m0} \frac{a^2}{2} (J_1(\gamma_{m,0}))^2 \tag{D.27}$$

$$A_{m0} = -\frac{2C_{sat}}{\gamma_{m,0} J_1(\gamma_{m,0})} \tag{D.28}$$

There, the solution of $C(r, \theta; t)$ can be written as

$$C(r, \theta; t) = C_{sat} - 2C_{sat} \sum_{m=1}^{\infty} \frac{1}{\gamma_{m,0} J_1(\gamma_{m,0})} J_0 \left(\frac{\gamma_{m,0}}{a} r \right) e^{-\frac{\gamma_{m,0}^2 D}{a^2} t} \tag{D.29}$$

Therefore, $\frac{\partial C}{\partial r}$ can be written as

$$\frac{\partial C}{\partial r} = -C_{sat} \sum_{m=1}^{\infty} \frac{1}{a J_1(\gamma_{m,0})} \left(J_{-1} \left(\frac{\gamma_{m,0}}{a} r \right) - J_1 \left(\frac{\gamma_{m,0}}{a} r \right) \right) e^{-\frac{\gamma_{m,0}^2 D}{a^2} t} \tag{D.30}$$

where we use the fact that

$$\frac{d J_0(r)}{dr} = \frac{J_{-1}(r) - J_1(r)}{2} \tag{D.31}$$

Continuing on with the calculation, since $\frac{dC}{dr}$ has no angular dependence, $\int_0^{\Phi} \frac{dC}{dr} d\theta = \Phi \frac{dC}{dr}$, whence

$$\frac{\Delta m}{m} = \frac{1}{\rho \frac{a^2}{2} \sin \Phi} \int_0^{t_C} \int_0^{\Phi} D \frac{dC}{dr} a d\theta dt \tag{D.32}$$

$$= -\frac{2\Phi D}{\rho a^2 \sin \Phi} C_{sat} \sum_{m=1}^{\infty} \frac{1}{J_1(\gamma_{m,0})} \left(J_{-1}(\gamma_{m,0}) - J_1(\gamma_{m,0}) \right) |_{r=a} \int_0^{t_C} e^{-\frac{\gamma_{m,0}^2 D}{a^2} t} dt \tag{D.33}$$

$$= \frac{2\Phi}{\rho \sin \Phi} C_{sat} \sum_{m=1}^{\infty} \frac{1}{J_1(\gamma_{m,0}) \gamma_{m,0}^2} \left(J_{-1}(\gamma_{m,0}) - J_1(\gamma_{m,0}) \right) \left(e^{-\frac{\gamma_{m,0}^2}{\gamma_{1,0}^2} t} - 1 \right) \tag{D.34}$$

$$\leq \frac{2\Phi}{\rho \sin \Phi} C_{sat} \sum_{m=1}^{\infty} \frac{1}{J_1(\gamma_{m,0}) \gamma_{m,0}^2} \left(J_{-1}(\gamma_{m,0}) - J_1(\gamma_{m,0}) \right) \tag{D.35}$$

$$\tag{D.36}$$

Using the property of Bessel functions that $J_{-1}(r) = -J_1(r)$ and that $\gamma_{m,0} \geq 2m$, we

conclude with the estimate that

$$\frac{\Delta m}{m} \leq \frac{4\Phi}{\rho \sin \Phi} C_{sat} \sum_{m=1}^{\infty} \frac{1}{\gamma_{m,0}^2} \tag{D.37}$$

$$\leq \frac{\Phi}{\rho \sin \Phi} C_{sat} \sum_{m=1}^{\infty} \frac{1}{m^2} \tag{D.38}$$

$$= \frac{\Phi \pi^2}{6\rho \sin \Phi} C_{sat} \tag{D.39}$$

Assuming the wedge is smaller than $\pi/2$, the function $\frac{\Phi}{\sin \Phi}$ achieves its max value of $\pi/2$ at $\theta = \pi/2$, whence

$$\frac{\Delta m}{m} \leq \frac{\pi^3}{12\rho} C_{sat} \tag{D.40}$$

Taking the value of C_{sat} from Table A.1 at a temperature of $295K$, we plug in the density and the saturation concentration of water and conclude that

$$\frac{\Delta m}{m} \leq \frac{\pi^3}{12\rho} C_{sat} \tag{D.41}$$

$$= 5 * 10^{-5} \tag{D.42}$$

Less than 0.005% of the total volume of the drop is evaporated as the concentration transitions towards steady state, which completely justifies our quasi-static assumptions.

Bibliography

[1] Md. Mahbub Alam and Y. Zhou. Fluid dynamics around an inclined cylinder with running water rivulets. *Volume 1: Symposia, Parts A and B*, 2006.

[2] Oleg Alekseev and Mark Mineev-Weinstein. Theory of stochastic laplacian growth. *Journal of Statistical Physics*, 168(1):68–91, 2017.

[3] S. David, K. Sefiane, and L. Tadrist. Experimental investigation of the effect of thermal properties of the substrate in the wetting and evaporation of sessile drops. *Colloids and Surfaces A: Physicochemical and Engineering Aspects*, 298(1-2):108–114, 2007.

[4] P. G. de Gennes. Soft matter. *Rev. Mod. Phys.*, 64, 1992.

[5] Robert D. Deegan. Pattern formation in drying drops. *Physical Review E*, 61(1):475–485, 2000.

[6] Robert D. Deegan, Olgica Bakajin, Todd F. Dupont, Greb Huber, Sidney R. Nagel, and Thomas A. Witten. Capillary flow as the cause of ring stains from dried liquid drops. *Nature*, 389(6653):827–829, 1997.

[7] Robert D. Deegan, Olgica Bakajin, Todd F. Dupont, Greg Huber, Sidney R. Nagel, and Thomas A. Witten. Contact line deposits in an evaporating drop. *Physical Review E*, 62(1):756–765, 2000.

[8] Misael Díaz-Maldonado and Ubaldo M. Córdova-Figueroa. On the anisotropic response of a Janus drop in a shearing viscous fluid. *Journal of Fluid Mechanics*, 770, 2015.

[9] Misael Díaz-Maldonado and Ubaldo M. Córdova-Figueroa. Dynamics and rheology of Janus drops in a steady shear flow. *International Journal of Multiphase Flow*, 85:2–13, 2016.

[10] G.J. Dunn, S.K. Wilson, B.R. Duffy, S. David, and K. Sefiane. The effect of the thermal conductivity of the substrate on droplet evaporation. *Progress in Industrial Mathematics at ECMI 2006*, 2007.

[11] G.J. Dunn, S.K. Wilson, B.R. Duffy, S. David, and K. Sefiane. A mathematical model for the evaporation of a thin sessile liquid droplet: Comparison between experiment and theory. *Colloids and Surfaces A: Physicochemical and Engineering Aspects*, 323(1-3):50–55, 2008.

[12] Miltiades Elliotis, Georgios Georgiou, and Christos Xenophontos. The solution of laplacian problems over l-shaped domains with a singular function boundary integral method. *Communications in Numerical Methods in Engineering*, 18(3):213–222, 2002.

[13] Miltiades Elliotis, Georgios Georgiou, and Christos Xenophontos. Solving laplacian problems with boundary singularities: a comparison of a singular function boundary integral method with the p/hp version of the finite element method. *Applied Mathematics and Computation*, 169(1):485–499, 2005.

[14] A.F.M. Kilbinger F. Wurm. Polymeric janus particles compartment. *Angew. Chem. Int. Edm*, 48, 2009.

[15] Ronald P Fedkiw, Tariq Aslam, Barry Merriman, and Stanley Osher. A non-oscillatory eulerian approach to interfaces in multimaterial flows (the ghost fluid method). *Journal of Computational Physics*, 152(2):457–492, 1999.

[16] Ronald P Fedkiw, Tariq Aslam, and Shaojie Xu. The ghost fluid method for deflagration and detonation discontinuities. *Journal of Computational Physics*, 154(2):393–427, 1999.

[17] Frédéric Gibou, Liguo Chen, Duc Nguyen, and Sanjoy Banerjee. A level set based sharp interface method for the multiphase incompressible Navier-Stokes equations with phase change. *Journal of Computational Physics*, 222(2):536–555, 2007.

[18] Abinand Gopal and Lloyd N. Trefethen. New laplace and helmholtz solvers. *Proceedings of the National Academy of Sciences*, 116(21):10223–10225, 2019.

[19] Abinand Gopal and Lloyd N. Trefethen. Solving laplace problems with corner singularities via rational functions. *SIAM Journal on Numerical Analysis*, 57(5):2074–2094, 2019.

[20] Björn Gustafsson, Razvan Teodorescu, and Alexander Vasil'Ev. Laplacian growth and random matrix theory. *Classical and Stochastic Laplacian Growth Advances in Mathematical Fluid Mechanics*, pages 187–210, 2014.

[21] Jeong-Mo Hong, Tamar Shinar, Myungjoo Kang, and Ronald Fedkiw. On boundary condition capturing for multiphase interfaces. *Journal of Scientific Computing*, 2006.

[22] Hua Hu and Ronald G. Larson. Evaporation of a sessile droplet on a substrate. *The Journal of Physical Chemistry B*, 106(6):1334–1344, 2002.

[23] Hua Hu and Ronald G. Larson. Analysis of the effects of marangoni stresses on the microflow in an evaporating sessile droplet. *Langmuir*, 21(9):3972–3980, 2005.

[24] Hua Hu and Ronald G. Larson. Analysis of the microfluid flow in an evaporating sessile droplet. *Langmuir*, 21(9):3963–3971, 2005.

[25] A. A. Ivanova, V. G. Kozlov, and A. V. Chigrakov. Dynamics of a fluid in a rotating horizontal cylinder. *Fluid Dynamics*, 39(4):594–604, 2004.

[26] J. Lahann J. Yoon, K.J.Lee. Multifunctional polymer particles with distinct compartments. *Angew. Chem. Int. Edm*, 21, 2011.

[27] T. Kawamura and K. Kuwahara. Computation of high reynolds number flow around a circular cylinder with surface roughness. *22nd Aerospace Sciences Meeting*, 1984.

[28] Henrik Kettunen, Henrik Wallén, and Ari Sihvola. Polarizability of a dielectric hemisphere. *Journal of Applied Physics*, 102(4):044105, 2007.

[29] Randall J. Leveque and Zhilin Li. The immersed interface method for elliptic equations with discontinuous coefficients and singular sources. *SIAM Journal on Numerical Analysis*, 31(4):1019–1044, 1994.

[30] Randall J. Leveque and Zhilin Li. Immersed interface methods for stokes flow with elastic boundaries or surface tension. *SIAM Journal on Scientific Computing*, 18(3):709–735, 1997.

[31] Zhilin Li and Ming-Chih Lai. The immersed interface method for the Navier-Stokes equations with singular forces. *Journal of Computational Physics*, 171(2):822–842, 2001.

[32] H. Ma and G. Peterson. Temperature variation and heat transfer in triangular grooves with an evaporating film. *Guidance, Navigation, and Control Conference*, 1996.

[33] H. B. Ma and G. P. Peterson. Experimental investigation of the maximum heat transport in triangular grooves. *Journal of Heat Transfer*, 118(3):740–746, 1996.

[34] Alexandre Noll Marques, Jean-Christophe Nave, and Rodolfo Ruben Rosales. A correction function method for poisson problems with interface jump conditions. *Journal of Computational Physics*, 230(20):7567–7597, 2011.

[35] Hassan Masoud and James D. Felske. Analytical solution for stokes flow inside an evaporating sessile drop: Spherical and cylindrical cap shapes. *Physics of Fluids*, 21(4):042102, 2009.

[36] A. D. Mcewan. Inertial oscillations in a rotating fluid cylinder. *Journal of Fluid Mechanics*, 40(3):603–640, 1970.

[37] Tuan A. H. Nguyen and Anh V. Nguyen. On the lifetime of evaporating sessile droplets. *Langmuir*, 28(3):1924–1930, 2012.

[38] Lorraine G Olson, Georgios C Georgiou, and William W Schultz. An efficient finite element method for treating singularities in laplaces equation. *Journal of Computational Physics*, 91(2):497, 1990.

[39] Charles S Peskin. Numerical analysis of blood flow in the heart. *Journal of Computational Physics*, 25(3):220–252, 1977.

[40] G. P. Peterson and H. B. Ma. Theoretical analysis of the maximum heat transport in triangular grooves: A study of idealized micro heat pipes. *Journal of Heat Transfer*, 118(3):731–739, 1996.

[41] Mikko Pitkonen. Polarizability of the dielectric double-sphere. *Journal of Mathematical Physics*, 47(10):102901, 2006.

[42] Mikko Pitkonen. An explicit solution for the electric potential of the asymmetric dielectric double sphere. *Journal of Physics D: Applied Physics*, 40(5):1483–1488, 2007.

[43] Yuri O. Popov. Evaporative deposition patterns: Spatial dimensions of the deposit. *Physical Review E*, 71(3), 2005.

[44] W. D. Ristenpart, P. G. Kim, C. Domingues, J. Wan, and H. A. Stone. Influence of substrate conductivity on circulation reversal in evaporating drops. *Physical Review Letters*, 99(23), 2007.

[45] Rodolfo Rosales and Pedro Saenz. Thermocapillary reorientation of Janus drops. In *APS Division of Fluid Dynamics Meeting Abstracts*, APS Meeting Abstracts, page G6.005, November 2017.

[46] Walter Rudin. *Real and Complex Analysis*, chapter 16. McCraw-Hill, New York, second edition, 1986.

[47] F. G. H. Schofield, S. K. Wilson, D. Pritchard, and K. Sefiane. The lifetimes of evaporating sessile droplets are significantly extended by strong thermal effects. *Journal of Fluid Mechanics*, 851:231–244, 2018.

[48] Feargus G. H. Schofield, Alexander W. Wray, David Pritchard, and Stephen K. Wilson. The shielding effect extends the lifetimes of two-dimensional sessile droplets. *Journal of Engineering Mathematics*, 120(1):89–110, 2020.

[49] S. Shklyaev, A. O. Ivantsov, M. Díaz-Maldonado, and U. M. Córdova-Figueroa. Dynamics of a Janus drop in an external flow. *Physics of Fluids*, 25(8):082105, 2013.

[50] Sergey Shklyaev. Janus droplet as a catalytic micromotor. *EPL (Europhysics Letters)*, 110(5):54002, 2015.

[51] J. M. Stauber, S. K. Wilson, B. R. Duffy, and K. Sefiane. On the lifetimes of evaporating droplets. *Journal of Fluid Mechanics*, 744, 2014.

[52] Jutta M. Stauber, Stephen K. Wilson, Brian R. Duffy, and Khellil Sefiane. On the lifetimes of evaporating droplets with related initial and receding contact angles. *Physics of Fluids*, 27(12):122101, 2015.

[53] Elias M. Stein and Rami Shakarchi. *Complex analysis*. Princeton Univ. Press, 2003.

[54] Bengt Sundén and Juan Fu. *Heat transfer in aerospace applications*. Elsevier Ltd., 2017.

[55] L. W. Swanson and G. P. Peterson. Evaporating extended meniscus in a v-shaped channel. *Journal of Thermophysics and Heat Transfer*, 8(1):172–180, 1994.

[56] J. M. Taylor. The condition of gram matrices and related problems. *Proceedings of the Royal Society of Edinburgh: Section A Mathematics*, 80(1-2):45–56, 1978.

[57] M. F. Unal and D. Rockwell. On vortex formation from a cylinder. part 1. the initial instability. *Journal of Fluid Mechanics*, 190:491–512, 1988.

[58] Dimitrij A. Varšalovič, Anatolij N. Moskalev, and Valerij K. Chersonskij. *Quantum theory of angular momentum: irreducible tensors, spherical harmonics, vector coupling coefficients, 3nj symbols*. World Scientific, 2008.

[59] Jinliang Wang and Ivan Catton. Enhanced evaporation heat transfer in triangular grooves covered with a thin fine porous layer. *Applied Thermal Engineering*, 21(17):1721–1737, 2001.